Tora Sund Morken

Brain development and metabolism after hypoxia-ischemia and varying oxygen levels in the neonatal rat studied with ^{13}C-MR spectroscopy and multimodal MR imaging

Thesis for the degree of Philosophiae Doctor

Trondheim, December 2013

Norwegian University of Science and Technology
Faculty of Medicine
Department of Laboratory Medicine,
Children's and Women's Health

NTNU – Trondheim
Norwegian University of
Science and Technology

NTNU
Norwegian University of Science and Technology

Thesis for the degree of Philosophiae Doctor

Faculty of Medicine
Department of Laboratory Medicine, Children's and Women's Health

ISBN 978-82-471-4861-7 (printed ver.)
ISBN 978-82-471-4862-4 (electronic ver.)
ISSN 1503-8181

Doctoral theses at NTNU, 2013:357

Printed by NTNU-trykk

Hjerneutvikling og metabolisme etter hypoksisk-iskemisk hjerneskade og varierende oksygennivå i nyfødte rotter studert via ^{13}C-MR spektroskopi og multimodal MR-avbildning

Barn som er født for tidlig er spesielt utsatt for redusert blod- og oksygentilførsel til hjernen som kan føre til hypoksisk-iskemisk hjerneskade (HI). Slike skader kan ha livslange konsekvenser for barnet og representerer derfor et betydelig folkehelseproblem. Når blodstrømmen til hjernen gjenopprettes etter HI vil det dannes oksygenradikaler, som fører til oksidativt stress. Barnets hjerne er på dette stadiet spesielt utsatt for slikt stress, og det er mulig at ekstra oksygentilførsel i denne reperfusjonsfasen vil øke skadeomfanget etter HI. Gjeldende internasjonale retningslinjer anbefaler derfor å starte gjenoppliving av barn som er født til termin med romluft i stedet for rent oksygen, men det har ikke vært mulig med en klar anbefaling for for tidlig fødte barn på grunn av lite bevisgrunnlag.

Antioksidanter er stoffer som kan begrense oksidativt stress, og når glukose metaboliseres via pentose-fosfat-shunten opprettholdes nivået av glutation, en viktig antioksidant i hjernen. Hos voksne er det vist at andelen glukose som kanaliseres via denne shunten øker som respons på skade, kanskje som en måte å beskytte hjernen på. Nivået av pentose-fosfat-shunten og dens respons på HI i nyfødt hjerne er imidlertid ukjent.

Etter HI er hjernens nerveceller, neuronene, avhengig av beskyttelse mot eksitotoksisk skade som følge av overdreven stimulering fra neurotransmitteren glutamat. Det er astrocytter som gir denne beskyttelsen, via opptak og resirkulering av glutamat i det som kalles glutamat-glutamin-syklusen. Astrocyttene sørger også i normal tilstand for å opprettholde neuronenes glutamatlagre via sin evne til nydanning av glutamat. Den nyfødte hjernen er spesielt utsatt for eksitotoksisitet fra glutamat, og det er mulig at årsaken til slik overfølsomhet ligger i at samspillet mellom neuroner og astrocytter i glutamat-glutamin-syklusen fungerer annerledes enn i den voksne hjerne.

I denne avhandlingen ble det undersøkt hvordan rent oksygen etter HI påvirker skadeomfanget over tid i en nyfødt dyremodell. Syv dager gamle rotter ble eksponert for to timer rent oksygen etter at de på forhånd var blitt påført HI. I tillegg ble det undersøkt hvordan langtidseksponering for varierende grad av høye og lave oksygennivå i nyfødtperioden påvirker hjerneutviklingen over tid. Skadeomfanget ble undersøkt med multimodal MR-avbildning fra skadetidspunkt og fram til nær voksen alder. I metabolismestudier via ^{13}C-MR spektroskopi ble glutamat-glutamin-syklusen, nivået av glukose som nedbrytes via pentose-fosfat-shunten og nydanning av glutamat studert før og etter HI.

Studiene viste at eksponering for rent oksygen sammenlignet med romluft ga et økt skadeomfang etter HI, og at forskjellen i skadeomfang i hjernen økte over tid mellom

disse to gruppene. Hjernens utviklingsstadium hos syv dager gamle rotter kan sammenlignes med moderat for tidlig fødte barn, det vil si barn som er født i svangerskapsuke 32-34. Studien støtter derfor opp under at man bør være forsiktig med å gi høye nivåer av oksygen også til for tidlig fødte barn etter en hypoksisk-iskemisk hjerneskade.

Videre ble det funnet at andelen glukose som metaboliseres via pentose-fosfat-shunten er relativt høy hos nyfødte, men at andelen nedreguleres etter HI. Siden perioden etter HI sannsynligvis karakteriseres av et økt behov for antioksidanter på grunn av oksidativt stress er det mulig at denne nedreguleringen kan være med på å forklare den nyfødte hjernens sårbarhet for slikt stress. Det ble også funnet at i den nyfødte hjernen har astrocytter en relativt høy nydannelse og overføring av glutamat til neuroner i glutamat-glutamin-syklusen. Videre ble det funnet at etter HI er denne nydanningen relativt bevart. Det er mulig at slik nydanning av glutamat kan bidra til eksitotoksisitet i akuttfasen etter nyfødt hypoksisk-iskemisk hjerneskade.

Kandidat: **Tora Sund Morken**
Institutt: **Institutt for Laboratoriemedisin, Barne- og Kvinnesykdommer**
Veiledere: **Ann-Mari Brubakk, Pål Erik Goa, Jon Skranes og Asta Håberg**
Finansieringskilde: **Samarbeidsorganet Helse Midt-Norge og NTNU**

Ovennevnte avhandling er funnet verdig til å forsvares offentlig
for graden Philosophiae Doctor i Nevrovitenskap.
Disputas finner sted i Auditoriet, Medisinsk teknisk forskningssenter, NTNU
Mandag 9.desember 2013 kl.12.15

Preface and acknowledgements

This thesis has been submitted in partial fulfilment of the requirements for the degree of Philosophiae Doctor (PhD) in Neuroscience at the Norwegian University of Science and Technology (NTNU). It is the result of work carried out at the Department of Laboratory Medicine, Children's and Women's Health, NTNU. Funding was provided by the Liaison Committee between the Central Norway Regional Health Authority (RHA) and NTNU.

It takes a village to raise a child, and in my case there were many villagers: First and foremost I offer my sincere gratitude to my main supervisor Ann-Mari Brubakk: your innovative ideas, vast knowledge and never dwindling enthusiasm started this project and pushed it to an end. I am also indebted to my "informal supervisor" Ursula Sonnewald, whose warm-heartedness and intellect I highly admire. Furthermore, I sincerely thank my co-supervisors: Pål Erik Goa, Asta Kristine Håberg and Jon Skranes for all their help and for sharing their knowledge with me. Each and every co-author is acknowledged for large contributions to this work. Special thanks to Marius Widerøe for close cooperation on animal models and *in vivo* MR imaging, and to Eva Mari Førland Brekke with whom I had the pleasure of working and writing during the last couple of years. Tina Bugge Pedersen and Lars Evje are acknowledged for their highly competent technical assistance. The staff at the Comparative Medicine Core Facility (CoMed), especially Venke-Lill Nygård, Knut Grøn and Erling Wold, is acknowledged for housing and caring for the animals. Unn Granli, Borgny Ytterhus, Eli Johannessen and Kathrin Torseth at the Cellular and Molecular Imaging Core Facility (CMIC), have contributed significantly to the performance and optimization of immunohistochemical procedures. I also thank Marit Martinussen for her mentorship and Tore Syversen for introducing me to neuroscience back when I was in Medical School. I have enjoyed being part of the research environments at the MR Core Facility, the Perinatal Brain Injury Group at the Department of Laboratory Medicine, Children's and Women's Health as well as the Metabolic Neuroscience Group at the Department of Neuroscience, where my many colleagues have provided a great workplace atmosphere.

My sisters and parents – your interest in this work and your belief in me have been invaluable, as well as countless baby-sittings. Anders, you helped me find occasional harmony in the work-life balance during these years and I believe I owe a lot to you. At the end of every day while writing this "book" I went to pick up my daughters Petra and Gunhild at pre-school. Thank you my blessed girls for that best moment of the day.

Trondheim, September 2013

Tora Sund Morken

Abbreviations

$\lambda_{\perp}$	radial diffusivity
$\lambda_{\parallel}$	axial diffusivity
ω_0	Larmor frequency
γ	gyromagnetic ratio
3D	three-dimensional
ADC	apparent diffusion coefficient
ATP	adenosine triphosphate
BBB	blood-brain barrier
B_0	static magnetic field
C	carbon
Ca^{2+}	calcium
CBF	cerebral blood flow
Cl^-	chloride
CO_2	carbon dioxide
DEHSI	diffuse excessive high signal intensity
DTI	diffusion tensor imaging
FA	fractional anisotropy
FOV	field of view
GABA	γ-amino butyric acid
GFAP	glial fibrillary acidic protein
GLAST	glutamate aspartate transporter
GLT-1	glutamine transporter-1
GLUT	glucose transporter
GS	glutamine synthetase
GSH	reduced glutathione
GW	gestational weeks
^1H	proton
HPLC	high performance liquid chromatography
HI	hypoxia-ischemia
IHH	intermittent hyperoxia-hypoxia
i.p.	intraperitoneal
K^+	potassium
LDH	lactate dehydrogenase
M	molar
MBP	myelin basic protein
MD	mean diffusivity
MR	magnetic resonance
MRS	magnetic resonance spectroscopy
MRI	magnetic resonance imaging
Na^{2+}	sodium
Na^{2+}/K^+-ATPase	sodium potassium pump
N_2	nitrogen
NAD^+	nicotinamide adenine dinucleotide
NADH	reduced nicotinamide adenine dinucleotide
NADP	nicotinamide adenine dinucleotide phosphate
NADPH	reduced nicotinamide adenine dinucleotide phosphate
NKCC1	Na^+-K^+-$2Cl^-$ cotransporter-1

NMDA	N-methyl-D-aspartate
NOE	nuclear Overhauser effect
O_2	oxygen
OL	oligodendrocyte
OL+	immature oligodendrocyte
P	postnatal day
PC	pyruvate carboxylase
PCA	perchloric acid
PDH	pyruvate dehydrogenase
ppm	parts per million
PPP	pentose phosphate pathway
PVL	periventricular leukomalacia
preOL	pre oligodendrocyte
RD	radial diffusivity
RF	radiofrequency
ROI	region of interest
ROP	retinopathy of prematurity
ROS	reactive oxygen species
TCA	tricarboxylic acid
TE	echo time
TR	repetition time
VOI	volume of interest
VEGF	vascular endothelial growth factor

Abstract

Background:

Pathological grey and white matter changes of the brain are abundant following preterm birth. Several characteristics may render the brain vulnerable to injury at this stage of development: immature cells are differentiating and migrating; a prolonged inflammatory process may be activated; there is a heightened susceptibility to oxidative stress and excitotoxicity and availability and preference of substrates for energy production is different from that in adult age. Infants born preterm are also often exposed to unphysiological and fluctuating oxygen levels as part of intensive care, and it is probable that such exposure may influence outcome. Specific for injury to an immature brain is that it may cause not only a static injured area, but also a change in the long-term trajectory of normal brain development.

In the brain, neurons and astrocytes are intimately connected. Neurons depend upon astrocytes for metabolic support as well as for their clearance of glutamate from the synaptic cleft to enable specific neurotransmission and to limit excitotoxicity. The role of neuron-astrocyte metabolic interactions in the developing brain is largely unexplored and may be of particular importance at this stage, e.g. because of the large increase in glutamatergic neurotransmission from neonatal to adult age. Furthermore, the metabolism of glucose via the pentose phosphate pathway (PPP) may be of specific significance during this period since it is essential in the synthesis of nucleotides and lipids as well as in the generation of antioxidants. Thus it has been proposed that the PPP may act as a protecting measure against oxidative stress, but its activity following neonatal brain injury has not earlier been investigated.

Aims:

The overall aim of this thesis was to study the structural changes in grey and white matter following hypoxia-ischemia (HI) and exposure to 100% oxygen as well as following prolonged exposure to fluctuating oxygen levels in neonatal rat brain. Furthermore, the aim was to elucidate metabolic pathways that might potentially affect the vulnerability of the neonatal brain to injury. This overall aim was investigated via the following specific aims: (I) Study longitudinal grey and white matter development in the neonatal rat brain after HI, hyperoxia and intermittent hyperoxia-hypoxia. (II) Study the neuronal-astrocytic interactions in the neonatal vs. the adult rat brain under physiological conditions. (III) Study the pentose phosphate pathway and the *de novo* synthesis of amino acid neurotransmitters via pyruvate carboxylation in the neonatal rat brain under physiological conditions and in the immediate recovery phase following HI.

Methods:

Longitudinal *in vivo* multimodal MR imaging was combined with immunohistochemistry to monitor grey and white matter development after HI and two hours of hyperoxia on postnatal day 7 (P7) and intermittent hyperoxia-hypoxia from birth until P14. Furthermore, to study neuron-astrocyte-interactions, *ex vivo* ^{13}C-MR spectroscopy was applied to quantify downstream metabolites following the simultaneous injection of [1,2-^{13}C]acetate and [1-^{13}C]glucose in P7 rats. The activity of the pentose phosphate and pyruvate carboxylation pathways was studied in the same manner via injection of [1,2-^{13}C]glucose.

Results and conclusions:
(I) Hyperoxia following HI in the neonatal brain led to a progressively increasing brain injury long-term in grey and white matter compared to exposure to room-air. Furthermore, fluctuating levels of oxygen led to reversible alterations in grey and white matter, although changes in the permeability of the blood brain barrier indicated long-term effects. (II) The neonatal rat brain prioritized available glucose for neuronal glutamate production, and the glutamate-glutamine cycle worked in favour of transfer of substrate from the astrocyte to the neuron. (III) The activity of the PPP was high in the neonatal brain. However, following a challenge like HI, the activity of the PPP was reduced. Also, pyruvate carboxylation was relatively preserved in the early recovery phase following HI.

Results from this thesis indicate that unphysiological levels of oxygen, even without a preceding insult, may induce alterations in brain development. This thesis also indicates that central metabolic pathways are very different in the neonatal vs. the adult brain. Whether these differences may influence the vulnerability of the neonatal brain to excitotoxicity and oxidative stress should be investigated in future studies.

List of publications

This thesis is based upon the following papers:

I. **Longitudinal diffusion tensor and manganese-enhanced MRI detect delayed cerebral gray and white matter injury after hypoxia-ischemia and hyperoxia**

   Tora Sund Morken, Marius Widerøe, Christina Vogt, Stian Lydersen, Marianne Havnes, Jon Skranes, Pål Erik Goa, Ann-Mari Brubakk

   Pediatric Research (2013) 73: 171-179.

II. **Brain development after intermittent hyperoxia-hypoxia in the rat studied by longitudinal MRI and immunohistochemistry**

   Tora Sund Morken, Axel Nyman, Ioanna Sandvig, Sverre Torp, Jon Skranes, Pål Erik Goa, Ann-Mari Brubakk, Marius Widerøe

   Accepted for publication in PLoS ONE

III. **Neuron-astrocyte interactions, pyruvate carboxylation and the pentose phosphate pathway in the neonatal rat brain**

   Tora Sund Morken, Eva Brekke, Asta Håberg, Marius Widerøe, Ann-Mari Brubakk, Ursula Sonnewald

   Neurochemical Research (2013) Mar 16 [Epub ahead of print]

IV. **The pentose phosphate pathway and pyruvate carboxylation after neonatal hypoxic-ischemic brain injury**

   Eva Brekke, Tora Sund Morken, Marius Widerøe, Asta Håberg, Ann-Mari Brubakk, Ursula Sonnewald

   Submitted to Journal of Cerebral Blood Flow & Metabolism

These papers are not included in this thesis:

V. **Effects of methylmercury on primary brain cells in mono- and co-culture**

   Tora Sund Morken, Ursula Sonnewald, Michael Aschner, Tore Syversen

   Toxicological Sciences (2005) 87:169-75.

VI. **Doxycycline treatment in a neonatal rat model of hypoxia–ischemia reduces cerebral tissue and white matter injury: a longitudinal magnetic resonance imaging study**

   Marius Widerøe, Marianne Havnes, Tora Sund Morken, Jon Skranes, Pål Erik Goa, Ann-Mari Brubakk

   European Journal of Neuroscience (2012) 36:2006-2016

Table of contents

1 Introduction

1.1 Brain cells during development

The brain consists of neurons, glial cells and extracellular matrix which on gross morphological inspection appear as grey and white matter. Grey matter contains predominantly astrocytes, neuronal soma and unmyelinated axons, while white matter is dominated by oligodendrocytes which ensheath neuronal axons with myelin.

The term "neuron" describes a type of cell which has the ability to create electrochemical gradients as an action potential across their membrane and thereby transmit information from one cell to another. Neurons are mainly either glutamatergic or GABAergic depending on which neurotransmitter they synthesize. Axons from which the presynaptic boutons extend can either be very long, such as those extending from the motor cortex to the spinal cord, or short such as intracortical interneurons. During human brain development, immature neurons – neuroblasts – migrate outwards from the neurogenic niche of the germinal matrix, a highly cellular and vascularized region in the wall of the lateral ventricles that exists from gestational week (GW) 8 until GW 36 (reviewed in (Ballabh *et al.*, 2004)). On their way to their final appropriate positions in the cortical layers I-VI, neuroblasts form the transient neuronal population of the subplate. This initial proliferation, migration and initial differentiation of neurons is around mid-gestation followed by a period in which neurogenesis is influenced by other cells, most importantly glial cells (Stolp *et al.*, 2012).

The term "glial cell" encompasses astrocytes, oligodendrocytes and microglia.

Astrocytes, the most abundant of the glial cells, are controllers of the extracellular environment and providers of neuronal metabolic support in the form of the glutamate-precursor glutamine (Danbolt, 2001). Furthermore, astrocytes take up glutamate from the synapse following presynaptic release, thereby ensuring rapid and precise neurotransmission. Astroglia are formed when the pluripotent stem cells creating neurons – radial glia – switch and start to form astrocyte precursors which will later differentiate into astrocytes and oligodendroglial progenitor cells (Malatesta *et al.*, 2000) around mid-gestation (Vaccarino *et al.*, 2007). This switch may be regulated by neurons by way of cytokine secretion, ensuring that gliogenesis does not occur until neurogenesis is complete (Barnabe-Heider *et al.*, 2005). Furthermore, this switch initiates the brain growth spurt around GW 20 that is largely due to gliogenesis (Bandeira *et al.*, 2009) and that continues until term (GW 40 weeks) in a period where the total brain surface area is also dramatically increased because of the formation of gyri and sulci.

Oligodendrocytes form the myelin sheath around axons that enables rapid propagation of action potentials. The myelin ensheathes axons in several-layers, and since one oligodendrocyte enwraps up to 40 axons, the oligodendroglial cell surface is very large (Brady & Tai, 2011). Myelin itself is a membrane consisting of lipids and proteins, creating the macroscopic bright appearance of the cerebral white matter. Axonal myelination begins around mid-gestation and continues into adulthood. The pre-oligodendrocytes (preOL) are in abundance from GW 23-30. Thereafter myelinating immature oligodendrocytes (OL+) dominate in relative numbers before finally the mature oligodendrocytes (OL) form the major part of oligodendroglial cells at term (reviewed by Volpe (2009)).

Microglial cells are widely distributed resident macrophages that invade the brain from the blood as early as GW 4 (Monier *et al.*, 2006; Monier *et al.*, 2007). During this early migration phase they have an amoeboid appearance and show features of reactivity. Microglia phagocyte cellular debris (Graeber, 2010), a process that is enhanced following injury (Neumann *et al.*, 2009). Furthermore, microglia may participate in plasticity in the adult brain (Tremblay *et al.*, 2010) and in the pruning of redundant neuronal synapses that allow for the maintenance and strengthening of others during brain development (Schafer *et al.*, 2012).

1.2 Brain Energy Metabolism

The brain is the organ of the body that needs the most energy per weight, and the energy need of grey matter far exceeds that of white matter (Clarke & Sokoloff, 1999). The large consumption is partly explained by the neuronal need to maintain their cell membrane potential and the ability to propagate action potentials (neurotransmission via electrochemical gradients). The major part of the energy production in the form of adenosine triphosphate (ATP) stems from oxidative phosphorylation in the mitochondria. This process require supply of the substrate glucose, the main energy substrate for the brain (32 ATP from one molecule of glucose), in the presence of the electron acceptor, oxygen (O_2) (McKenna *et al.*, 2012). Glucose in blood is taken up over the blood-brain barrier (BBB) via facilitating specialized glucose transporters (GLUTs). In the cytosol of the cell, glucose is trapped in the form of glucose-6-phosphate via the enzyme hexokinase. Glucose-6-phosphate may then enter glycogen synthesis for storage, glycolysis for generation of ATP or the pentose phosphate pathway (PPP; Figure 1a). The PPP generates pentoses for nucleotide synthesis and NADPH, a reducing agent that is essential in lipid synthesis and the regeneration of reduced glutathione (GSH). The PPP communicates with glycolysis via fructose-6-phosphate and glyceraldehyde. Via glycolysis, three molecules of glucose yield six pyruvate molecules, six ATP and six NADH molecules that may enter oxidative phosphorylation in the mitochondria.

Pyruvate, the end product of aerobic glycolysis, may have several fates. In the absence of O_2, pyruvate may be converted to lactate via lactate dehydrogenase (LDH), thereby reoxidizing NADH to NAD+. NAD+ is an essential oxidizing agent for the continuation of glycolysis during anaerobic conditions (by donating a proton to regenerate NADH). Therefore there is no net production of NADH under anaerobic conditions, and the ATP yield is two molecules from one glucose molecule versus 38 molecules produced under aerobic conditions when glycolysis is followed by oxidative phosphorylation and the tricarboxylic acid (TCA) cycle. In the presence of O_2 pyruvate will enter the TCA cycle as acetyl CoA via pyruvate dehydrogenase (PDH) in the mitochondria of both astrocytes and neurons or via conversion to oxaloacetate by pyruvate carboxylase (PC). Neurons depend heavily upon astrocytes for metabolic support because PC, the major anaplerotic enzyme of the brain (Patel, 1974), is localized in astrocytes only (Yu *et al.*, 1983). An anaplerotic reaction replenishes the constant drain of intermediates of the TCA cycle by the addition of carbon dioxide (CO_2, carboxylation) to pyruvate, forming “new” oxaloacetate. This is opposed to cataplerotic reactions that extract TCA cycle intermediates.

Even though glucose is an essential energy substrate for both the mature and immature brain, lactate and ketone bodies constitute a large source of energy and carbon atoms during brain development (Cremer, 1982; Nehlig, 2004). Ketone bodies are converted to acetyl CoA via β-oxidation while lactate may enter the TCA cycle via conversion to pyruvate by LDH and is subsequently converted to acetyl CoA. Furthermore is the developing brain characterized by a low number of glucose transporters (Vannucci *et al.*, 1994; Vannucci & Simpson, 2003) and a

lower energy demand than in adults, which is thought to account for the ability of the immature brain to survive prolonged periods of hypoxia as compared to adult age (Duffy *et al.*, 1975; Rice *et al.*, 1981; McKenna *et al.*, 2012).

1.3 Amino acid neurotransmitters

The TCA cycle is intimately involved in the synthesis of amino acid neurotransmitters glutamate, glutamine and y-amino-butyric acid (GABA), and it has been proposed that these transmitters are key regulators of neurodevelopment (Danbolt, 2001; Wang & Kriegstein, 2009).

1.3.1 Glutamate and glutamine

Glutamate is the main excitatory amino acid in the brain. When stimulated, glutamate reseptors depolarize the cell by an inward flux of Na^{2+} and Ca^{2+}. The inward current of Na^{2+} is created by the Na^{2+}/K^{+}/ATPase-transporter that creates a negative membrane potential. Glutamate is stored in synaptic vesicles in glutamatergic neurons (Storm-Mathisen *et al.*, 1983). After release in neurotransmission, glutamate is taken up via specialized transporters mainly on astrocytes (Danbolt *et al.*, 1992; Danbolt, 2001). In astrocytes, glutamate is either rapidly converted to glutamine via the enzyme glutamine synthetase (GS), exclusively localized in astrocytes (Norenberg & Martinez-Hernandez, 1979), or converted to α-ketoglutarate, thereby entering the TCA cycle (McKenna *et al.*, 1996). The ability of astrocytes to take up glutamate from the synapse and convert it into glutamine is vital for normal metabolic homeostasis and as a defence mechanism against excitotoxicity (Danbolt, 2001). When glutamine is released into the synapse it is taken up by high affinity transporters on neurons (Varoqui *et al.*, 2000) where it is converted to glutamate by phosphate activated glutaminase (Hogstad *et al.*, 1988). This closes what is termed *the glutamate-glutamine cycle* (McKenna *et al.*, 2012). The main functions of this cycle are to ensure precise neural signalling, preserve carbon atoms for neuronal glutamate synthesis and limit excitotoxicity by way of excessive glutamate receptor stimulation (Danbolt, 2001).

In rat the number of glutamine transporters on astrocytes on postnatal day seven (P7) is similar to adult levels but increases over the next seven days and peaks on P14 with twice the number found on adult astrocytes (Boulland *et al.*, 2003). Neuronal glutamine transporters are also present from late-gestation (Weiss *et al.*, 2003), setting the stage for transport of glutamine from astrocytes to neurons and the subsequent utilization of glutamine for glutamate synthesis. However, there is low expression of astrocytic glutamate transporters (GLT-1 and GLAST) early in brain development (Danbolt, 2001) suggesting that the ability of astrocytes to take up glutamate from the synapse is limited in the neonatal brain. In humans the density of N-methyl-D-aspartate (NMDA) binding sites, a glutamate receptor, peaks at GW 24 at levels higher than in the adult brain (Represa *et al.*, 1989) and in the rat a similar peak at 150 - 200% of adult levels occurs at P7 (Tremblay *et al.*, 1988), coinciding with the peak in synapse formation (Semple *et al.*, 2013). Furthermore, glutamate levels are two-fold lower than at term at GW 32, increase during the first year of life (Kreis *et al.*, 2002) and then remain stable after the first year until adult age (Pouwels *et al.*, 1999). Thus in humans the major increase in glutamate levels appears to happen in late pregnancy and in the early neonatal period, while in the rat this increase happen in the postnatal period and adult levels of glutamate are attained at P14 (Tkac *et al.*, 2003).

1.3.2 GABA

GABA is synthesized from glutamate via glutamate decarboxylase in the subset of neurons with relatively short processes called interneurons that constitute 20-30% of the total neuronal population (Markram *et al.*, 2004). After release, GABA is taken up via specialized GABA transporters mainly on neurons (reviewed by Schousboe (2000)). GABA is catabolized via GABA aminotransferase eventually forming succinate, and thus re-enters the TCA cycle in what is known as the GABA-shunt. Glutamine also plays an essential role in GABA homeostasis in what is referred to as the GABA-glutamate-glutamine cycle (McKenna *et al.*, 2012).

GABA is the main inhibitory amino acid neurotransmitter in the brain, but exerts excitatory neurotransmission during development (reviewed by Ben-Ari et al. (2012)). This is probably due to high intracellular Cl^- content during development created by the Na^+-K^+-$2Cl^-$ cotransporter-1 NKCC1 (Dzhala *et al.*, 2005). As a consequence of the high intracellular Cl^- content, opening of Cl^- channels via GABA stimulation will create an outward flux of Cl^- ions and depolarization of the cell. During brain development, it has been proposed that GABA play a significant role in modulating cortical complexity, differentiation and migration (Wang & Kriegstein, 2009). GABAergic neurons are present in human brain as early as GW 17 (Yan *et al.*, 1992) and GABA appears to be the first neurotransmitter to establish signalling in the developing brain (Tyzio *et al.*, 1999). On P7 in the rat the density of GABAergic neurons is similar to that of the adult brain (Micheva & Beaulieu, 1995) and the concentration of GABA at birth is similar to levels in the adult (Tkac *et al.*, 2003; Chowdhury *et al.*, 2007). Furthermore, GABAergic neurons have the ability to take up GABA from the synapse early in brain development (Vitellaro-Zuccarello *et al.*, 2003; Sipilä *et al.*, 2004) and may thus be less dependent upon delivery of substrate from astrocytes. In humans *in vivo* data on GABA levels in the preterm brain are scarce, but suggest a less steep increase during development than for glutamate (Kreis *et al.*, 2002).

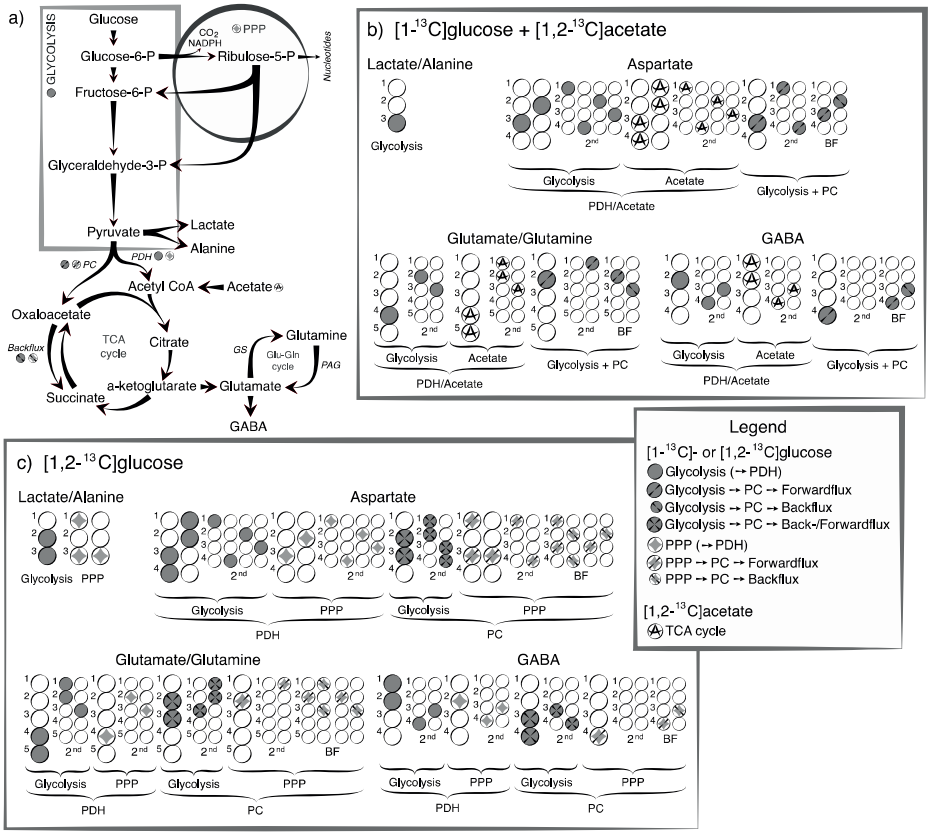

Figure 1 Simplified presentation of ^{13}C labelling patterns of metabolites following injection of [1-^{13}C]glucose and [1,2-^{13}C]acetate, or [1,2-^{13}C]glucose. a) An overview over the principal metabolic pathways discussed. b) The labelling patterns in lactate, alanine, aspartate, glutamate, glutamine and GABA following metabolism of [1-^{13}C]glucose and [1,2-^{13}C]acetate. c) The labelling patterns in the same metabolites following metabolism of [1,2-^{13}C]glucose. The circles symbolize the carbon backbone of the molecules. *Dark grey filled circles* mark the position of the label resulting from glycolysis, followed by conversion to acetyl CoA by PDH where applicable. A *middle line crossing the dark grey circle* indicates that the pyruvate has instead undergone pyruvate carboxylation before being converted to the metabolite depicted. The direction of the middle line indicates if the pattern is derived from backflux or not. *Two lines crossing* indicate that the labelling pattern from backflux cannot be distinguished from the labelling pattern from forwardflux. An "**A**" in the middle of the circle indicates that the labelling pattern is derived from [1,2-^{13}C]acetate metabolism. *Light grey diamonds mark* the position of the label resulting from the PPP. The middle lines crossing symbolize the same as mentioned above. For simplicity, only condensation of oxaloacetate with unlabeled acetyl CoA is shown for the 2nd turn. Abbreviations: α-KG, α-ketoglutarate; BF, backflux; gln, glutamine; glu, glutamate; GS, glutamine synthetase P, phosphate; PAG, phosphate activated glutaminase; PC, pyruvate carboxylase; PDH, pyruvate dehydrogenase; PPP, pentose phosphate pathway. The figure was made by Eva Brekke and utilized in paper III.

1.4 Preterm brain injury

The brain has a large ability to change permanently upon physiological and pathological stimuli in what is called plasticity. This ability is thought to be age-related (Kolb *et al.*, 2012) and forms hypothesis of fetal and/or perinatal origins for such diverse neurological and mental disorders as autism, epilepsy, cerebral palsy and schizophrenia (Stolp *et al.*, 2012). The injury mechanism may among others be early inflammation or exposure to environmental toxins *in utero* and a secondary hit such as hypoxia-ischemia (HI) that in combination cause neurodevelopmental disorders. Being born preterm (birth < GW 37) is evidently a pathological stimuli that may permanently change the normal trajectory of brain development. Indeed, preterm birth is a risk factor for long-term structural brain changes (Martinussen *et al.*, 2005) and the degree of prematurity closely correlates with IQ (Bhutta *et al.*, 2002; Johnson, 2007). The term "encephalopathy of prematurity" has been proposed to describe the complex of white matter injury combined with grey matter axonopathy that may ensue following preterm birth (Volpe, 2009).

1.4.1 White matter

The spectrum of brain injury in preterm born children has changed over the years. Earlier, focal periventricular leukomalacia (PVL) and germinal matrix haemorrhages with cysts in the white matter areas around the ventricles were abundant. Presently, a more diffuse developmental disorder seen as widespread gliosis of white matter is the most common pathological finding in this population (Volpe, 2009) and cognitive impairment is now a larger problem than cerebral palsy among survivors of extremely preterm birth (Platt *et al.*, 2007; Larroque *et al.*, 2008). On magnetic resonance imaging (MRI) ventricular dilatation (Skranes *et al.*, 1998; Dyet *et al.*, 2006) and DEHSI (Diffuse Excessive High Signal Intensity) (Maalouf *et al.*, 1999; Dyet *et al.*, 2006) in white matter are abundant as well as long-term white matter diffusion abnormalities that may persist into young adulthood (Eikenes *et al.*, 2010).

1.4.2 Grey matter

Neuronal injury and gliosis is often found in cases of PVL (Pierson *et al.*, 2007), and encephalopathy of prematurity is now acknowledged to be accompanied by neuronal loss (Volpe, 2005; Leviton & Gressens, 2007; Volpe, 2009). Furthermore, grey matter volumes are lower in preterm born infants with white matter injuries (Inder *et al.*, 1999), and cortical thinning and reduced surface area correlate with lower IQ, suggesting that such grey matter abnormalities affect neurodevelopmental outcome (Martinussen *et al.*, 2005).

1.4.3 Hypoxia-ischemia

In HI there is a combined stop in delivery of glucose and O_2 to brain cells and compromised drainage of metabolites into the blood from the brain due to the compromised cerebral blood flow (CBF). Preterm born infants are at higher risk of such hypoxic-ischemic events before and during birth as well as in the postnatal period, and HI may be caused by intraventricular or germinal matrix haemorrhage, embolism or birth asphyxia with systemic circulatory failure.

Lack of O_2, the major electron acceptor in the electron transport chain, reduces oxidative phosphorylation and the activity of the TCA cycle in the mitochondria. Then anaerobic glycolysis becomes the principal source of ATP, generating 2 ATP molecules for every glucose molecule, which is 19-times less than during aerobic conditions (38 ATP per glucose molecule). The abrupt need for energy is met by the breakdown of glycogen to glucose, increased glucose

uptake from the blood (Vannucci *et al.*, 1996) and upregulation of glycolysis in the brain (Vannucci *et al.*, 2005). The utilization of glucose for anaerobic glycolysis is highly inefficient, and together with limited glycogen storage in the brain it causes a rapid depletion of brain glucose while plasma glucose levels remain normal (Yager *et al.*, 1992).

Eventually, in spite of adaptive measures, ATP falls after minutes of HI in neonatal rats (Welsh *et al.*, 1982). This primary energy failure initiates a cascade of events of which the initial is a failure of the ATP-dependent Na^{2+}/K^{+} pump. The consequential Na^{2+} influx leads to influx of Cl^{-} and H_2O, cell swelling, cytotoxic edema and early necrosis. Furthermore, glutamate is released into the synapse in large amounts because the cell membrane is depolarized, causing overstimulation of glutamate receptors. Overstimulation of the NMDA-receptor leads to an influx of Ca^{2+} into the cytosol that starts off a series of events resulting in late apoptotic cell death. During and after HI, free oxygen radicals or reactive oxygen species (ROS) arise from several sources: (I) processes initiated by increased intracellular Ca^{2+} (II) microglial activation (III) initiation of oxidative phosphorylation upon reperfusion and delivery of oxygen to the tissue. ROS are highly reactive oxidative agents that may directly damage cellular structures (Maltepe & Saugstad, 2009).

1.5 Which factors make the preterm brain susceptible to injury?

1.5.1 Oligodendrocytes

The diffuse component of PVL is thought to be caused by injury to the immature forms of oligodendrocytes, namely preOL and OL+ (Haynes *et al.*, 2003; Back *et al.*, 2005) which are abundant in the preterm brain (Back *et al.*, 2001). Failure in their capacity to mature properly into myelin-producing oligodendrocytes (OLs) is now thought to be important for the ensuing delayed myelination and hypomyelination (Billiards *et al.*, 2008; Buser *et al.*, 2012). In neonatal rats it has been shown that immature white matter has an increased susceptibility to HI (Segovia *et al.*, 2008), inflammation (Favrais *et al.*, 2011), oxidative stress (Back *et al.*, 1998; Gerstner *et al.*, 2008) and excitotoxicity (Follett *et al.*, 2000).

1.5.2 Neurons

There is a paucity of subplate neurons in preterm infants with PVL (Kinney *et al.*, 2012) and it has been proposed that this transient population of neurons during brain development may be targets for injury (Leviton & Gressens, 2007; Volpe, 2009). These neurons are susceptible to HI in neonatal rats (McQuillen *et al.*, 2003) and it has also been proposed that they may be injured when wandering out from the germinal matrix to the cortex when passing through an abundance of activated microglia in white matter (Leviton & Gressens, 2007). Furthermore, the term “dying back” of neurons has been introduced since secondary necrosis after axonal damage due to PVL is frequent (Andiman *et al.*, 2010). Also, coinciding with the peak vulnerability period for PVL (Xu *et al.*, 2011), GABAergic interneurons migrate around mid-gestation, possibly making them susceptible as targets for injury.

1.5.3 Increased susceptibility to excitotoxicity

As mentioned earlier, there are indications that the ability of astrocytes to limit excitotoxicity is lower in the neonatal than the adult brain since the expression of the predominantly astrocytic glutamate transporters GLT-1 on astrocytes is low ((Danbolt, 2001) and references

therein). This may limit the ability of astrocytes to rapidly reduce the glutamate concentration in the synaptic cleft and thereby increase the danger of excitotoxic events. Furthermore, the mentioned abundance of NMDA receptors early in brain development coincide with a hypersensitivity of these receptors because of subunits that create a prolonged influx of Ca^{2+} into the cell upon stimulation (reviewed in (Sanchez & Jensen, 2001)). This may explain the heightened susceptibility of the immature brain to excitotoxicity in case of excessive glutamate release such as after HI (Johnston, 2005).

1.5.4 Vulnerability to oxidative stress

The preterm brain is susceptible to oxidative stress because of low-levels of anti-oxidant enzymes and a pro-oxidant environment during development because of high concentrations of fatty acids and iron (McQuillen & Ferriero, 2004; Volpe, 2008). Haemorrhage, a common feature in preterm brain injury, may also contribute iron that together with hydrogen peroxide will generate hydroxyl radicals in what is called the Fenton reaction. The PaO_2 *ex utero* is considerably higher than the PaO_2 in fetal circulation of 25-30 mmHg. Furthermore, the sick premature child will often be in need of oxygen therapy. Both these factors, a relative hyperoxic environment together with additional oxygen as part of treatment may increase oxidative stress following a preceding insult such as HI. Indeed, resuscitation with 100% O_2 after birth asphyxia increase oxidative stress (Vento *et al.*, 2001), neonatal mortality and possibly also the risk of hypoxic-ischemic encephalopathy (Saugstad *et al.*, 2008). Consequently the current recommendation from the International Liaison Committee on Resuscitation (ILCOR) is to start resuscitation in term infants with room-air (21% O_2) (Perlman *et al.*, 2010). However guidelines are not conclusive in preterm born infants since experimental evidence in this group is scarce. Apnoeic episodes (temporary absence or cessation of breathing) are also frequent in preterm infants, creating large fluctuations in oxygen levels that are non-physiological. Such non-physiological fluctuations are implicated in the pathogenesis of retinopathy of prematurity (ROP), a potentially blinding disorder with perturbed neurovascular development in the retina (Hartnett & Penn, 2012), and it has been proposed that such an exposure may also affect normal brain development (Martin *et al.*, 2011).

1.5.5 Activation of microglial cells

Inflammation is a risk factor for preterm delivery (Andrews *et al.*, 1995; Vrachnis *et al.*, 2010), potentiates preterm brain injury (Schlapbach *et al.*, 2011) and create white matter alterations in neonatal animals (Favrais *et al.*, 2011). Furthermore is the injury cascade following neonatal HI characterized by a continuum of necrosis, apoptosis and delayed inflammation that may continue for weeks (Northington *et al.*, 2001; Nelson & Lynch, 2004) and possibly even years (Fleiss & Gressens, 2012). The pathogenesis of both inflammation and HI converge upon one cell: the microglia, and these innate immune cells of the brain has therefore recently become subject to massive investigations. During their invasion of the developing brain they migrate into foci that correspond to susceptible areas in white matter injury (Monier *et al.*, 2007; Verney *et al.*, 2010) and there attain an activated amoeboid morphology (Billiards *et al.*, 2006). It has therefore been proposed that such activated microglia may be key effectors in injury to the developing white matter since “they are in the right place at the right time” (Volpe, 2009). Persistent alteration in the immune response following neonatal brain injury has been named one of many *tertiary* mechanism of prolonged brain damage (Fleiss & Gressens, 2012), and may represent a window of opportunity for treatment.

1.5.6 Immature vascularization

During brain development the vasculature grows with close proximity to the neurogenic tissue (Stubbs *et al.*, 2009), and important regulators of vasculogenesis like vascular endothelial growth factor (VEGF) (Carmeliet *et al.*, 1996) may also regulate neurogenesis (Darland *et al.*, 2011). Early in fetal life vascular supply to the basal parts of the brain dominates via Heubner's artery that perforates to the germinal matrix and basal ganglia from around GW 23-24. However, during the brain growth spurt the pattern of vascular supply is progressively more dominated by the branches of the carotid internal artery. By GW 32-34, when the organization of the cortical and white matter is still ongoing, the main arterial supply to the brain comes from penetrating arteries into the cortex, and the relative size of Heubner's artery is successively getting smaller (Wigglesworth & Pape, 1978; Pape & Wigglesworth, 1979). The localization of the most severe forms of preterm brain injury in water-shed areas with poor circulation around the ventricles and in the germinal matrices strongly suggests that vascular patterns are implicated in the pathogenesis. These water-shed areas may be particularly susceptible to ischemia because the preterm brain has a narrow autoregulatory plateau of CBF causing a pressure-passive perfusion (Wigglesworth & Pape, 1978). Furthermore, the rich vasculature of the germinal matrices appears to be fragile, possibly making them susceptible to haemorrhage upon variations in CBF (El-Khoury *et al.*, 2006; Braun *et al.*, 2007). Immature neurovasculature is also implicated in another disorder of the premature, namely ROP. Like in the brain, neural and vascular tissue grow in close proximity in the retina during the last part of gestation, and perturbations of this growth is followed by hypersecretion of VEGF and ensuing retinal neovascularization in the most severe forms of ROP (Hartnett & Penn, 2012). Albeit this knowledge, research into the cerebrovascular contribution to preterm brain injury has been limited (Baburamani *et al.*, 2012).

1.6 Magnetic Resonance (MR)

Magnetic resonance imaging (MRI) and spectroscopy (MRS) represent powerful tools to describe long-term brain development since they may be utilized *in vivo* and have no described toxic effects. MRI and MRS are both based on the manipulation of the nuclear spin of atoms with uneven nuclear mass numbers like ^{1}H, ^{13}C and ^{31}P when placed within a magnetic field (B_0) (Friebolin, 1993). In MRI only ^{1}H (also referred to as "proton") is studied due to its abundance in biological tissue, whereas in MRS all of the above mentioned nuclei may be studied. Only proton- and ^{13}C-MRS will be considered in this thesis.

1.6.1 Principles of magnetic resonance

The nuclear spin will in its resting state be randomly oriented. However when placed in a magnetic field (B_0), the nuclear spin will precess around an axis parallel to the direction of the B_0 at a frequency called the Larmor frequency (ω_0). The Larmor frequency is determined by the specific nuclei's gyromagnetic ratio (γ) and the applied magnetic field:

Eq. 1 $$\omega_o = \mathrm{B}_o\gamma$$

For proton spins two allowed energy states exist; a low-energy state (α) aligning parallel to the magnetic field (spin-up) and a high-energy state (β) aligning anti-parallel (spin-down), to the magnetic field. Normally the energy difference between these two states (ΔE) is small, but nevertheless a small majority of the spins will be in the low energy state, creating a net

magnetization vector (M_0) that aligns with B_0. The ratio between the two populations at thermal equilibrium can be described by Boltzmann statistics:

Eq. 2 $$\frac{N_\alpha}{N_\beta} = e^{\frac{\Delta E}{K_B T}}$$

where N_α is the number of spins in the low energy state (spin-up), N_β is the number of spins in the high-energy state (spin-down), ΔE is the energy difference between the N_α spin-up and N_β spin-down, K_B is the Boltzmann's constant and T is the absolute temperature. ΔE is determined by the specific individual gyromagnetic ratio (γ), Plank's constant ($\hbar$) and the B_0:

Eq. 3 $$\Delta E = \gamma \hbar B_o$$

It follows from Eq. 2 and 3 that as the magnitude of the magnetic field increases so does the surplus of atoms in the low-energy state.

Magnetic resonance techniques exploit that the spins can be manipulated by adding energy to the system via the application of a radio frequency pulse (the RF-pulse). For such a transfer of energy to occur, the RF-pulse must be applied at the Larmor frequency of the spins, thereby the use of the term *resonance*. When applied perpendicular to the B_0 (usually defined along the z-axis) the RF pulse will force the net magnetization vector (M_0) from the z-axis down into the x-y plane. This causes more spins to be in the high-energy state. The resulting M_0 will precess around the B_0 with the Larmor frequency and induce an alternating current in the receiving RF coil. After the RF-pulse is turned off, the spin system will return to the thermal equilibrium state, and the energy is emitted to the surroundings at the Larmor frequency and induces an alternating decaying signal in a receiving RF-coil. This is known as the Free-induction decay (FID) and forms the basis for the MR signal.

The MR signal is usually averaged over several scans to increase the signal-to-noise ratio (SNR). To double the SNR one must increase the number of scans four times since the ratio is proportional to the root of the number of scans needed to obtain the signal:

Eq. 4 $$\frac{S}{N} \sim \sqrt{(n\ scans)}$$

1.6.2 T_1 relaxation and T_2 relaxation

The mechanism which brings the z-axis magnetization vector (M_z) back to the thermal equilibrium value (M_0) is termed longitudinal relaxation or T_1-relaxation, and follows the equation:

Eq. 5 $$M_z = M_o(1 - e^{-\frac{t}{T1}})$$

where T_1 is the time constant for the T_1-relaxation process.

Pari passu with T_1 relaxation, transverse or T_2 relaxation occurs in the x-y plane. Nuclear spins act upon each other to dephase and loose coherence, gradually nulling each other out. This is called spin-spin or T_2 relaxation and follows the equation:

Eq. 6 $$M_{xy} = M_o^{(-\frac{TE}{T2})}$$

where echo time (TE) is the time delay between RF-excitation and signal acquisition. It is common to distinguish between native T_2 and T_2*, where the latter is always shorter than T_2 and includes so-called static dephasing effects.

1.6.3 Spatial Encoding

In order to get an image from the acquired MR signal, one needs a method for spatial encoding. This is achieved by letting the applied magnetic field B_0 vary linearly with physical position in different ways during the MR sequence. This linear variation in the applied field is obtained using so-called gradient coils, which can be switched on and off very quickly. By the application of such gradients, the *location* of the spin along this gradient field will determine its specific Larmor frequency. The mathematical method called Fourier transformation identifies the different frequencies and amplitudes that make the MR signal. This transformation converts the signal from amplitude against time into amplitude against frequency. Spatial encoding enables the correct location of where to plot signal intensities so that an MR image can be created.

1.6.4 Spin-echo

In a standard FID-experiment, the MR signal will decay by a rate given by T_2*. However, by using a technique called the spin-echo, the MR signal amplitude can be partly regained to an amplitude defined by T_2 instead of T_2*, meaning that only the static dephasing contributions is refocused. By the application of a second RF-pulse that is at 180° at a specific time after the 90° pulse, spins will be flipped 180° and start to rephase again at the same rate as they were dephasing. At double the time of the 180° pulse the spins will be in phase again and form one large magnetization vector in the xy-plane in what is known as an echo. The TE is given by twice the delay between the 90° pulse and the 180° pulse.

1.6.5 MR contrast formation

The acquired MR signal is a function of the proton density and T_1 and T_2 relaxation properties of the tissue. The relative contribution to the acquired signal from these three properties is controlled through the TE and the repetition time (TR) of the MR-sequence where TR is the time delay between each excitation RF-pulse.

When the image contrast between tissue types is mainly determined by differences in T_1-relaxation time, we have what we call a T_1-weighted image. To obtain such an image, one must choose the shortest possible TE in order to minimize the sensitivity to T_2-differences, while TR should be in between the T_1-values of the tissue types one wants to distinguish. In a T_1-weighted image, tissue with short T_1 like fat will be brighter than tissue with longer T_1 like fluids.

Similarly, in order to obtain a T_2-weighted image the sensitivity to T_1-differences must be minimized while maximizing the T_2-sensitivity. T_2-relaxation time is always shorter than T_1. Maximizing the T_2-sensitivity is achieved by choosing a long TR and TE, thereby avoiding that

differences in T_1 relaxation will affect the contrast since all protons will have had time to regain its net magnetization vector along the B_0. In tissue with long T_2 such as water the transfer of energy in the spin-spin relaxation is slow, leading to a high signal in a T_2-weighted MR image.

The MR signal can be manipulated via the application of contrast agents that have magnetic properties like manganese (Mn^{2+}). Such agents will facilitate energy transfer from excited protons and thereby facilitate both T_1 and T_2 relaxation, but mainly T_1-relaxation. Thereby T_1-relaxation time will be shortened and there will be increased signal contrast between manganese-enhanced tissue and tissue with less manganese-enhancement.

1.6.6 Diffusion weighted imaging

Diffusion is the free and random movement of small particles in a medium, as can be observed when putting a drop of ink in a glass of water. In tissue the diffusion of water molecules is restricted due to the architecture of the tissue like cell membranes. Magnetic resonance techniques can be applied to quantify the degree of diffusion in a specific tissue via the application of a linear magnetic field gradient along the y-axis just before and after the 180°pulse in a spin-echo sequence. The water molecules that diffuse will have moved between the first and the second signal and the rephasing induced by the 180° pulse will be incomplete compared to molecules that have not shifted position, thereby reducing the magnitude of the subsequent echo. This reduction in signal magnitude between the signal before diffusion weighing (S_0) and the weakened signal (S) is given by the following equation:

Eq. 7
$$S = S_0 e^{-b \cdot D}$$

where *b* is a number quantifying the amount of diffusion weighting that is determined by the applied gradients, and D is the diffusion coefficient of the tissue under study. It follows that the weakening of the signal increases with increasing *b*-values. In tissue the diffusion coefficient is named the apparent diffusion coefficient (ADC). When applying systematically increasing *b*-values and measuring the subsequent decrease in signal, the slope of the resulting curve is determined by the ADC, and ADC maps of the tissue may be created. ADC is high if the free movement of water molecules (diffusion) is unrestricted.

1.6.7 Diffusion Tensor Imaging

In free water, as well as in most tissue types, the diffusion coefficient is the same in every direction and we have what we call isotropic diffusion. However, in some tissue types the water diffusion is highly directional which is termed anisotropic diffusion. An example of such tissue is cerebral white matter axons where myelin sheets highly restrict diffusion of water molecules.

By varying the directions of the linear magnetic gradients in diffusion-weighted sequences, the overall *directionality* of the diffusion in a tissue can be determined. This is exploited in diffusion tensor imaging (DTI). Water diffusion is described by three vector directions (λ_1 , λ_2 and λ_3) that in the case of anisotropic diffusion are either parallel to the main direction of diffusion (λ_1) or perpendicular to it (λ_2 and λ_3). λ_1 is the longest vector of the vectors that describe the ellipsoid of the so-called diffusion tensor.

Radial diffusivity ($\lambda_\perp$) is the diffusion perpendicular to the main direction of diffusion and is given by:

Eq.8 $$\lambda_\perp = \frac{(\lambda_2+\lambda_3)}{2}$$

Axial diffusivity ($\lambda_\parallel$) is the average diffusivity along the primary diffusion direction and is given by:

Eq. 9 $$\lambda_\parallel = (\lambda_1)$$

Mean diffusivity (MD) is the average directional diffusivity within a voxel of the tissue and is equivalent to the ADC. It is given by:

Eq. 10 $$MD = \frac{(\lambda_1+\lambda_2+\lambda_3)}{3}$$

The overall directionality of the diffusion in a voxel, the fractional anisotropy (FA), describes the sum of the distance of all the directional vectors from the mean diffusivity, standardized divided by the sum of all the vectors. When it is close to 1 water movement is totally anisotropic, and when it is 0 there is no anisotropy.

Eq. 11 $$\mathrm{FA} = \sqrt{\frac{3}{2}}\,\frac{\sqrt{((\lambda_1-\lambda)^2+(\lambda_2-\lambda)^2+(\lambda_3-\lambda)^2}}{\sqrt{(\lambda_1+\lambda_2+\lambda_3)}}$$

1.6.8 Magnetic resonance spectroscopy

In MR spectroscopy the magnetic field strength is held constant and the amplitude of the Larmor frequencies of individual nuclei like ^{1}H, ^{13}C and ^{31}P are recorded. The same nucleus in different molecules will experience unique chemical environments that will slightly change their gyromagnetic ratios and thus their Larmor frequencies in a phenomenon called chemical shift. Therefore individual peaks reflecting the same nuclei but within different molecules will occur at varying distances from a reference compound in a unitless scale of parts per million (ppm). This scale is independent of the magnetic field and forms the x-axis of the spectrum (Figure 2). The ppm of each metabolite is usually known from the literature (Fan & Lane, 2008), and the peak intensity is a function of the T_1 of the nuclei in that specific molecule.

In ^{13}C-MR spectroscopy the ^{13}C nuclei are excited. The low natural abundance of ^{13}C (1.1%) may be exploited for metabolic studies in MR spectroscopy by the addition of ^{13}C-labelled substrates like [1-^{13}C]glucose or [1,2-^{13}C]acetate to a biological system like a research animal. The ^{13}C-label and its position in downstream metabolites (Figure 1b & c) may be seen as characteristic peaks in a spectrum and may be quantified relative to a standard (Figure 2). Unique Larmor frequencies for each position of ^{13}C in isotopes of a molecule allows for identification and quantification of downstream metabolites.

Combined with the knowledge of metabolic compartments in the brain, i.e. the pools of neurotransmitters and the localization of key enzymes, this technique enables mapping of distinct metabolic pathways and neurotransmitter synthesis and cycling between cellular compartments.

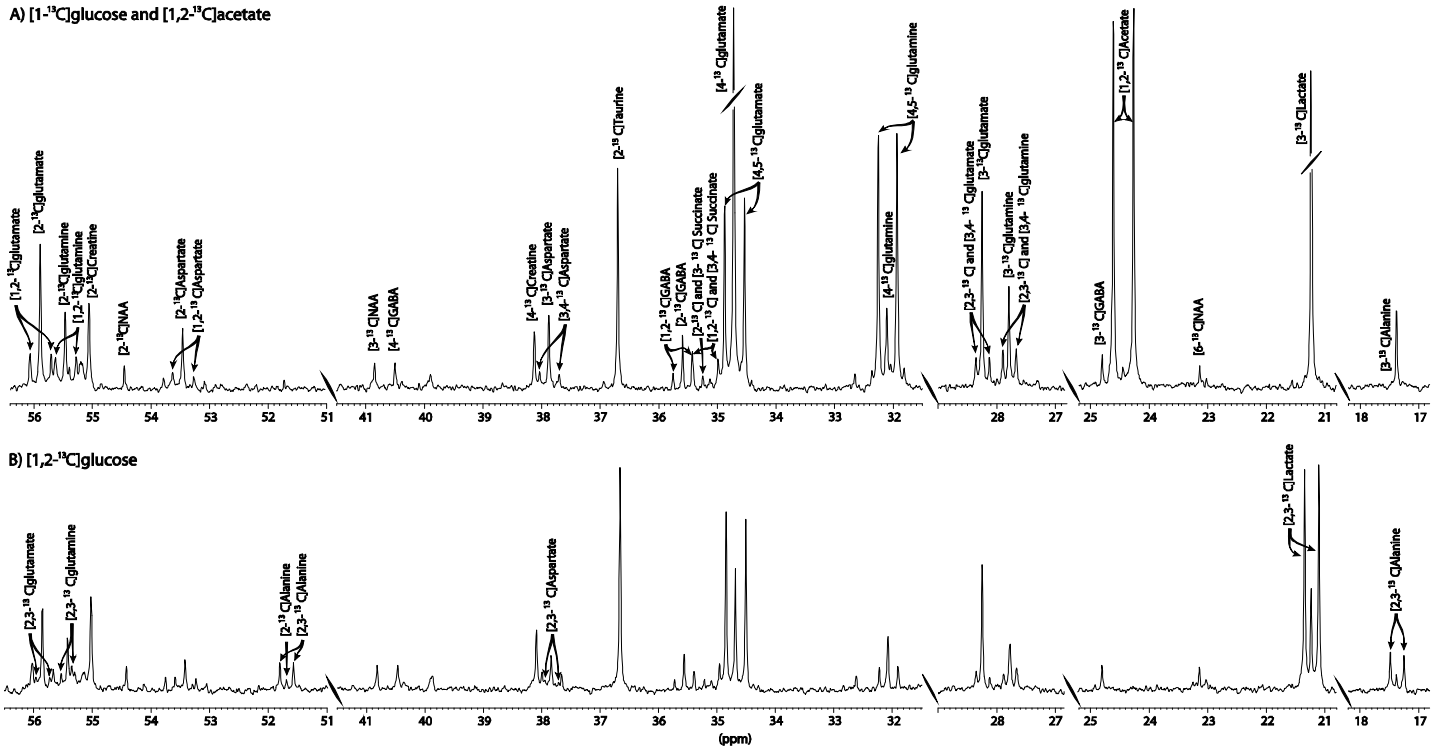

Figure 2 ^{13}C-MR spectra of the brain extracts from postnatal day 7 rats. The horizontal axis has been truncated in several places. (a): Spectrum resulting from metabolism of [1-^{13}C]glucose and [1,2-^{13}C]acetate. The peaks of [4-^{13}C]glutamate and [3-^{13}C]lactate have been truncated. (b): Spectrum resulting from metabolism of [1,2-^{13}C]glucose. Most of the peaks are only marked in (a), but some additional doublets and singlets have been marked in (b). Abbreviations: NAA, n-acetyl aspartate; ppm, parts per million.

1.7 The glutamate-glutamine cycle

It is known that the neonatal brain is susceptible to excitotoxic injury and that a heightened sensitivity to glutamate may be involved (Johnston, 2005). The glutamate-glutamine cycle is central in glutamate homeostasis (McKenna *et al.*, 2012). However, the actual transfer of glutamate and glutamine between the neuronal and glial compartment has not earlier been characterized in the immature brain. The utilization of a precursor that will be taken up in the glial compartment, incorporated into glutamine and then transported to the neuronal compartment for conversion to glutamate may answer whether this transfer is different in the neonatal compared to the adult brain. [1,2-^{13}C]acetate is such a precursor since it is exclusively metabolized in astrocytes (Sonnewald *et al.*, 1993; Waniewski & Martin, 1998). Via simultaneous injection together with [1-^{13}C]glucose, which is mainly metabolized in neurons (Qu *et al.*, 2000), ^{13}C MRS makes it possible to study astrocytic and neuronal metabolism in the same animal and the transfer of substrates between these two cellular compartments.

1.7.1 Labelling patterns from [1-^{13}C]glucose

Via glycolysis, [1-^{13}C]glucose will yield one unlabelled pyruvate and one [3-^{13}C]pyruvate molecule which can enter the TCA cycle as [2-^{13}C]acetyl CoA via PDH after condensation with oxaloacetate. After several steps α-[4-^{13}C]ketoglutarate will be formed, and can give rise to [4-^{13}C]glutamate, [4-^{13}C]glutamine and [2-^{13}C]GABA (from [4-^{13}C]glutamate; Figure 1b). If α-[4-^{13}C]ketoglutarate stays in the cycle, the ^{13}C label will be scrambled in the symmetrical molecule succinate to yield equal parts of [2-^{13}C] or [3-^{13}C]succinate, fumarate, malate, oxaloacetate and aspartate. [2-^{13}C] or [3-^{13}C]oxaloacetate can condense with acetyl CoA and yield [2-^{13}C] or [3-^{13}C]glutamate/glutamine and [3-^{13}C] or [4-^{13}C]GABA from the 2nd turn of the TCA cycle if the acetyl-CoA is unlabelled. If [2-^{13}C] or [3-^{13}C]oxaloacetate condense with [2-^{13}C]acetyl CoA, the molecules will in addition be labelled in the positions mentioned above from the 1st turn of the TCA cycle.

1.7.2 Labelling patterns from [1,2-^{13}C]acetate

[1,2-^{13}C]acetate will enter the TCA cycle via acetyl CoA and yield [4,5-^{13}C]glutamate/glutamine and [1,2-^{13}C]GABA (Figure 1b). If the label remains in the TCA cycle for a 2nd turn, it will lead to glutamate and glutamine equally labelled in either [1,2-^{13}C] or [3-^{13}C]glutamate/glutamine and [3-^{13}C] or [4-^{13}C]GABA.

1.8 The pentose phosphate pathway and pyruvate carboxylation

The utilization of alternate energy sources like ketone bodies is higher in the neonatal than the adult brain, as mentioned earlier (Cremer, 1982; Nehlig, 2004). Nevertheless, glucose is still an essential substrate, and one proposed explanation is the activity of the PPP, which can only be fuelled by glucose. The PPP is essential in nucleotide and lipid synthesis as well as in the regeneration of GSH. GSH acts together with glutathione peroxidase in the reduction of ROS. These are all processes that are important during brain development, and it has been proposed that levels of the PPP are higher in the neonatal brain than in the adult brain (Ben-Yoseph *et al.*, 1996; McKenna *et al.*, 2012). Furthermore, it has been reported in animal and human studies that the PPP in the adult brain can be upregulated several-fold in response to injury that cause oxidative stress (Bartnik *et al.*, 2005; Dusick *et al.*, 2007). However, neither the significance of this pathway nor its activity following similar insults has earlier been studied

in the neonatal brain. To quantify the PPP with ^{13}C - MR spectroscopy, a ^{13}C - labelled precursor which will create specific labelling patterns via the PPP vs. glycolysis would be required. [1,2-^{13}C]Glucose is such a precursor.

Furthermore, to increase glutamate reserves in neurons during brain development, *de novo* synthesis of glutamate must take place. This requires anaplerosis, and as mentioned it is pyruvate carboxylase (PC), which is exclusively localised in astrocytes (Yu *et al.*, 1983), that is the main anaplerotic enzyme of the brain (Patel, 1974). The level of PC is low during brain development in the rat and its activity has a steep increase towards adulthood in the period of glutamatergic increase (Wilbur & Patel, 1974). However, the actual extent of carboxylation of pyruvate from glucose in the neonatal brain has not earlier been quantified. To do this a ^{13}C-labelled precursor that would lead to distinct labelling patterns following PC derived metabolites would be needed in combination with ^{13}C -MR spectroscopy. [1,2-^{13}C]Glucose can also be utilized for this purpose.

1.8.1 Labelling patterns from [1,2-^{13}C]glucose

It is possible to distinguish the labelling patterns in metabolites derived from the PPP from those resulting from glycolysis via [1,2-^{13}C]glucose. If [1,2-^{13}C]glucose is metabolized via the PPP, one of the labelled ^{13}C atoms will be discarded as $^{13}CO_2$, thus forming one molecule of [1-^{13}C]ribulose. Three molecules of [1-^{13}C]ribulose are involved when one [1,3-^{13}C]- and one [1-^{13}C]fructose-6-P as well as one unlabelled glyceraldehyde-3-P are formed. The labelled [1,3-^{13}C]- and [1-^{13}C]fructose-6-P will generate [1,3-^{13}C]- and [3-^{13}C]glyceraldehyde and subsequently pyruvate labelled in the same positions (Brekke *et al.*, 2012). Three molecules of [1,2-^{13}C]glucose will generate one [1,3-^{13}C]pyruvate, one [3-^{13}C]pyruvate and three unlabelled molecules of pyruvate which can either enter the TCA cycle and lead to labelling in glutamate/glutamine/GABA, or be reduced to lactate or transaminated to alanine maintaining the same labelling patterns as pyruvate. The sum of [1,3-^{13}C]- and [3-^{13}C]lactate/alanine can be quantified in the C3-positions in the spectra (Figure 2b). Via PDH both [3-^{13}C]pyruvate and [1,3-^{13}C]pyruvate will be converted to [2-^{13}C]acetyl CoA, which can enter the TCA cycle forming [2-^{13}C]citrate. Metabolism of [2-^{13}C]citrate in the TCA cycle leads to [4-^{13}C]glutamate/glutamine, [2-^{13}C]GABA and equal amounts of [2-^{13}C]- and [3-^{13}C]aspartate in the 1st turn. In the 2nd turn, it will lead to [2-^{13}C]glutamate/glutamine, [3-^{13}C]glutamate/glutamine, [3-^{13}C]GABA, [4-^{13}C]GABA, and aspartate labelled equally in all four positions. PPP followed by PC will generate label in [2-^{13}C]glutamate/glutamine and [4-^{13}C]GABA. The part of the labelled oxaloacetate which backfluxes to the symmetrical molecule fumarate before it is again reverted to oxaloacetate, can be detected due to the formation of [3-^{13}C]glutamate/glutamine and [3-^{13}C]GABA which appears in addition to [2-^{13}C]glutamate/glutamine and [4-^{13}C]GABA.

Via glycolysis, three molecules of [1,2-^{13}C]glucose will generate three molecules of [2,3-^{13}C]pyruvate and three unlabelled molecules of pyruvate, with corresponding labelling patterns in lactate and alanine. If this pyruvate is metabolized via PDH, the 1st turn of the TCA cycle will lead to formation of α-[4,5-^{13}C]ketoglutarate and thus [4,5-^{13}C]glutamate/glutamine and [1,2-^{13}C]GABA. If [2,3-^{13}C]pyruvate is instead subjected to PC, this will lead to the formation of [2,3-^{13}C]oxaloacetate. [2,3-^{13}C]Oxaloacetate can be transaminated to form [2,3-^{13}C]aspartate, or it can condense with acetyl CoA forming [3,4-^{13}C]citrate. After several steps, α-[2,3-^{13}C]ketoglutarate is formed, which can exit the TCA cycle and give rise to [2,3-^{13}C]glutamate, [2,3-^{13}C]glutamine and [3,4-^{13}C]GABA. If the label remains in the TCA cycle

for a 2nd turn, it will give rise to equal amounts of [3-^{13}C]glutamate and [1,2-^{13}C]glutamate, [3-^{13}C]glutamine and [1,2-^{13}C]glutamine, and [3-^{13}C]GABA and [4-^{13}C]GABA.

2 Aims

The overall aim of this thesis was to study the structural longitudinal changes in grey and white matter following HI and/or unphysiological oxygen exposure and to elucidate central metabolic pathways in the neonatal brain that might potentially explain the vulnerability of the neonatal brain to injury. This overall aim was investigated via the following specific aims:

- Investigate whether hyperoxic exposure after HI in the P7 rat will impact long-term injury in grey and white matter measured by multimodal *in vivo* MRI and immunohistochemical methods (Paper I).
- Investigate whether long-term exposure to intermittent hyperoxia-hypoxia from birth until P14 in the rat will impact grey and white matter brain development measured by multimodal *in vivo* MRI and immunohistochemical methods (Paper II).
- Study the temporal incorporation of label in downstream metabolites from [1-^{13}C]glucose and [1,2-^{13}C]acetate in the P7 rat brain via *ex vivo* ^{13}C-MR spectroscopy (Paper III).
- Study neuron-astrocytic interactions in the P7 vs. the adult rat brain under physiological conditions via injection of [1-^{13}C]glucose and [1,2-^{13}C]acetate and *ex vivo* ^{13}C-MR spectroscopy (Paper III).
- Study the pyruvate carboxylation and pentose phosphate pathways in the P7 rat brain under physiological conditions and in the immediate recovery phase following HI via injection of [1,2-^{13}C]glucose and *ex vivo* ^{13}C-MR spectroscopy (Paper III & IV).

3 Methods and materials

3.1 Animal models

3.1.1 Animals

All experiments were approved by the Animal Care and Use Committee at the Norwegian University of Science and Technology (NTNU; Forsøksdyrutvalget) and conducted in accordance with the European Communities Council Directive of 1986 (86/609/EEC). All animals were from Scanbur AS (Nittedal, Norway). Pups were weaned at the age of 4 weeks and animals were kept on a 12:12 hours light: dark cycle with food and water *ad libitum* throughout the experiments.

Paper I: Six Wistar rats mated at the Comparative Medicine Core Facility, NTNU gave birth to six litters of 9 - 14 pups, total n = 60.

Paper II: Time-mated Sprague-Dawley rats gave birth to three litters of 8 - 13 pups, total n = 30.

Paper III: 10 adult Sprague-Dawley rats (~3 months old) and 22 Sprague-Dawley pups were utilized in the experiments.

Paper IV: Sprague-Dawley rats mated at the Comparative Medicine Core Facility, NTNU gave birth to two litters of 8 and 11 pups, total n = 19.

3.1.2 Hypoxia-ischemia

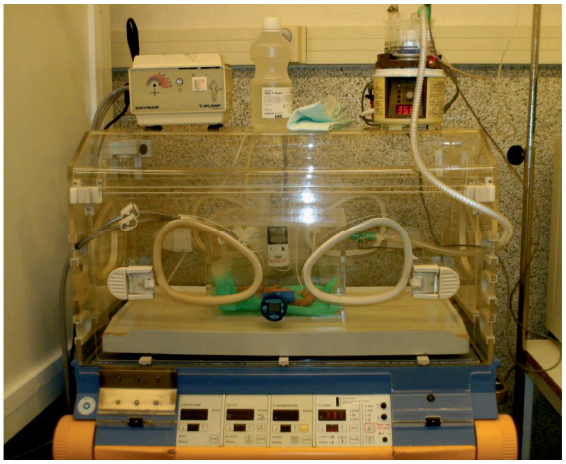

Figure 3 Hypoxia fibreglass box with rat pups inside a neonatal incubator with heated and humidified environment. Animals are atop of a water-heated bed, and the air of the box holds a temperature of 36 ± 0.5 °C. The box is flushed with humidified and heated gas.

The Vannucci model for HI was utilized in papers I & IV (Rice *et al.*, 1981). P7 rats were placed on a water-heated thermal pad (Gaymar Industries Ltd., Orchard Park, NY) and anaesthetized with isoflurane (4% induction, 2% maintenance in O_2; Baxter, Allerød, Denmark). The right common carotid artery was identified, thermo-cauterized and severed. In sham-operated littermates the carotid artery was identified under anaesthesia, but not severed. The pups were returned to their dam for recovery and feeding for minimum two hours and maximum four hours. Thereafter pups were put in a fibreglass box inside an incubator where temperature and oxygen concentrations were constantly monitored and temperature was kept at 36 ± 0.5 °C for the whole period that the pups were in the box (Figure 3). The box was flushed with pre-heated humidified 8% O_2 in 92% N_2 and the oxygen concentration was kept constant for 75 minutes (paper I) or 90 minutes (paper IV). This model creates ischemia of the ipsilateral hemisphere with reduced CBF during hypoxia (Vannucci *et al.*, 1988) that returns to normal levels immediately upon end of hypoxia (Mujsce *et al.*, 1990). Like in the adult rat, severing only the common carotid artery does not produce brain injury (Levine, 1960) which is most likely due to the rich cerebral collateral circulation of the rat (Coyle & Jokelainen, 1982). Immediately after hypoxia ended the box was flushed with either 100% O_2 or room-air (20.9% O_2; paper I). After saturating the box with the desired gas concentration, flow was kept at a minimum during exposure. Four litters (n = 28) were exposed to 100% O_2 and two litters (n = 19) were exposed to room-air for 2 hours. Manganese chloride ($MnCl_2$; # 7773-01-5, Sigma-Aldrich Inc., St. Louis, USA) was given as a single dose (40mg/kg bodyweight) by intraperitoneal (i.p.) injection six hours after hypoxia ended (one litter from each experiment group with sham-operated littermates; n = 20). Animals that did not receive $MnCl_2$ were injected with 0.15 ml of 0.9% NaCl (B. Braun, Melsungen, Germany).

3.1.3 Intermittent hyperoxia-hypoxia

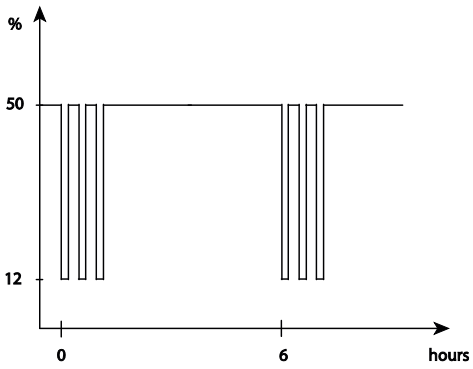

Figure 4 Every sixth hour of hyperoxia (50% O_2) was interrupted by a cluster of three consecutive episodes of hypoxia (12% O_2) 10 minutes apart, each of 2 minutes. This profile was applied continuously from <four hours after birth until postnatal day 14.

An A84 Oxycycler (Biospherix Ltd., Lacona, NY) was used to create a profile of intermittent hyperoxia-hypoxia (IHH) that creates neovascularization, immature vascular bed and retinal haemorrhage in the neonatal rat reminiscent of changes seen in ROP (Coleman *et al.*, 2008). Within four hours after delivery of the last pup, litter and dam were placed in specialized controlled oxygen chambers (A-30524, Biospherix Ltd., New York, USA) in their cages. In the IHH profile, continuous hyperoxia (50% O_2) for 14 days was interrupted every six hours by a cluster of three consecutive two–minute long episodes of hypoxia (12% O_2), each ten minutes apart (Figure 4). The ramp time between hyperoxia and hypoxia was approximately two minutes. Bedding was changed during a 50% cycle on day seven. The chamber was then opened for < three minutes. Inside the chamber, oxygen was controlled via a sensor and a computerized feed-back system where nitrogen was used to lower and oxygen was used to raise the oxygen concentration inside the chamber. CO_2, temperature and relative humidity were continuously monitored and kept within physiological levels via the use of Soda lime (Anmedic AB, Stockholm, Sweden), ventilation and a built-in fan. One group (n = 22) was exposed to IHH while controls (n = 8) were exposed to room-air (20.9% O_2) from P0 to P14. Controls were reared in the same room in an identical controlled oxygen chamber.

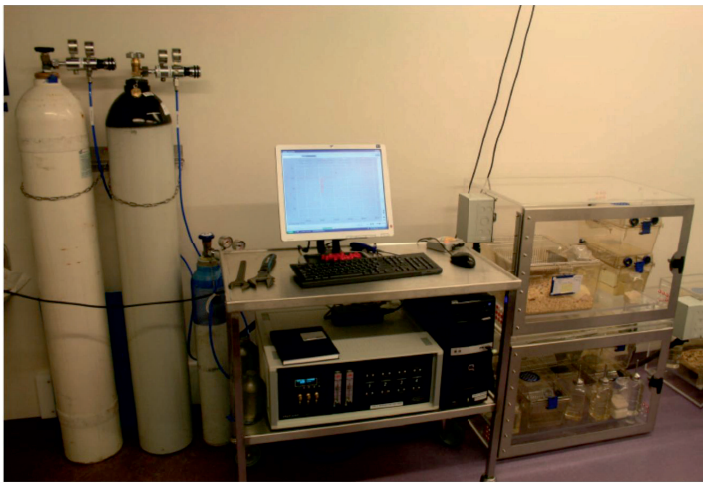

Figure 5 Experimental set-up of the intermittent hyperoxia-hypoxia model with oxygen, nitrogen and calibration gas flasks (left) connected to the computerized Oxycycler (middle) that controls gas delivery into the animal chambers that contain cages with litter and dam (right).

3.2 Histology and Immunohistochemistry

3.2.1 Perfusion-fixation and tissue processing

In papers I & II animals were euthanized by an overdose of pentobarbital (300 mg/kg; Vétoquinol, Lure Cedex, France) and were then perfused via an intracardial injection of 4% paraformaldehyde (PAH; Fluka Chemie AG, Buchs, Switzerland) in phosphate-buffered saline (PBS; Oxoid Limited, Hampshire, UK). Before fixation in formalin, brains were removed while in paper II also eyes were enucleated and the orbita were inspected for gross abnormalities. Thereafter brains and the right eye (paper II) were embedded in paraffin and coronal brain sections, corresponding to –3.25 mm from the bregma (Paxinos & Watson, 2008), and retinal cross-sections were cut at 8 (paper I) or 4 µm (paper II) and mounted onto Super Frost glass (Thermo Fisher Scientific Inc., Waltham, MA*)* for further processing*.* The retina of the left eye (paper II) was dissected and then whole-mounted onto Super Frost object glass.

3.2.2 Immunohistochemistry

Coronal brain and retinal cross-sections were stained with Haematoxylin & Eosin (H&E; Cell Path Ltd., Newtown, UK and Sigma-Aldrich Inc., St. Louis, MO) and examined for morphological changes. Thereafter corresponding sections were incubated with: *Paper I*: anti-ED1-fitc (1:400; Serotec, Raleigh, NC) for CD68-positive microglia, anti-glial fibrillary acidic protein (GFAP; 1:200; Cymbus Biotechnology, Southampton, UK) for reactive astrocytes or anti-cleaved-caspase-3 (1:100; Cell Signaling, Danvers, MA) for apoptosis. Sections were then incubated with rat-anti-FITC-biotin (Roche, Basel, Switzerland), horse-anti-mouse-biotin (Vector Laboratories, Burlingame, CA) or goat-anti-rabbit-biotin (Vector Laboratories Inc.). *Paper 2:* anti-rat-albumin (1:16000) (Nordic Immunology, Eindhoven, the Netherlands) for albumin leakage, Biotinylated *Griffonia (Bandeiraea) Simplicifolia* lectin I Isolectin B4 (1µg/ml) (Vector Laboratories Inc.) for vascular density, anti-glial fibrillary acid protein for astrogliosis and anti-ED1-fitc for activated microglia. Sections were then incubated with labelled polymer HRP anti-rabbit (Dako A/S, Glostrup, Denmark), streptavidin-conjugated FITC (Vector Laboratories Inc.), horse-anti-mouse-biotin (Vector Laboratories Inc.) and rat-anti-FITC-biotin. Visualization was performed using a Vectastain ABC kit (Vector Laboratories Inc.) and a Diaminobenzidine (DAB) kit (Vector Laboratories Inc.). Full section images were captured with a MIRAX MIDI system (Carl Zeiss MicroImaging GmbH, Jena, Germany) and examined. Sections in which the primary immunobody was omitted were blank, and they were used as negative controls. Retinal whole-mounts were incubated with Isolectin B4 (12.5 µg/ml) and thereafter with streptavidin-conjugated FITC, embedded in DEPEX and visualized using a fluorescence-microscope in the FITC channel.

3.2.3 Evaluation of brain sections

In paper I, sections were evaluated semi-quantitatively for the presence of CD-68 or GFAP positive cells in 13 defined regions; parietal cortex divided into six subregions, CA1, CA2, CA3, CA4, dentate gyrus, thalamus and caudate putamen (Grafe *et al.*, 2008). The following scale was used for scoring; 0: no positive cells; 1: <33% of cells in area stained; 2: 33-67% stained to 3: >67% stained. In paper II the presence (score = 1) or not (score = 0) of increased albumin immunoreactivity in the neuropil in the hippocampus, cortex, thalamus and hypothalamus was scored.

Quantitative methods were applied in paper I for caspase-3 immunoreactive cells that were counted in ipsi- and contralateral hemisphere. In paper II vessel density was quantified in three

areas of the cortex (parietal and temporal), thalamus, hippocampus (CA2, CA3 and dentate gyrus) and periventricular white matter at x400 magnification using ImageJ (v1.42q, National Institute of Health, Bethesda, MD) and normalized relative to control.

3.3 MR

3.3.1 MR Imaging

Figure 6 The 7 Tesla magnet (Biospec 70/20) utilized for longitudinal *in vivo* MR imaging of rats with designated animal bed.

In vivo MR imaging was performed on a 7 Tesla magnet (Biospec 70/20 AS, Bruker Biospin MRI, Ettlingen, Germany; Figure 6) with water-cooled (BGA-12, 400 mT/m) gradients. All animals were imaged longitudinally until euthanization. During scanning the anaesthetized (2% isoflurane in 30% O_2/70% N_2) pups lay prone in a dedicated water-heated bed (Bruker Biospin MRI) and the head of every animal was fixated in the same position with tooth-bar, nose-mask and polystyrene. Temperature and respiration were monitored during the scanning procedure. A volume resonator (Bruker Biospin MRI) was used for RF transmission and actively decoupled head surface coils (Rapid Biomedical Gmbh, Rimpar, Germany) were used for RF reception.

Diffusion weighted images (DWI) were obtained using an Echo Planar Imaging (EPI) sequence with six *b*-values (100/200/400/600/800/1000 ms) in three orthogonal directions; echo time (TE) = 37.50 ms; repetition time (TR) = 3000 ms; four averages; field-of-view (FOV) = 25 × 30 mm^2; acquisition matrix (MTX) = 160 × 192; 15 coronal slices á 1mm.

Manganese-enhanced T_1-weighted 3D data sets were obtained using a gradient echo fast low angle shot (FLASH) sequence with flip-angle = 30°; TR = 12ms; TE = 3.0ms; FOV = 25 × 25 × 17.5mm^3, and MTX = 160 × 160 × 112.

T_2-maps were obtained with a turbo spin-echo (RARE) sequence with slightly different parameters in papers I & II: *Paper I:* Effective TE = 25, 75, 125 ms; TR = 4000 ms; RARE-factor = 4; FOV = 25 × 20 mm^2 (day one and seven) 30×20 mm^2 (day 21 and day 42); MTX = 160 × 96 (day one and day seven after HI) and 192 × 96 (day 21 and day 42 after HI) reconstructed to 160 × 128 and 192 × 128 respectively; 15 slices á 1 mm. *Paper II:* Effective TE = 16, 48, 80, 120 ms and TR = 3750 ms; RARE-factor = 4; FOV = 25 x 20 mm^2; MTX = 160 x 96 reconstructed to 164 x 128; 15 slices á 0.75 mm.

DTI was performed with an echo planar imaging (EPI) sequence using 30 directions with the following parametres: *Paper I: b* = 1000 ms; 5 *b*0 images; TE = 40 ms; TR = 3750 ms; FOV = 40 × 49.5 mm^2 ; MTX = 172 × 212; 25 axial slices á 0.5 mm. *Paper II: b* = 1000 ms; 5 *b*0 images and TE = 32; TR = 3750 ms; FOV = 25 x 25 mm^2; MTX = 128 x 128 and 15 coronal slices á 0.75 mm.

3.3.2 MR image data analyses

From the DWI, ADC maps were calculated by fitting a mono-exponential model to the signal intensity of the images with different *b*-values. Regions-of-interest (ROI) were drawn in parasagittal cortex, thalamus, hippocampus and basal ganglia in one slice corresponding to -3.25 mm from the bregma (Paxinos & Watson, 2008) and the mean ADC in each ROI was calculated (for placement of ROI, see Figure 7). ADC maps were also utilized for qualitative scoring of injury severity on day I.

On the T_1 weighted 3D image stacks, manganese-enhanced areas in the ipsilateral hemisphere were defined as those having higher signal intensity than the corresponding contralateral area. Areas of manganese-enhancement were manually drawn in each relevant image slice and the manganese-enhanced volumes were calculated.

T_2-maps were calculated by fitting a mono-exponential model to the images with different TE in all the voxels creating a parametric map giving the actual T_2 in the voxels in msec using in-house developed software (MATLAB ver. R2010a, Math Works Inc, Natick, MA). Thereafter T_2 -maps were imported to ImageJ, and the area of the remaining brain tissue in each hemisphere and porencephalic cysts (paper I) and of the whole brain (paper II) were drawn manually in each slice using a Wacom© pen-tablet LCD-screen. Volumes were then calculated by adding the areas in the stack and multiplying with the slice thickness (paper I & II). Furthermore, the actual T_2-relaxation time was measured in ROI that were drawn in the parasagittal cortex, thalamus, hippocampus and putamen in two slices corresponding to –3.25 and –1.5 mm from the bregma (Figure 7a & b).

DTI analyses were performed with the tools of the FMRIB software library (FSL ver 4.1.4, Oxford Centre for Functional MRI of the Brain, UK; Hwww.fmrib.ox.ac.uk/fslH).

Images were pre-processed to reduce image artifacts due to motion and eddy current distortions by affine transformation and co-registration of the diffusion-encoded images to the *b*0 images. Brains were segmented out using the Brain Extraction Tool before FDT ver 2.0 (FMRIB's Diffusion Toolbox; both part of FSL) was used to fit a voxelwise diffusion tensor model to the diffusion image data. Maps for the fractional anisotropy (FA), radial ($\lambda_\perp$), mean (MD) and axial ($\lambda_\parallel$) diffusivity were created. ROI were manually drawn in the centre of white matter structures at all relevant image slices on the FA-maps (Figure 7 c & d). In paper I these were combined to three volumes of interest (VOI) that

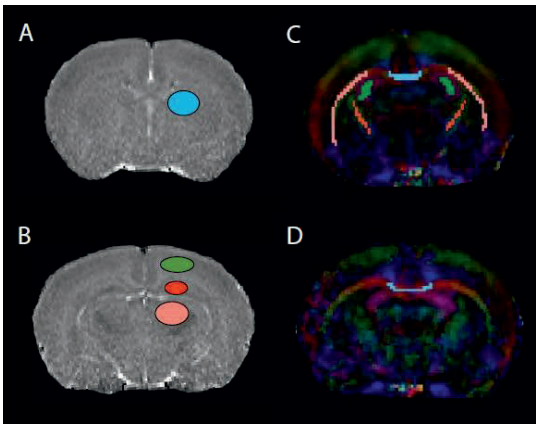

Figure 7 (a) T_2-map corresponding to –1.5 mm from the bregma with regions of interest (ROI) marked in putamen (blue). (b) T_2 -map corresponding to –3.25 mm from the bregma with ROI in parasagittal cortex (green), hippocampus (red) and thalamus (pink). (c) Colour-encoded directional FA-maps from postnatal day 14 (c) and 28 (d) with ROI in corpus callosum (blue), hippocampal fimbriae (green), internal capsule (red) and external capsule (pink). The ROI in corpus callosum encompassed three slices anterior and three posterior to the one shown. The ROI in hippocampal fimbriae, external and internal capsule encompassed two posterior to the one shown.

were used in the analyses: corpus callosum (comprising the genu, body and splenium), contralateral major white matter structures (external capsule, internal capsule, hippocampal fimbriae and cingulum). Due to severe tissue loss ROIs were not drawn in ipsilateral white matter. ROI were also placed in the contralateral caudate putamen. In paper II ROIs were combined to five VOI at P14: corpus callosum (body), external capsule, internal capsule, hippocampal fimbriae and total white matter (comprising all of the aforementioned areas). Due to low signal-to-noise (SNR) in the deeper brain structures in the DWI on P28, masks were only drawn in the body of the corpus callosum where SNR was adequate for robust calculations of DTI metrics at this time-point. Mean FA, radial, axial and mean diffusivity were calculated in each of these volumes of interest in each animal.

3.3.3 Administration of [^{13}C]glucose and [^{13}C]acetate

In paper III, metabolism under physiological conditions was studied, and pups were left undisturbed with their dam from birth until i.p. injection with ^{13}C-labelled substrates at P7. Pups were injected with [1-^{13}C]glucose (543 mg/kg, 0.3M; 99% ^{13}C enriched; Cambridge Isotope Laboratories, Woburn, MA) and [1,2-^{13}C]acetate (504 mg/kg, 0.6M; 99% ^{13}C enriched; Cambridge Isotope Laboratories) and decapitated 5, 10, 15, 30 and 45 minutes after injection (n= 3 - 4 at each time-point). One group of P7 rats (n = 4) was injected with [1,2-^{13}C]glucose (564 mg/kg, 0.3M; 99% ^{13}C enriched; Cambridge Isotope Laboratories) and decapitated after 30 minutes. In separate experiments, adult rats were injected i.p. with [1-^{13}C]glucose and [1,2-^{13}C]acetate and decapitated after 15 minutes. Heads were snap-frozen in liquid N_2 and stored at −80°C until extraction. In paper IV, following the HI (n = 10) or sham-procedure (n = 9) described above, pups were allowed to recover for 30 minutes with their dam before i.p. administration of [1,2-^{13}C]glucose (564 mg/kg, 0.3M) and decapitation after 30 minutes. After injections all pups were kept separate from their dam in a heated environment of 36 ± 0.5 °C until decapitation. Heads were snap-frozen in liquid nitrogen (N_2) and stored at −80°C until extraction.

3.3.4 Dissection and extraction of brain tissue

In paper III entire cerebri (P7) and cortex cerebri (adults) were dissected for extraction while in paper IV the ipsilateral and contralateral hemisphere of the cerebrum was dissected separately. Tissue was thereafter extracted using either methanol-chloroform or perchloric acid (PCA; paper I: 5-15 minute injection time in P7 animals and in adults). 7% PCA was added and tissue was homogenized using a Vibra Cell sonicator (Model VCX 750, Sonics & Materials, Newtown, CT). The homogenates were centrifuged at 3000*g* at 4°C for 5 minutes. The neutralized supernatants were lyophilized and re-suspended in D_2O (99.9%; CDN Isotopes, Pointe-Claire, Canada) before being lyophilized once more in order to minimize the proton content of water. When methanol-chloroform extraction was applied, methanol was added and tissue was homogenized using the same sonicator. Subsequently, chloroform and water were added, the samples were centrifuged at 3000*g* for 15 minutes, and the supernatants were transferred to a new tube. Following that, the procedure was repeated once more, using only water in order to separate the lipids from the supernatant with the cellular extracts. Finally, the supernatants were transferred to a third tube, lyophilized, and re-suspended in D_2O. At this point, a proportion was taken out for analysis with high performance liquid chromatography (HPLC; paper IV) before the remaining sample was lyophilized once more in order to minimize the proton content of water before analysis with MR spectroscopy.

3.3.5 ^{13}C- and ^{1}H-MR spectroscopy

Lyophilized samples were dissolved in 400 µl (paper III) or 120 µl (paper IV) D_2O containing 0.01% ethylene glycol (Acros Organics, Geel, Belgium) and 0.018% 3-(trimethylsilyl)-1-propane-sulfonic acid (DSS; Sigma-Aldrich, St. Louis, MA). The supernatants were transferred to SampleJet tubes (5.0 x 103.5 mm or 3.0 x 103.5 mm, respectively) for insertion into the SampleJet autosampler (Bruker BioSpin GmbH, Rheinstetten, Germany). All samples were analyzed on a 14.1 Tesla Ultrashielded Plus Avance III magnet (Bruker BioSpin GmbH) operating at 600 MHz (for ^{1}H) using a QCI CryoProbe™. ^{1}H-MR spectra were accumulated with a pulse angle of 90°, acquisition time was 2.7 s and relaxation delay was 10 s. The number of scans was 32 or 128, respectively. Proton decoupled ^{13}C MR spectra were obtained on the same spectrometer using an acquisition time of 1.7 s, a relaxation delay of 0.5 s and a flip angle of 30°. Scans were accumulated at 30 kHz spectral width with 98 K data points. The number of scans in paper III and IV was typically 2400 or 11000, respectively.

3.3.6 Post processing of MR spectroscopy data

Relevant peaks in the spectra were identified and integrated using TopSpin™ 3.0 software (Bruker BioSpin GmbH). Concentrations of metabolites were calculated from the integrals of the peaks using DSS (^{1}H-MR spectra) or ethylene glycol (^{13}C-MR spectra) as internal standards. Concentrations from the ^{1}H-MR spectra were corrected for the numbers of protons that constituted the peak.

The singlets in the ^{13}C MR data were corrected for naturally abundant ^{13}C by subtracting 1.1 % of the total cellular contents obtained from ^{1}H spectra. % ^{13}C excess enrichment was calculated after subtracting natural abundance of ^{13}C, and was referred to as % enrichment. All peaks were corrected for tissue weight. If a ^{13}C nucleus is coupled to another ^{13}C nucleus, i.e. when there are two ^{13}C in a molecule, homonuclear spin-spin coupling, also known as J-J coupling, will cause splitting of peaks in the carbon spectra. The probability of this to occur naturally is very low (0.01%). Therefore these peaks represent enrichment with ^{13}C in the compound in question in the studies presented here.

Depending on the pulse sequence used to obtain the ^{13}C-MR spectrum there can also be splitting of peaks due to heteronuclear spin-spin coupling between neighbouring ^{1}H and ^{13}C nuclei which is caused by the two energy states of the ^{1}H population. To avoid this, one may eliminate the ΔE between these two populations by irradiating the ^{1}H frequency with a weak RF-pulse during acquisition in what is called a proton decoupling. The ^{13}C peaks will then appear as singlets since the protons are impaired from interacting with the ^{13}C nuclei or from releasing energy into its surroundings. This only happens between nuclei that are in close proximity, e.g. in protons that are covalently bound to a ^{13}C nucleus. However, if the proton decoupling is carried out constantly, the addition of energy to the ^{13}C atoms will cause enhancement of the ^{13}C signal in what is termed the Nuclear Overhauser Effect (NOE), and this signal enhancement needs to be corrected for. Furthermore, to obtain full T_1-relaxation one must wait 5* T_1 of the longest T_1 in the sample or tissue. Since the signal in ^{13}C is small one needs to scan many times, and such a long relaxation delay (TR) is not possible for all nuclei, especially not for the carboxylic acid groups with long T_1. This relative loss of amplitude in the T_1 signal must be corrected for to be able to measure absolute quantities. Since we used a short relaxation delay of 0.5 sec in a ^{13}C sequence, full relaxation of all the spins was not achieved at the time of the new RF-pulse. Combined correction factors for T_1 and NOE can be obtained via the comparison of spectra with constant proton decoupling and short relaxation delay (our normal experiment) to a spectrum in which proton decoupling was just done shortly

before sampling of the signal and the relaxation delay was long enough to allow for full relaxation of the nuclei used in the study. After calibration of the reference compound ethylene glycole, integrals from the fully relaxed spectra were divided by the respective integrals from the proton-decoupled spectra with short relaxation delay. The resulting correction factors for incomplete T_1-relaxation and Nuclear Overhauser Effects (NOE) in the ^{13}C spectra were later applied to the integration values of all metabolites in the ^{13}C MR spectra of all samples.

3.4 High-Performance Liquid Chromatography

Amino acids in brain extracts were quantified by HPLC on a 1200 system (Agilent Technologies, Palo Alto, CA). The amino acids were pre-column derivatized with *o*-phthaldialdehyde (Geddes & Wood, 1984) and components were subsequently separated on a ZORBAX SB-C18 (4.6 × 150 mm, 3.5 µm) column from Agilent using a phosphate buffer (50 mM, pH = 5.9) and a solution of methanol (98.75 %) and tetrahydrofurane (1.25 %) as eluents. α-Amino butyric acid (α-ABA) was used as internal standard. The separated amino acids were detected with fluorescence and quantified by comparison to a standard curve derived from standard solutions of amino acids. All amounts were corrected for tissue weight.

3.5 Statistics

Statistical analyses were performed in SPSS 16 (SPSS Inc., Chicago, IL) and STATA 10 (Stata Corp, College Station, TX) and a two-sided *p*-value of < 0.05 was considered significant. Depending on the number of the groups, Student's *t*-test or ANOVA followed by *post hoc* tests with Bonferroni correction were applied to test for differences between experiment groups, while paired *t*-tests were applied to test for differences between time-points. When data were not considered to have a normal distribution, non-parametric tests were applied. In paper I data were analyzed at each time-point with linear mixed models with experiment group as fixed effect and litter as random effect, measuring the effect of the fixed effects (experiment groups) taking into account random effects (litters).

4 Synopsis of papers

Paper I

Longitudinal diffusion tensor and manganese–enhanced MRI detect delayed cerebral grey and white matter injury after hypoxia-ischemia and hyperoxia

Tora Sund Morken, Marius Widerøe, Christina Vogt, Stian Lydersen, Marianne Havnes, Jon Skranes, Pål Erik Goa, Ann-Mari Brubakk. *Pediatric Research (2013) 73: 171-179.*

The aim of this study was to evaluate the possible difference in long-term development of injury after hypoxia-ischemia (HI) and exposure to hyperoxia (100% O_2) or room-air (20.9% O_2) via multimodal MRI and immunohistochemistry.

HI was induced in seven days old rats and was followed by two hours of either hyperoxia or room-air exposure. Six hours after HI animals were injected i.p. with $MnCl_2$ for later manganese-enhanced MRI. Thereafter an *in vivo* multimodal MRI study of injury development until near-adult age at 42 days after HI was performed at 7 Tesla. Apparent Diffusion Coefficient (ADC)-maps were acquired at day one, T_1-weighted manganese-enhanced images at day seven, Diffusion tensor images (DTI) at day 21 and 42 and T_2-maps at all time-points.

The long-term brain tissue destruction on T_2-maps was more severe in HI+hyperoxia than HI+room-air. ADC was lower in HI+hyperoxia versus HI+room-air and sham, and was positively correlated with long-term tissue destruction. Manganese-enhancement indicating inflammation was seen in both groups along with more microglial activation in HI+hyperoxia on day seven. Fractional anisotropy (FA) in corpus callosum was lower and radial diffusivity higher in HI+hyperoxia than HI+room-air and sham on day 21. From day 21 to day 42 FA and radial diffusivity in HI+hyperoxia was unchanged, while in HI+room-air FA increased and radial diffusivity decreased to values similar to sham.

In this study we found that HI+hyperoxia induced irreversible white matter injury and caused a progressively increasing long-term tissue destruction compared to exposure to room-air after HI.

Paper II

Brain development after neonatal intermittent hyperoxia-hypoxia in the rat studied by longitudinal MRI and immunohistochemistry

Tora Sund Morken, Axel Nyman, Ioanna Sandvig, Sverre Torp, Jon Skranes, Pål Erik Goa, Ann-Mari Brubakk, Marius Widerøe. *Accepted for publication in PLoS One*

The aim of this study was to evaluate whether an exposure of fluctuating oxygen levels that create retinopathy in the neonatal rat would also induce pathological changes in brain development long-term.

To this end rat pups with their dam were reared continuously in intermittent hyperoxia-hypoxia (IHH) from birth until postnatal day 14. IHH was induced by exposure to hyperoxia (50% O_2) that was interrupted by three consecutive two-minute episodes of hypoxia

(12% O_2) every sixth hour. Controls were reared in room-air. Thereafter longitudinal *in vivo* MRI (Diffusion Tensor Imaging and T_2-mapping) was performed on postnatal days 14 and 28, and retinal and brain tissue were examined for histopathological changes.

Mean, radial and axial diffusivity were higher in white matter of IHH versus controls at postnatal day 14, while fractional anisotropy (FA) was lower in the hippocampal fimbria and tended to be lower in corpus callosum and external capsule. White matter diffusivity in IHH was similar to controls at postnatal day 28. Higher cortical vessel density was observed at postnatal day 14. Cortical and thalamic T_2-relaxation time was higher in the IHH group at postnatal day 14, and albumin leakage was present at postnatal day 28. Rats in the IHH group ran for a longer time on a Rotarod than the control group. Pups with lower bodyweight had more severe MRI alterations and albumin leakage.

In this study we found that IHH had reversible effects on brain white matter diffusivity, grey matter water content and vascular density while alterations in BBB permeability were long-term. Furthermore the study may indicate that lower bodyweight may interact with effects of IHH.

Paper III

Neuron-astrocyte interactions, pyruvate carboxylation and the pentose phosphate pathway in the neonatal rat brain

Tora Sund Morken, Eva Brekke, Asta Håberg, Marius Widerøe, Ann-Mari Brubakk, Ursula Sonnewald. *Neurochemical Research (2013) Mar 16 [Epub ahead of print]*

The aim of this study was to investigate glucose and acetate metabolism and the synthesis of amino acid neurotransmitters in neonatal vs. adult rat brain. Furthermore we wanted to study pyruvate carboxylation and the pentose phosphate pathway (PPP) in the neonatal brain.

To this end postnatal day 7 rats were injected i.p. with [1-^{13}C]glucose and [1,2-^{13}C]acetate and euthanized 5, 10, 15, 30 and 45 minutes later. Adult rats were injected with the same substrates and euthanized after 15 minutes. To analyze pyruvate carboxylation and PPP activity during development, postnatal day 7 rats received [1,2-^{13}C]glucose and were euthanized 30 minutes later. Thereafter brain extracts were analyzed via ^{1}H- and ^{13}C-MR spectroscopy.

Numerous differences were found between the neonatal and adult brain. The neonatal brain contained lower levels of glutamate, aspartate and *N*-acetylaspartate, but similar levels of GABA and glutamine. Metabolism of [1-^{13}C]glucose at the acetyl CoA stage was reduced much more than that of [1,2-^{13}C]acetate. The transfer of glutamate from neurons to astrocytes was much lower, while transfer of glutamine from astrocytes to glutamatergic neurons was relatively higher. However, transfer of glutamine from astrocytes to GABAergic neurons was lower. Using [1,2-^{13}C]glucose it could be shown that despite much lower pyruvate carboxylation, relatively more pyruvate from glycolysis was directed towards anaplerosis than pyruvate dehydrogenation in astrocytes in the neonatal brain compared to in adults. Moreover, the ratio of PPP/glucose metabolism was higher than in adult reports.

This study indicated that the glutamate-glutamine cycle works in favour of transfer of substrate from astrocyte to neuron early in brain development and that, compared to in adults, the activity of the PPP and pyruvate carboxylation pathways are relatively high.

Paper IV

The pentose phosphate pathway and pyruvate carboxylation after neonatal hypoxic-ischemic brain injury

Eva Brekke, Tora Sund Morken, Marius Widerøe, Asta Håberg, Ann-Mari Brubakk, Ursula Sonnewald. *Submitted to Journal of Cerebral Blood Flow & Metabolism*

The aim of this study was to evaluate pyruvate carboxylation and the pentose phosphate pathway (PPP) in the immediate recovery phase following hypoxia-ischemia (HI) in the neonatal rat brain.

To this end postnatal day 7 rats were subjected to HI or sham-operated and injected with [1,2-^{13}C]glucose. Rats were euthanized 60 minutes after HI ended, and extracts of ipsi- and contralateral cerebral hemispheres were analyzed separately via ^{1}H- and ^{13}C-MR spectroscopy and HPLC.

After HI, glucose levels were increased and there was evidence of mitochondrial hypometabolism in both hemispheres. The labelling via PPP as well as labelling following PDH and PC was reduced in both hemispheres. However, the ratio of PC vs. PDH was preserved and even increased in glutamate.

In this study we demonstrated that following an insult like HI, the activity of the PPP was reduced, and that in the early recovery phase following HI, a period of ongoing excitotoxicity, pyruvate carboxylation and thereby *de novo* synthesis of glutamate was relatively preserved.

5 Discussion

5.1 Methodological considerations

5.1.1 How well is preterm brain injury reproduced in neonatal rat models?

A central assumption in this thesis is that the neonatal rat brain is relevant for studies of early human brain development and injury. In this context it is of importance to consider the similarities and differences in normal development between these species. Although the human newborn infant is highly dependent on its mother for an extended period of time compared to other species, most neural events occur *in utero*, and the human brain at birth is complex and advanced. This is illustrated by how the human newborn can interact with and learn from its surroundings in sophisticated ways; for instance, at birth the human newborn can recognize its mother's voice (Beauchemin *et al.*, 2011) and syllables from her mother tongue (Moon *et al.*, 2013) as well as the mother's face (Field *et al.*, 1984). The advanced stage of the human brain at birth is in contrast to the rat that is born immature with many major neural events occurring in the postnatal period. Furthermore, the rat brain remains lissencephalic throughout life, while the newborn human brain has a complex gyrencephalic structure causing a large cortical surface area (White *et al.*, 2010), and events that span weeks and months in humans happen over a few days in rat. Nevertheless, animal models remain highly valuable despite such inter-species differences since they create the opportunity to study aspects of brain development and injury *in vivo* as opposed to *in vitro* or in patients.

The Vannucci model of HI in the P7 rat (Rice *et al.*, 1981) is well-described, reproducible, cost-efficient and relatively simple to prepare. However, regarding the relevance of the model to preterm brain injury in humans, one must consider whether the P7 rat may be likened to a specific time-point in human brain development, whether the injury pattern that arise after HI reproduce features of the modelled condition in humans (face validity) and whether the factor that induce injury in the model is similar to the theoretical cause in the modelled condition (causative validity).

Regarding the comparison of the P7 rat to a specific time-point in human brain development, it has been common in the literature to liken the P7 rat brain to a late-preterm newborn of GW 32-34, while P10 has been compared to the term infant and P3 to GW 22-25. This is because of histological similarities (Vannucci & Vannucci, 2005), the stage of oligodendroglial differentiation (Back *et al.*, 2001; Craig *et al.*, 2003) and the timing of the brain growth spurt (Dobbing & Sands, 1979). Pre-OLs dominate at P2 - P5 (Dean *et al.*, 2011) while by P7 OL^+ dominate and myelination begins, making the P7 rat comparable to GW 32-34 in humans with regards to oligodendroglial maturation. By P10 mature oligodendrocytes (OLs) are in abundance such as in the term human infant (reviewed by Volpe (2009)). However, this is an oversimplification that can be debated, not the least because of the reasons listed above. Also, glutamatergic receptors peak later in the rat than in humans; making a P7 rat comparable to GW 24 in humans in that sense (Tremblay *et al.*, 1988; Represa *et al.*, 1989). Furthermore, the switch from neurogenesis to gliogenesis occurs at mid-gestation in humans vs. at birth in the rat (Vaccarino *et al.*, 2007) and synaptogenesis occurs from birth and during the first 2-3 postnatal weeks in rat vs. from GW 20 and through the first years of life in humans (Semple *et al.*, 2013).

The injury pattern following HI in the P7 rat in this thesis was a mixture of both long-term grey and white matter tissue destruction, susceptibility of the hippocampal and basal ganglia areas, hypotrophic longitudinal growth of the ipsi- and contralateral brain hemispheres and alterations in white matter diffusivity. Preterm encephalopathy is dominated by white matter injury while brain injury following term-born asphyxia mainly affects grey matter. However, also in the preterm brain is white matter injury accompanied by grey matter neuronal loss (Volpe, 2005; Leviton & Gressens, 2007; Volpe, 2009), as mentioned earlier, and areas of increased susceptibility in the term brain like the basal ganglia and thalamus (Sie *et al.*, 2000) are also involved in preterm brain injury (Volpe, 2009). When white matter injury is seen in term infants it is thought to be the result of a more subacute injury of repeated hypoxia *in utero* that thus has happened at an earlier time-point (Sie *et al.*, 2000). Furthermore, cyst formation in the most severe forms of preterm brain injury is rare nowadays, but does still occur. In this thesis there was disintegration of ipsilateral brain tissue and development of a porencephalic cyst following HI reminiscent of such cyst formation. The presence and distribution of such porencephalic cysts were markers of the most severe response to HI, in line with earlier reports (Towfighi *et al.*, 1991; Ten *et al.*, 2004). As a conclusion, the injury pattern in the Vannucci model at P7 share characteristics with both term (increased susceptibility of hippocampal, basal ganglia and thalamic areas) and preterm brain injury (white matter areas accompanied by grey matter loss and cyst formation) (Volpe, 2009) and may have relevance (face validity) for injury at both these developmental time-points in the human brain.

Regarding the causative validity of the model, both hypoxia and also ischemia, or compromised cerebral blood supply, are thought to be important in the development of preterm encephalopathy. It has been proposed that insufficient oxygen supply in the water-shed areas or variation in blood pressure outside of the short autoregulatory plateau of the circulation in the preterm brain may lead to ischemia of the periventricular zone. In the Vannucci model, carotid artery severing and subsequent hypoxia compromise ipsilateral CBF resulting in ischemia (Vannucci *et al.*, 1988) and thereby mimick the potential ischemic component in the pathogenesis of preterm brain injury.

5.1.2 Did mode of euthanization affect the metabolite levels and labelling?

MR *ex vivo* spectroscopy should ideally be a “snap-shot” of the brain metabolites at the time of death and should not reflect post mortem metabolism. Micro-wave fixation is superior for fast euthanization (Beaver *et al.*, 2001) and in the preservation of metabolites due to fast degradation of enzymes and thus rapid arrest of all cerebral metabolic processes (Rabin *et al.*, 1997). Our laboratory did not have suitable equipment for micro-wave fixation of neonatal animals at the time experiments were performed. However, results from this thesis indicate that also decapitation as the mode of euthanization with subsequent snap-freezing in N_2 to preserve metabolites stopped metabolism quickly in the P7 rat. The clearest indication of this was the occasional finding of phosphocreatine in ^{1}H-spectra (unpublished results). Phosphocreatine is a high-energy phosphate that is rapidly depleted following death, and its presence therefore indicate rapid arrest of cerebral metabolic processes. It is probable that because of the small size of the P7 rat head the whole brain was nearly instantly frozen, contrasting the much larger adult brain with thicker skull bone where brain tissue most likely does not freeze as rapidly. ATP-independent processes like anaerobic glycolysis may continue post mortem and cause lactate to increase post mortem e.g. during thawing for tissue extraction. However, lactate levels in papers III & IV were comparable to levels measured by *in*

vivo MR spectroscopy (Tkac *et al.*, 2003), indicating that thawing did not cause a major continuation of such ATP-independent processes.

5.1.3 What is the optimal time frame for studying P7 brain metabolism?

Several kinetic studies from the adult rat brain exist (Kanamatsu & Tsukada, 1994; Hassel *et al.*, 1995; Kanamatsu & Tsukada, 1999), while I am unaware of similar studies in the P7 rat. In a study by Cruz et al. (1998), [1,2-^{13}C]acetate was injected into P7 rats, but no details were given about labelling other than that related to pyruvate recycling. Thus in paper III the time-course of ^{13}C-labelling of metabolites after i.p. injection of [1-^{13}C]glucose and [1,2-^{13}C]acetate in the P7 rat was investigated to determine the ideal time-point for euthanization. In adult rats 15 minutes injection time was chosen due to information from the references cited above and from our own kinetic studies (unpublished results), in which there was clear labelling from the 1st and 2nd turns of the TCA cycle after 15 minutes. Labelling from the 1st and 2nd turns of the TCA cycle is necessary for detailed interpretation of results. The ideal time-interval between injection and euthanization should be to the left of the plateau of rise in amount of ^{13}C-labelled isotopomers downstream from glucose metabolism when there is still supply of [^{13}C]glucose without wash-out of label and extensive 2nd turn labelling. Excessive labelling from further turns appearing after longer time-intervals make interpretation of labelling from [^{13}C]glucose and [^{13}C]acetate impossible due to peak overlap. The equivalent time-point to 15 minutes in adults was 30 minutes in the P7 rats, and this injection time was subsequently implemented in paper IV.

5.1.4 The impact of sham-operation on brain metabolism

Sham-operated litter-mates are considered the gold standard for control animals in experimental studies since they correct for factors that one do not want to measure the effect of. In this thesis such factors were the litter-effect, isoflurane exposure, isolation of the carotid artery and handling during the HI procedure, *in vivo* MR scanning and euthanization. Since animals in paper III were undisturbed prior to injection of ^{13}C-labelled substrate and decapitation, comparisons can be made between these and sham-operated animals from paper IV to investigate possible contributions of the sham-procedure to changes in brain metabolism. In addition to the above mentioned factors may differences between sham-operated animals and animals under physiological conditions also arise from the separation from the dam during the time HI-operated littermates were subject to hypoxia (90 minutes).

In paper IV both amounts and % enrichment of 1st turn metabolites derived from [1,2-^{13}C]glucose in glutamate, glutamine, GABA and aspartate were higher in shams than in animals from paper III, except % enrichment in [4,5-^{13}C]glutamate (paper IV: 4.8 ± 1.2 % vs. paper III: 3.4 ± 0.8 % , p = 0.09). Therefore, this may indicate that brain metabolism of glucose was increased in sham animals. Nevertheless, when comparing the PC/pyruvate metabolism ratio (Eq. 7, paper III) it was similar in shams in paper IV (0.16 ± 0.02) and in animals from paper III (0.15 ± 0.02, p = 0.3). Thus, the relative level of anaplerosis was not altered in sham-animals. Furthermore PPP/glucose metabolism ratio was lower in shams than in animals in physiological conditions (paper III: 12.8 ± 1.5 % vs. paper IV: 6.3 ± 1.7 %, p < 0.001).

The conclusion is that the brain metabolism in sham-animals did differ from animals under physiological conditions in papers III & IV. Even though the cause for this difference cannot be determined from the present experiments, these results confirm that sham-operated litter-mates should be the gold-standard for controls also in metabolic studies of HI.

5.2 Major findings

5.2.1 What can be learned about the role of oxygen in perinatal brain injury from this thesis and from earlier studies?

In this thesis, two models of hyperoxia exposure were explored: early and short exposure following HI at P7 (paper I) and long-term fluctuating oxygen levels between hyperoxia and hypoxia from birth until P14 (paper II). It may be argued that the former paradigm may be more relevant to acute treatment with O_2 following neonatal HI while the latter is more relevant for the long-term treatment of an infant in need of long-term O_2 treatment during intensive care and that experience apnoeic attacks.

Regarding paper I, several meta-analysis and systematic reviews have found that 100% O_2 during resuscitation following birth asphyxia in term born infants increase mortality (Davis *et al.*, 2004; Rabi *et al.*, 2007; Saugstad *et al.*, 2008) and that there is a trend of reduced risk for hypoxic-ischemic encephalopathy following resuscitation with room-air (Saugstad *et al.*, 2008). Furthermore, healthy term-born infants breathing room-air utilize 8 minutes to achieve a O_2-saturation above 90% (Rabi *et al.*, 2006), suggesting that it may be unphysiological for newborns, coming from the lower oxygen tension *in utero* to rapidly achieve a high O_2-saturation. Reflecting the mounting evidence for an injurious effects of resuscitation with 100% O_2, the most recent guidelines from the International Liaison Committee on Resuscitation (ILCOR) state that resuscitation should start with room-air (21% O_2) rather than 100% O_2 in term-born infants (Perlman *et al.*, 2010). However, these guidelines do not conclude on therapy aims for preterms, making paper I highly relevant since, as discussed earlier, the developmental stage of the P7 rat brain may be likened to that of a late-preterm infant. However, regarding the translational value of the paradigm in paper I, several issues must be considered:

First, the rat pups are not newborns, but have lived for seven days after birth. Thus their respiratory and circulatory system have been adapted to an *ex utero* environment, and importantly they are adapted to the higher O_2 tension versus the *in utero* environment. Furthermore they have also established metabolism suitable for the high fat diet of maternal milk. Secondly, since cardiac or respiratory arrest is not part of the model, the animals are not *resuscitated* as such, but only *exposed* to high oxygen levels inside a fibreglass box. One may therefore argue that the paradigm in Paper I merely models HI with subsequent hyperoxia *exposure*. Thirdly, the animals are spontaneously breathing and hyperventilating during hypoxia and therefore get hypocapnic (Vannucci *et al.*, 1995), contrasting a clinical situation of birth asphyxia where the infant is usually *hyper*capnic due to respiratory problems. A refinement of the Vannucci model to make it more similar to a clinical situation of birth asphyxia would have been to add CO_2 during hypoxia. This has earlier been done by Vannucci et al. (1997) in a study where the authors found that hypercapnia restores CBF more rapidly than hypocapnia. Finally, animals were exposed to two hours of hyperoxia following HI. The rationale for this was to be able to demonstrate an effect on trajectories of grey and white matter injury development. However, this rather long exposure to a high concentration of O_2 does not translate directly to a clinical setting in which exposure is typically repeated, shorter, and fluctuating between low and high concentrations. The addition of experiment groups with shorter and lower levels of hyperoxia would have added information of a possible dose-dependent relationship in the development of anatomical injury after HI. Such a relationship for markers of injury following resuscitation with increasing levels of O_2 has earlier

been found e.g. in a piglet model of hypoxemia in the liver (Solberg *et al.*, 2010) and in urinary markers of oxidative injury to DNA (Solberg *et al.*, 2007).

In paper I, exposure to hyperoxia after HI led to more severe longitudinal tissue destruction as demonstrated by the more pronounced brain tissue loss and larger porencephalic cysts in HI+hyperoxia than HI+room-air long-term. Furthermore, white matter alterations seemed to be reversible in HI+room-air while there was no normalization of DTI metrics in the HI+hyperoxia group, indicating an irreversible effect on white matter diffusivity. There seem to be increasing evidence for the negative effects of hyperoxia on the outcome after a preceding insult to the brain. Nevertheless, the progressively larger injury long-term in HI+hyperoxia vs. HI+room-air shown in paper I has to my knowledge not earlier been reported. Alterations in white matter diffusivity was also found by Bockhorst et al. (2010) in a study utilizing a similar paradigm as in paper I with long-term multimodal MRI, although with follow-up only until P28. A frequently cited study by Shimabuku et al. (2005) found a higher frequency of cortical damage in P7 rats exposed to 100% O_2 for 24 hours after HI at one week follow-up, although 24 hours exposure represents a dramatically more severe exposure than what is relevant in the clinic. However, mice exposed to as little as 30 min of 100% O_2 post-HI had disrupted myelination and deficits in motor testing after four weeks (Koch *et al.*, 2008). It has also been reported that a moderately *hypoxic* exposure after HI in P10 mice is beneficial, via a proposed mechanism of limiting ROS generation from the mitochondria upon reperfusion (Niatsetskaya *et al.*, 2011). In that study an increased CBF during reperfusion was found following post-HI exposure to 100% O_2, contrasting a study by Fabian et al. (2008) that found a decreased CBF in P7 rats exposed to in HI. Reduced CBF following hyperoxia has also been demonstrated in preterm born infants (Lundstrom *et al.*, 1995). Beneficial effects or no-effects of hyperoxia have also been reported (Presti *et al.*, 2006; Grafe *et al.*, 2008), although less frequently. Calvert et al. (2007) report that oxygen exposure attenuates the energy deficit after an HI-insult and decreases brain damage. Furthermore, Bagenholm et al. (1996) was not able to demonstrate any difference in brain weight between animals exposed to oxygen versus room-air one week after insult.

In paper II a different paradigm of oxygen exposure was explored, namely long-term fluctuations between hyperoxic and hypoxic levels during the two first postnatal weeks in rat. As mentioned, this may be a relevant paradigm to model a sick preterm infant in need of long-term intensive care, since they are often in need of extra oxygen that, in combination with apnoeic episodes, creates large fluctuations in oxygen levels. In ROP immature vessel growth is inhibited by high oxygen levels. This is followed by hypersecretion of VEGF due to tissue hypoxia and ensuing retinal neovascularization (Hartnett & Penn, 2012). It seems that the avoidance of large fluctuations in oxygen levels is important in preventing ROP (Penn *et al.*, 1993; Penn *et al.*, 1995; Di Fiore *et al.*, 1996; Di Fiore *et al.*, 2012), and it has been proposed that similar fluctuations may also adversely influence brain development (Martin *et al.*, 2011). However, data on the influence of such fluctuations on brain development are scarce. An interesting model that reproduces ROP in neonatal rats has been developed from recordings of the fluctuating oxygen saturations of a preterm boy that later developed severe ROP (Cunningham *et al.*, 2000), and authors report alterations in myelin expression in white matter following exposure (Sedowofia *et al.*, 2008). Furthermore, impaired memory and increased cerebral apoptosis has been found in adult mice exposed to fluctuating hyperoxia and hypoxia in the neonatal period (Ratner *et al.*, 2007). This concurs with a potentiating effect of the *fluctuations* between high and low oxygen levels not only in the retina, but also in the neonatal brain. In paper II exposure to IHH seemed to give subtle changes in brain white matter

diffusivity, grey matter water content and vascular density that were reversible. However, alterations in BBB permeability may point to more long term effects in the brain. Interestingly, these findings point to the neurovascular unit as a target point for injury in both the brain and the retina following IHH.

Although the control of oxygen is rigid in neonatal intensive care nowadays, ROP still occurs, warranting a search for other factors that may contribute in the pathogenesis. There is an emerging realization that several factors work synergistically and possibly potentiate each other also in the development of preterm brain injury, in accordance with the hypothesis of multiple hits in the genesis of neurodevelopmental disorders (Stolp *et al.*, 2012). For instance, being born small-for-gestational-age (SGA) deteriorates neurodevelopmental outcome in preterm born infants, and inflammation potentiates this effect (Leviton *et al.*, 2013). In paper II alterations in brain development were most severe in animals from the largest litter with the lowest bodyweight. This finding could have been caused by confounding maturational differences due to age with IHH exposure, since changes in white matter diffusivity and in T_2-relaxation time is part of normal brain development (Thornton *et al.*, 1999; Bockhorst *et al.*, 2008). Furthermore, lower body weight may lead to later achievement of developmental milestones (Chahoud & Paumgartten, 2009) and it is conceivable that it may also delay brain development in neonatal rats, thereby leading to differences in maturity. However, because of rigorous control of the time of birth, the age of the pups was comparable in the present study. Also, the albumin leakage over the BBB that was most pronounced in pups with the lowest bodyweight was a pathological finding that could not have been related to maturation. The pups were not weighed at birth as to not disturb the dam prior to IHH exposure, and therefore the actual growth curve during IHH exposure is unknown. Nevertheless, albeit the limited number of litters, findings from paper II may generate the hypothesis that a relative growth restriction, even within the normal range may sensitize the brain to adverse events such as IHH. This hypothesis should be investigated in future studies where growth restriction is induced as a controlled condition and where animals subsequently are exposed to a similar paradigm of IHH.

5.2.2 Early MRI markers for outcome following HI

Of major interest in preterm encephalopathy is to establish biomarkers that early can identify children more or less prone to lasting neurodevelopmental impairments following neonatal brain injury and identify both those that are eligible for therapy but also those that are in need of special intervention and long-term care (Ment *et al.*, 2009). The applicability of ADC -mapping as such a marker was investigated in paper I.

ADC-mapping is used in the clinic for early qualitative assessment of perinatal brain injury because diffusion abnormalities appear more rapidly than signal abnormalities on T_2 and T_1 imaging. Animal studies of HI have found that lesion volumes on ADC can predict later injury volume in the Vannucci model at P7 (Widerøe *et al.*, 2012). Paper I in this thesis adds that the actual ADC value in thalamus, if reduced, can predict ensuing long-term volume destruction, meaning that quantitative evaluation of ADC is valuable in the early phase after injury. This is in agreement with a human study in which low early ADC in this area predicted long-term MRI injury patterns and neurologic outcome after HI (Rutherford *et al.*, 2004; Boichot *et al.*, 2006).

The ADC value is the coefficient to the negative slope of the reduced signal when increasing the diffusion weighing (*b*-value) in a diffusion weighted sequence. Thus a lower ADC may indicate a more restricted movement of extracellular water molecules (lower diffusion e.g. because of cytotoxic edema) while high ADC may indicate more free movement (higher

diffusion e.g. because of vasogenic or extracellular edema). Since extracellular space is smaller compared to intracellular space (Lehmenkuhler *et al.*, 1993), even a subtle change in extracellular space could rapidly perturb water diffusion properties. ADC was most severely reduced in HI+hyperoxia in comparison with HI+room-air in paper I. One may speculate that a more severe cytotoxic edema, possibly caused by oxidative stress following hyperoxia, caused a restriction of water movement due to cellular swelling and reduction of extracellular space.

High ADC indicates more free movement of water molecules. In paper I an increase in white matter ADC was a hallmark for an injury affecting predominantly white matter, together with hypotrophic and impeded brain growth (paper I). A similar observation has earlier been reported as a sign of subtle white matter injury after HI in P7 rat (Meng *et al.*, 2006; Lodygensky *et al.*, 2011) and authors speculated that the high ADC was caused by vasogenic edema extending into white matter from adjacent injured areas or cellular reactions in oligodendrocytes or microglia. Cellular shrinkage caused by apoptosis with a resulting increase in extracellular space may be an alternative explanation for higher ADC. The presence of more free extracellular water is supported by the concurrent high T_2 observed in white matter in the same animals in paper I. Increased water content leads to an increase in T_2 relaxation time. In some parallel to the mentioned experimental studies, high ADC in white matter has also been reported by Counsell et al. (2003) in a study of preterm born babies with white matter Diffuse Excessive High Signal Intensity (DEHSI) at term-equivalent age.

As a conclusion early high ADC in white matter may be a marker of a favourable outcome following HI, while low thalamic ADC may be a sign of a less favourable outcome.

5.2.3 Grey matter maturation

The decrease in T_2 relaxation time in brain tissue during maturation in paper II is known from the literature (Thornton *et al.*, 1999). It is presumably caused by the decrease in extracellular space that in the rat has been measured to fall from 46% of the total brain volume at P1 to 20% at P20 (Lehmenkuhler *et al.*, 1993) because of an increase in neuronal size and glial cell numbers during the brain growth spurt (Bandeira *et al.*, 2009). It follows that the number of extracellular free water molecules is reduced and that the T_2 relaxation time becomes shorter. This is responsible for the lower contrast in T_2-maps from older vs. younger animals (paper I, Figure 2) because the difference in signal decay between tissues with short T_2 and long T_2 will be less when utilizing the same echo times, as was applied on the different developmental time-points in papers I & II. The ADC also decreases during the same period of brain maturation (Meng *et al.*, 2006; Sizonenko *et al.*, 2007) which is in agreement with a reduction in free water diffusion in the extracellular compartment.

When the amount of extracellular water is relatively high, such as in the neonatal compared to the adult brain, the need for an osmolyte must also be high. Indeed, the level of the osmolyte taurine was higher in the neonatal vs. the adult brain (paper III), in line with earlier reports in humans (Pouwels *et al.*, 1999) and rats (Tkac *et al.*, 2003). A reduction in taurine has been reported 24 hours after neonatal HI in rat, and the authors suggested that post-HI protective measures against cytotoxic edema and cellular swelling may have been the cause (van de Looij *et al.*, 2011). However, in the immediate recovery phase following HI (after 60 minutes) such a decrease in taurine was not found (paper IV). It is possible that this time-point was too early for protective measures against cytotoxic edema to become activated.

5.2.4 What do alterations in white matter directional diffusivity mean?

Diffusion tensor imaging (DTI) is an excellent method to study directional water diffusion, and is therefore applied in the study of white matter based on the knowledge that in white matter tracts, axons are aligned and oriented in the same direction, and that water diffusion along these axons must be highly directional since they are ensheathed by oligodendrocytes that contain the water-impermeable lipid myelin. Thus, an assumption is made that changes in the anisotropic diffusion measured in these areas reflect changes in white matter myelination or also axonal integrity (Mori & Zhang, 2006), and this assumption is widely utilized both in clinical and experimental work. The differentiation between myelination deficit and axonal injury may not be distinguished from DTI, although it is often interpreted so that diffusion parallel to the main diffusion direction (axial) is affected when there is axonal injury while diffusivity perpendicular to the main direction (radial) is affected when there are alterations in myelination.

During the first postnatal weeks the white matter of rats undergoes maturational changes such as increased oligodendrocyte coverage and myelination of white matter axons. This maturation is reflected in the directional water diffusivity with decreasing mean diffusivity, increasing FA and decreasing radial diffusivity of the white matter (Bockhorst *et al.*, 2008). However, as seen in data from papers I & II, these parameters are similar to adult levels by P14 and P21.

In paper I lower FA and higher radial diffusivity was reported in HI+hyperoxia and the HI+room-air groups vs. shams at P14, suggesting white matter injury at this time-point. One may speculate whether reduced myelination or axonal injury and loss of transcallosal fibres may have contributed to the lower FA and increased radial diffusivity. However, in the HI+room-air group parameters were normalized by 42 days following HI, while in HI+hyperoxia they were not, suggesting irreversible injury. Hyperoxia is thought to play an important role in the pathogenesis of white matter injury in the preterm brain (Volpe, 2009). There is experimental evidence for selective vulnerability of immature white matter to prolonged hyperoxia (Felderhoff-Mueser *et al.*, 2004). Gerstner et al. (2008) report that hyperoxia at P3 and P6, but not at P10, led to apoptosis in the oligodendroglial cell line. Schmitz et al. (2011) observed long-term alterations in white-matter diffusivity on *in vivo* DTI following neonatal hyperoxia, and proposed a role for excitotoxicity in the pathogenesis, since white matter astrocytes in the same study had an impaired uptake of glutamate from the extracellular milieu. It follows from these reports that the hyperoxia exposure in the present thesis (Paper I: 100% O_2 for two hours at P7, Paper II: 50% O_2 continuously from P0 to P14 in paper II) was applied in a period of heightened susceptibility of the white matter to injury by unphysiological levels of O_2.

A normalization of DTI parameters similar to in HI+room-air in paper I was also seen among IHH exposed animals from P14 to P28 in paper II. One may speculate that this normalization may be related to white matter maturational *delay* or repair rather than to permanent injury. In paper II such an interpretation is supported by a study by Cai et al. (2011), in which neonatal intermittent hypoxia for six hours per day arrested the maturation of oligodendrocytes rather than injured axons permanently. However, our DTI findings contrast reports of permanent white matter diffusivity alterations after neonatal hypoxia (Chahboune *et al.*, 2009) and hyperoxia (Schmitz *et al.*, 2012). The IHH profile had lower hyperoxia (50% versus 80%) and shorter hypoxia (three two-minute episodes every 6^{th} hour versus 10 days continuous

exposure) than the aforementioned studies. It may be speculated that this less severe exposure may have caused transient white matter affection with a preserved ability to catch-up maturation rather than a permanent injury.

Apart from alterations in myelination and axonal integrity, directional diffusivity may also reflect alterations in extracellular water content in white matter. Increased extracellular water such as in extracellular edema would decrease the overall directional diffusivity (FA) and increase the radial and axial diffusivity while the mean diffusivity would also increase because water molecules will be able to move more freely in all directions. In paper II a higher mean, axial and radial diffusivity was found among IHH animals at P14 combined with lower FA and a similar tendency in axial and radial diffusivity was also found in HI+hyperoxia animals vs. sham in paper I. In addition to injury to white matter tracts, this may also indicate extracellular increased water content.

5.2.5 [^{13}C]glucose uptake and utilization

To be able to quantify downstream metabolites, [^{13}C]glucose must pass the BBB and enter the cells in which it is metabolized. Since the number of glucose transporters in the BBB, GLUT-1, is low in the neonatal brain (Vannucci & Simpson, 2003) it is conceivable that transport of [^{13}C]glucose over the BBB is slower than in the adult brain. The % enrichment in [^{13}C]glucose was ~30% in both papers III & IV, which is comparable to adult studies (Melø *et al.*, 2006; Eyjolfsson *et al.*, 2011) and that indicates a consistent injection and uptake following i.p. injection also in the neonatal rat. Furthermore, according to data from paper III (Table 1) there was uptake of [^{13}C]glucose already after 5 minutes. Since amounts did not change considerably over 5 - 45 minutes past injection, a limitation in glucose transport over the BBB in the P7 rat was not responsible for the demonstrated differences in glucose metabolism vs. adult rats.

After entry into the brain, a low glucose utilization rate in P6 rat has been reported (Dombrowski *et al.*, 1989). In agreement with this, lower glycolytic activity was shown by the lower levels of ^{13}C incorporation from [1-^{13}C]glucose at all time-points in lactate and alanine compared to data published for the adult brain (Melø *et al.*, 2006; Eyjolfsson *et al.*, 2011).

Furthermore, TCA cycle enzyme activity is low in the neonatal brain compared to in adults (Wilbur & Patel, 1974), corresponding well with the six-times lower labelling of [4,5-^{13}C]glutamate derived from [1-^{13}C]glucose via the TCA cycle. Lower TCA cycle activity is also supported by the smaller amount of the TCA cycle intermediate succinate and the lower cycling ratio of [^{13}C]glucose-derived isotopomers of glutamate and glutamine compared to those in adults (Kondziella *et al.*, 2006). Interestingly, the smaller amount of [4-^{13}C]glutamate derived from [1-^{13}C]glucose is consistent with findings in one of very few existing ^{13}C-MRS studies of a preterm infant, which suggested a reduced rate of glucose utilization for the TCA cycle also in the immature human brain (Bluml *et al.*, 2001).

Following HI there were increased amounts of glucose in both hemispheres. An increased uptake could contribute to this, possibly explained by the reported increased expression of GLUT-1 in the BBB following HI in the P7 rat (Vannucci *et al.*, 1996; Vannucci *et al.*, 1998). Furthermore, in combination with the normal % enrichment in glucose, our findings are in agreement with rapid reperfusion in the Vannucci model (Mujsce *et al.*, 1990).

Glucose utilization via anaerobic glycolysis increases dramatically during HI to continue ATP generation (Vannucci *et al.*, 2005), resulting in an accumulation of lactate and a rapid depletion of brain glucose in both ipsi- and contralateral hemispheres (Yager *et al.*, 1991).

Interestingly, an increase in glucose reserves by hyperglycaemia *within* the brain prior to the insult is protective for the neonatal brain, while the opposite is the case in the adult where hyperglycaemia exacerbates outcome after stroke (Volpe (2008) and references therein). Such a differential effect of glucose levels prior to insults may be related to a more pronounced lactacidosis resulting from anaerobic glycolysis in the adult (Folbergrova *et al.*, 1995) than in the neonatal brain, where lactate levels are rapidly normalized (Yager *et al.*, 1991). In the present thesis such a rapid decline in lactate was supported by normalized levels of lactate at 60 minutes recovery time (paper IV) while we have also found an increase in lactate after 30 minutes of recovery (three-fold, unpublished results). Furthermore, this indicates that the glycolytic flux had indeed been increased during HI, but that it was rapidly normalized during recovery in both hemispheres. The rapid normalization of lactate levels may also be due to that unlabelled lactate accumulated during HI is rapidly metabolized or released into the blood upon reperfusion, since the neonatal brain both has an increased ability to utilize lactate as an energy substrate (Dombrowski *et al.*, 1989) and an increased transport capacity for lactate over the BBB (Vannucci & Simpson, 2003; Halestrap & Meredith, 2004).

5.2.6 Acetate utilization

In the adult, transport of [1,2-^{13}C]acetate over the BBB must be slower than metabolism of acetate since [1,2-^{13}C]acetate is present in serum (Melø *et al.*, 2005) but usually not in the brain following injection. However, in the P7 brain [1,2-^{13}C]acetate was readily detected following injection (Figure 2a), indicating that transport over the BBB must exceed metabolism. This may be due to the high expression of monocarboxylate transporters, which transport acetate across the BBB (Halestrap & Meredith, 2004), in the neonatal vs. the adult brain (Vannucci & Simpson, 2003).

GS, exclusively localized in astrocytes (Norenberg & Martinez-Hernandez, 1979) synthesize [4,5-^{13}C]glutamine from the small pool of glutamate in astrocytes that arise from [1,2-^{13}C]acetate. [4,5-^{13}C]Glutamine is then transferred to glutamatergic neurons and is there converted to [4,5-^{13}C]glutamate. The amounts and % enrichment of [4,5-^{13}C]glutamine was much higher than those of [4,5-^{13}C]glutamate (paper III), in line with a report by Chowdhury et al. (2007) in P10 rats. This confirms that acetate in the P7 rat brain as well as in that of adults is utilized predominantly by astrocytes (Sonnewald *et al.*, 1993).

The metabolism of [1,2-^{13}C]acetate in the neonatal brain 15 minutes past injection was 50 % lower than in adults, seen in % enrichment in [4,5-^{13}C]glutamine. However, 30 minutes past injection, both metabolism as well as TCA cycling of label was similar. Acetate metabolism has earlier been reported to be higher in P10 versus P30 rat brain (Chowdhury *et al.*, 2007). Furthermore, relatively more [1,2-^{13}C]acetate was utilized for both glutamine, glutamate and GABA synthesis than [1-^{13}C]glucose compared to in the adult brain (acetate/glucose utilization ratios in paper III), indicating that the neonatal brain utilized more acetate relative to glucose in neurotransmitter synthesis.

5.2.7 Mitochondrial hypometabolism following HI

After HI, there was a clear reduction in labelling from PDH in glutamate, glutamine, aspartate and GABA in both hemispheres. At the same time there was a decrease in the total amount of glutamate and an increase in the amounts of amino acids that can be substrates for transamination of α-ketoglutarate for glutamate formation; alanine, valine, phenylalanine, isoleucine, leucine and lysine. The above may indicate that glutamate formation and turnover were reduced following HI and that this reduction was also reflected in its products glutamine

and GABA. Summarized, this suggests that mitochondrial glucose metabolism was reduced in the immediate recovery phase following HI. Since glutamine is only synthesized in glia (Norenberg & Martinez-Hernandez, 1979) and most of the glutamate is localized in neurons (Storm-Mathisen *et al.*, 1983), the proportional decrease in labelling via PDH in glutamine and glutamate suggests a similar inhibition of mitochondrial metabolism in both cellular compartments. Such mitochondrial hypometabolism may also contribute to the observed accumulation of glucose following HI. Utilization of unlabeled lactate accumulated during HI could account for part of the bilateral reduction in labelling. However, the measured % enrichment in lactate in the ipsilateral hemisphere was not significantly reduced, while those of glutamate, glutamine, aspartate and GABA was reduced by more than 40%, indicating that such a dilution from unlabeled lactate may not explain the entire difference.

5.2.8 Pyruvate carboxylation and the glutamate-glutamine cycle

The ability of astrocytes to take up glutamate from the synapse and convert it to glutamine in the glutamate-glutamine cycle is vital for normal metabolic homeostasis and as a defence mechanism against excitotoxicity (Danbolt, 2001). In this thesis there were indications that this cycle is different in the neonatal versus the adult brain.

Glutamate levels were much lower in the P7 vs. the adult rat brain, in agreement with Tkac et al. (2003) who found that adult levels of glutamate are not attained until P14 in the rat. In this period of synaptogenesis (Semple *et al.*, 2013) the increase in glutamate that is mainly localized in neurons (Storm-Mathisen *et al.*, 1983) must happen via *de novo* synthesis of neurotransmitter amino acids which is only possible via PC in astrocytes (Patel, 1974; Yu *et al.*, 1983). Since GS is also exclusively localized in astrocytes (Norenberg & Martinez-Hernandez, 1979), [2,3-^{13}C]glutamine, labelled via PC when derived from [1,2-^{13}C]glucose, will be transferred from astrocytes to neurons and there be converted to [2,3-^{13}C]glutamate. Since the level of [2,3-^{13}C]glutamine was higher than [2,3-^{13}C]glutamate in both papers III & IV, it can be deduced that also in the neonatal brain is PC predominantly localized in astrocytes (Yu *et al.*, 1983). The activity of PC has been reported to increase several-fold from birth to adult age, like other enzymes involved in pyruvate metabolism (Wilbur & Patel, 1974). However, the ratio for the amount of pyruvate metabolized via PC relative to the sum of total pyruvate metabolism was calculated to be 15% (paper III) while the reported value in adult brain is approximately 10% (Hertz, 2011). Furthermore, in astrocytes ~50% of glucose was metabolized via PC which is higher than in the adult brain (Kunnecke *et al.*, 1993), indicating that more of the glucose that enter the astrocytic compartment in the neonatal brain is utilized for anaplerosis. The conspicuously higher glutamine transfer from astrocytes to neurons in the P7 brain compared to adults, probed by the astrocyte-specific marker [1,2-^{13}C]acetate, bears evidence for a significant role of astrocytes in anaplerosis in the neonatal brain. This may indicate that the glutamate-glutamine cycle does not operate as a cycle in the neonatal brain, but rather as a delivery system of glutamine from astrocytes to neurons.

In this context, it is of interest to note that PC, representing actual *de novo* synthesis of glutamate, was relatively preserved in the immediate recovery phase following neonatal HI, and that the PC/PDH ratio was increased in glutamate in the ipsilateral hemisphere. Anaplerosis may be beneficial if the neurons following HI have a reduction in TCA cycle intermediates (such as α-ketoglutarate) following the massive release of glutamate into the extracellular space that happen because of depolarization of the cellular membrane during and after HI. Under these conditions, glutamine transferred from astrocytes may be necessary for neurons to re-establish oxidative metabolism. The presence of both PC activity and synthesis

of glutamine, two ATP demanding processes, suggests that astrocytes have at least partly maintained or re-established their energy balance at this time-point after neonatal HI. However, extracellular glutamate release has been shown to continue during recovery after HI with a secondary rise around six hours (Puka-Sundvall *et al.*, 1997; Vannucci *et al.*, 1999), associated with what is known as the secondary energy failure (Kusaka *et al.*, 2004). It is conceivable that continued replenishment of the glutamate neurotransmitter pool via PC in astrocytes in a period of continuous glutamate release may contribute to excitotoxicity in cells with dysfunctional energy metabolism.

On the other hand there was negligible transport of glutamate from neurons to astrocytes. This may be due to a number of factors: limited glutamate release by neurons which are building up their glutamate pool during synaptogenesis (Semple *et al.*, 2013), increased reuptake by neurons and/or reduced uptake by astrocytes. A decreased uptake by astrocytes could possibly be due to the low number of glutamate transporters in the neonatal brain (Danbolt, 2001) and in case of excessive release of glutamate to the extracellular space would a low uptake heighten the danger for excitotoxicity.

5.2.9 GABA

GABA content in the neonatal brain was only slightly lower in the neonatal compared to the adult brain, in line with earlier reports from the rat (Tkac *et al.*, 2003; Chowdhury *et al.*, 2007) and human brain (Kreis *et al.*, 2002). Also, the PC/PDH ratio was not quantifiable in GABA, and incorporation and turnover of ^{13}C-label was much lower in the neonatal compared to adult brain. This may indicate that the main *de novo* synthesis of GABA has already happened before P7. Furthermore, the transfer of glutamine from astrocytes to GABAergic neurons was lower than in the adult brain. GABA transporters, mainly on GABAergic neurons (Schousboe, 2000), are functional from early in brain development (Vitellaro-Zuccarello *et al.*, 2003; Sipilä *et al.*, 2004). These findings support that GABAergic neurons in the neonatal brain may be less dependent upon anaplerosis by astrocytes and therefore more metabolic independent than their glutamatergic counterparts.

GABA content in the ipsilateral hemisphere increased following HI, in accordance with earlier reports from the neonatal brain (Wallin *et al.*, 2000) and from adult brain ischemia (Håberg *et al.*, 2001). The decreased amounts of label and the proportionally more reduced % enrichment in [1,2-^{13}C]GABA compared to [4,5-^{13}C]glutamate indicate that both the production and degradation of GABA were decreased. Consequently, the accumulation of total GABA was mainly due to decreased degeneration.

5.2.10 The pentose phosphate pathway

In paper III it was found that the PPP activity was higher than reports from the adult brain. This is in agreement with a proposed essential role for the PPP during growth and development (McKenna *et al.*, 2012).

Since the PPP generates NADPH that reduces glutathione and thereby restores the defence against ROS, it has been hypothesized that directing glucose via the PPP in response to injury may be beneficial for the brain. Therefore, the pronounced bilateral down-regulation in the neonatal brain after HI was surprising, compared to the reported up-regulation of the PPP after insults which induce oxidative stress in adults (Bartnik *et al.*, 2005; Dusick *et al.*, 2007), However, this may be in agreement with higher vulnerability to oxidative stress in the neonatal brain (McQuillen & Ferriero, 2004).

Via glycolysis, three molecules of glucose yield six pyruvate molecules, six adenosine tri-phosphate (ATP) and six NADH molecules, as mentioned earlier. However, via the PPP one carbon atom is lost in the first oxidative step. It follows that three molecules of glucose yield five molecules of pyruvate and five ATP, thus a ~17% reduction in ATP generation when compared to glycolysis. In the immediate recovery phase after neonatal HI there is severe energy deprivation and, as was found in paper IV, continued mitochondrial bilateral hypometabolism. It therefore seems probable that ATP production via glycolysis is maximized. From *in vitro* experiments with neurons there is evidence for a tight regulatory link between the PPP and glycolysis (Herrero-Mendez *et al.*, 2009). Moreover, there are indications that glutamate excitotoxicity increase glycolysis and reduce PPP activity *in vitro* (Rodriguez-Rodriguez *et al.*, 2012). Since glycolysis was no longer increased, as discussed above, it may be speculated that the depression of PPP in the immediate recovery following neonatal HI was mediated by a mechanism that deactivates PPP without enhancing glycolysis, or that deactivates PPP for a longer time than it stimulates glycolysis.

5.2.11 Contralateral hemisphere affection in the Vannucci model

It has been proposed that the contralateral hemisphere may be utilized as a control in the Vannucci model (Towfighi *et al.*, 1994). However, although reduced CBF is not present in the contralateral hemisphere (Vannucci *et al.*, 1988) it is rendered hypoxic. In agreement with an affection of the contralateral hemisphere, several alterations in short- and long-term development of the contralateral hemisphere following HI were found in papers I & IV.

24 hours following HI a decrease in ADC, i.e. restricted diffusion, was found in the contralateral cortex of animals with the most severe pattern of injury. This is in line with a similar report of increased signal of the contralateral hemisphere on DWI three days after injury, albeit in P10 rats (Ashwal *et al.*, 2007). Furthermore, an increased contralateral BBB permeability up to seven days after HI with persistent edema up to three weeks has been reported (Ferrari *et al.*, 2010). Such a persisting edema could explain the increased axial diffusivity at P49 concurrent with a normal FA that was also found in paper I. In addition it should be noted that microglial activation in contralateral white matter at P14 was observed after HI, supporting that also the contralateral white matter is involved in the injury response.

Restricted longitudinal contralateral hemispheric growth, such as was found following HI in this thesis, has also been reported by others (Andiné *et al.*, 1990; Tuor *et al.*, 2001; Calvert *et al.*, 2002; Ten *et al.*, 2004), but is in contrast with one report of normal long-term growth of the contralateral hemisphere (Towfighi *et al.*, 1994). However, Towfighi et al. utilized histological sections as basis for volume measurements, which is a less accurate method than longitudinal *in vivo* MRI measurements such as those provided in paper I.

The glucose content in contralateral hemisphere was increased in the immediate recovery phase following HI and more so than in the ipsilateral side. This is in line with the earlier mentioned up-regulation of the gene expression of GLUT-1 transporters in the BBB following HI that is in fact more pronounced in the contralateral hemisphere (Vannucci *et al.*, 1996; Vannucci *et al.*, 1998). There was a reduction in the synthesis of major neurotransmitters via PDH in both ipsi- and contralateral hemispheres in the immediate reperfusion phase following HI (paper IV), possibly caused by the global hypoxia that will hinder oxidative phosphorylation also in the contralateral hemisphere. Furthermore, the PPP activity was reduced also in the contralateral hemisphere in glutamate and alanine, as mentioned earlier.

As a conclusion both early and late signs of contralateral involvement in the injury following neonatal HI were found in this thesis. This warrants caution against utilizing the contralateral hemisphere as an uninjured control in the Vannucci model.

6 Concluding remarks

In this thesis, different MR imaging and spectroscopy modalities were utilized to quantify and visualize *in vivo* short- and long-term structural and metabolic alterations following insults to the neonatal brain.

Several interesting findings require further investigation. Structural studies demonstrated that hyperoxia following neonatal HI induced a larger injury that progressively increased from neonatal to near-adult age vs. room-air exposure. Furthermore, fluctuating levels of oxygen led to reversible alterations in grey and white matter, although changes in the permeability of the BBB indicated long-term effects. In the preterm born population it seems that about half of the children fare well while the other half will have long-term functional deficits ((Volpe, 2009) and references therein). This may suggest that *in utero* events preceding preterm birth, like growth retardation or infections, may be important determinants for later brain development, in line with the hypothesis of multiple hits (Stolp *et al.*, 2012). The contributions of such multiple hits to resulting brain injury may be studied in experimental models. From the present thesis, the indication of a differential response to fluctuating levels of oxygen related to body weight should be investigated in future studies that aim at disentangling the possible interactions between growth restriction and unphysiological oxygen exposure to brain injury and to the pathogenesis of ROP.

Furthermore, the glutamate-glutamine cycle seemed to function rather as a delivery system of glutamine from astrocytes to neurons in the neonatal brain. In future studies it should be investigated whether a lower uptake of glutamate by astrocytes in neonatal brain vs. in adults is indeed a cause for the lower transfer of glutamate from neurons to astrocytes that was found. Such a low uptake may potentially contribute to a heightened vulnerability to excitotoxicity in the neonatal brain. It should also be investigated whether *de novo* glutamate synthesis is accompanied by preserved transfer of substrate from astrocytes to neurons during recovery following HI. It is conceivable that a continued replenishment of the glutamate pool during the secondary depolarization and glutamate release following HI may contribute to excitotoxic injury. Also, even though the PPP activity was high in the neonatal brain, it was down-regulated in response to HI. Whether this lowers the defense against oxidative stress should be investigated. Finally, the PPP activity further on in the recovery phase after HI should be studied to assess whether this down-regulation is only short-term, possibly to maximize ATP yield during the primary energy failure, or if it is later followed by normalization or upregulation of PPP activity.

7 Bibliography

Andiman, S.E., Haynes, R.L., Trachtenberg, F.L., Billiards, S.S., Folkerth, R.D., Volpe, J.J. & Kinney, H.C. (2010) The cerebral cortex overlying periventricular leukomalacia: analysis of pyramidal neurons. *Brain Pathol*, **20**, 803-814.

Andiné, P., Thordstein, M., Kjellmer, I., Nordborg, C., Thiringer, K., Wennberg, E. & Hagberg, H. (1990) Evaluation of brain damage in a rat model of neonatal hypoxic-ischemia. *J Neurosci Methods*, **35**, 253-260.

Andrews, W.W., Goldenberg, R.L. & Hauth, J.C. (1995) Preterm labor: emerging role of genital tract infections. *Infect Agents Dis*, **4**, 196-211.

Ashwal, S., Tone, B., Tian, H.R., Chong, S. & Obenaus, A. (2007) Comparison of two neonatal ischemic injury models using magnetic resonance imaging. *Pediatr Res*, **61**, 9-14.

Baburamani, A.A., Ek, C.J., Walker, D.W. & Castillo-Melendez, M. (2012) Vulnerability of the developing brain to hypoxic-ischemic damage: contribution of the cerebral vasculature to injury and repair? *Front Physiol*, **3**, 424.

Back, S.A., Gan, X., Li, Y., Rosenberg, P.A. & Volpe, J.J. (1998) Maturation-dependent vulnerability of oligodendrocytes to oxidative stress-induced death caused by glutathione depletion. *J Neurosci*, **18**, 6241-6253.

Back, S.A., Luo, N.L., Borenstein, N.S., Levine, J.M., Volpe, J.J. & Kinney, H.C. (2001) Late oligodendrocyte progenitors coincide with the developmental window of vulnerability for human perinatal white matter injury. *J Neurosci*, **21**, 1302-1312.

Back, S.A., Luo, N.L., Mallinson, R.A., O'Malley, J.P., Wallen, L.D., Frei, B., Morrow, J.D., Petito, C.K., Roberts, C.T., Jr., Murdoch, G.H. & Montine, T.J. (2005) Selective vulnerability of preterm white matter to oxidative damage defined by F2-isoprostanes. *Ann Neurol*, **58**, 108-120.

Bagenholm, R., Hagberg, H. & Kjellmer, I. (1996) Impact of reoxygenation with oxygen and air on the extent of the brain damage after hypoxia-ischaemia in neonatal rats. *Acta Paediatr*, **85**, 1228-1231.

Ballabh, P., Braun, A. & Nedergaard, M. (2004) The blood-brain barrier: an overview: structure, regulation, and clinical implications. *Neurobiol Dis*, **16**, 1-13.

Bandeira, F., Lent, R. & Herculano-Houzel, S. (2009) Changing numbers of neuronal and non-neuronal cells underlie postnatal brain growth in the rat. *Proc Natl Acad Sci U S A*, **106**, 14108-14113.

Barnabe-Heider, F., Wasylnka, J.A., Fernandes, K.J., Porsche, C., Sendtner, M., Kaplan, D.R. & Miller, F.D. (2005) Evidence that embryonic neurons regulate the onset of cortical gliogenesis via cardiotrophin-1. *Neuron*, **48**, 253-265.

Bartnik, B.L., Sutton, R.L., Fukushima, M., Harris, N.G., Hovda, D.A. & Lee, S.M. (2005) Upregulation of pentose phosphate pathway and preservation of tricarboxylic acid cycle flux after experimental brain injury. *J Neurotrauma*, **22**, 1052-1065.

Beauchemin, M., Gonzalez-Frankenberger, B., Tremblay, J., Vannasing, P., Martinez-Montes, E., Belin, P., Beland, R., Francoeur, D., Carceller, A.M., Wallois, F. & Lassonde, M. (2011) Mother and stranger: an electrophysiological study of voice processing in newborns. *Cereb Cortex*, **21**, 1705-1711.

Beaver, B.V., Reed, W., Leary, S., McKiernan, B., Bain, F., Schultz, R., Bennett, B.T., Pascoe, P., Shull, E., Cork, L.C., Francis-Floyd, R., Amass, K.D., Johnson, R., Schmidt, R.H., Underwood, W., Thornton, G.W. & Kohn, B. (2001) Report of the AVMA panel on euthanasia. *J Am Vet Med Assoc*, **218**, 669-696.

Ben-Ari, Y., Woodin, M.A., Sernagor, E., Cancedda, L., Vinay, L., Rivera, C., Legendre, P., Luhmann, H.J., Bordey, A., Wenner, P., Fukuda, A., van den Pol, A.N., Gaiarsa, J.-L. & Cherubini, E. (2012) Refuting the challenges of the developmental shift of polarity of GABA actions: GABA more exciting than ever! *Front Cell Neurosci*, **6**.

Ben-Yoseph, O., Boxer, P. & Ross, B. (1996) Noninvasive assessment of the relative roles of cerebral antioxidant enzymes by quantitation of pentose phosphate pathway activity. *Neurochem Res*, **21**, 1005-1012.

Bhutta, A.T., Cleves, M.A., Casey, P.H., Cradock, M.M. & Anand, K.S. (2002) Cognitive and behavioral outcomes of school-aged children who were born preterm: A meta-analysis. *JAMA*, **288**, 728-737.

Billiards, S.S., Haynes, R.L., Folkerth, R.D., Borenstein, N.S., Trachtenberg, F.L., Rowitch, D.H., Ligon, K.L., Volpe, J.J. & Kinney, H.C. (2008) Myelin abnormalities without oligodendrocyte loss in periventricular leukomalacia. *Brain Pathol*, **18**, 153-163.

Billiards, S.S., Haynes, R.L., Folkerth, R.D., Trachtenberg, F.L., Liu, L.G., Volpe, J.J. & Kinney, H.C. (2006) Development of microglia in the cerebral white matter of the human fetus and infant. *J Comp Neurol*, **497**, 199-208.

Bluml, S., Moreno, A., Hwang, J.H. & Ross, B.D. (2001) 1-(^{13})C glucose magnetic resonance spectroscopy of pediatric and adult brain disorders. *NMR Biomed*, **14**, 19-32.

Bockhorst, K.H., Narayana, P.A., Dulin, J., Liu, R., Rea, H.C., Hahn, K., Wosik, J. & Perez-Polo, J.R. (2010) Normobaric hyperoximia increases hypoxia-induced cerebral injury: DTI study in rats. *J Neurosci Res*, **88**, 1146-1156.

Bockhorst, K.H., Narayana, P.A., Liu, R., Ahobila-Vijjula, P., Ramu, J., Kamel, M., Wosik, J., Bockhorst, T., Hahn, K., Hasan, K.M. & Perez-Polo, J.R. (2008) Early postnatal

development of rat brain: In vivo diffusion tensor imaging. *J Neurosci Res*, **86**, 1520-1528.

Boichot, C., Walker, P.M., Durand, C., Grimaldi, M., Chapuis, S., Gouyon, J.B. & Brunotte, F. (2006) Term neonate prognoses after perinatal asphyxia: contributions of MR imaging, MR spectroscopy, relaxation times, and apparent diffusion coefficients. *Radiology*, **239**, 839-848.

Boulland, J.-L., Rafiki, A., Levy, L.M., Storm-Mathisen, J. & Chaudhry, F.A. (2003) Highly differential expression of SN1, a bidirectional glutamine transporter, in astroglia and endothelium in the developing rat brain. *Glia*, **41**, 260-275.

Brady, S.T. & Tai, L. (2011) Cell biology of the nervous system. In Brady, S.T., Siegel, G.J., Albers, R.W., Price, D.L. (eds) *Basic Neurochemistry*. Elsevier, London.

Braun, A., Xu, H., Hu, F., Kocherlakota, P., Siegel, D., Chander, P., Ungvari, Z., Csiszar, A., Nedergaard, M. & Ballabh, P. (2007) Paucity of pericytes in germinal matrix vasculature of premature infants. *J Neurosci*, **27**, 12012-12024.

Brekke, E.M., Walls, A.B., Schousboe, A., Waagepetersen, H.S. & Sonnewald, U. (2012) Quantitative importance of the pentose phosphate pathway determined by incorporation of ^{13}C from [2-^{13}C]- and [3-^{13}C]glucose into TCA cycle intermediates and neurotransmitter amino acids in functionally intact neurons. *J Cereb Blood Flow Metab*, **32**, 1788-1799.

Buser, J.R., Maire, J., Riddle, A., Gong, X., Nguyen, T., Nelson, K., Luo, N.L., Ren, J., Struve, J., Sherman, L.S., Miller, S.P., Chau, V., Hendson, G., Ballabh, P., Grafe, M.R. & Back, S.A. (2012) Arrested preoligodendrocyte maturation contributes to myelination failure in premature infants. *Ann Neurol*, **71**, 93-109.

Cai, J., Tuong, C.M., Zhang, Y., Shields, C.B., Guo, G., Fu, H. & Gozal, D. (2011) Mouse intermittent hypoxia mimicking apnoea of prematurity: effects on myelinogenesis and axonal maturation. *J Pathol*, **226**, 495-508.

Calvert, J.W., Yin, W., Patel, M., Badr, A., Mychaskiw, G., Parent, A.D. & Zhang, J.H. (2002) Hyperbaric oxygenation prevented brain injury induced by hypoxia-ischemia in a neonatal rat model. *Brain Res*, **951**, 1-8.

Calvert, J.W. & Zhang, J.H. (2007) Oxygen treatment restores energy status following experimental neonatal hypoxia-ischemia. *Pediatr Crit Care Med*, **8**, 165-173.

Carmeliet, P., Ferreira, V., Breier, G., Pollefeyt, S., Kieckens, L., Gertsenstein, M., Fahrig, M., Vandenhoeck, A., Harpal, K., Eberhardt, C., Declercq, C., Pawling, J., Moons, L., Collen, D., Risau, W. & Nagy, A. (1996) Abnormal blood vessel development and lethality in embryos lacking a single VEGF allele. *Nature*, **380**, 435-439.

Chahboune, H., Ment, L.R., Stewart, W.B., Rothman, D.L., Vaccarino, F.M., Hyder, F. & Schwartz, M.L. (2009) Hypoxic injury during neonatal development in murine brain:

correlation between in vivo DTI findings and behavioral assessment. *Cereb Cortex*, **19**, 2891-2901.

Chahoud, I. & Paumgartten, F.J. (2009) Influence of litter size on the postnatal growth of rat pups: is there a rationale for litter-size standardization in toxicity studies? *Environ Res*, **109**, 1021-1027.

Chowdhury, G.M.I., Patel, A.B., Mason, G.F., Rothman, D.L. & Behar, K.L. (2007) Glutamatergic and GABAergic neurotransmitter cycling and energy metabolism in rat cerebral cortex during postnatal development. *J Cereb Blood Flow Metab*, **27**, 1895-1907.

Clarke, D.D. & Sokoloff, L. (1999) Circulation and energy metabolism. In Siegel, G.J., Agranoff, B.W., Albers, D.S., Fisher, S.K., Uhler, M.D. (eds) *Basic Neurochemistry*. Lippincott Williams and Wilkins, Philadelphia.

Coleman, R.J., Beharry, K.D.A., Brock, R.S., Abad-Santos, P., Abad-Santos, M. & Modanlou, H.D. (2008) Effects of brief, clustered versus dispersed hypoxic episodes on systemic and ocular growth factors in a rat model of oxygen-induced retinopathy. *Pediatr Res*, **64**, 50-55

Counsell, S.J., Allsop, J.M., Harrison, M.C., Larkman, D.J., Kennea, N.L., Kapellou, O., Cowan, F.M., Hajnal, J.V., Edwards, A.D. & Rutherford, M.A. (2003) Diffusion-weighted imaging of the brain in preterm infants with focal and diffuse white matter abnormality. *Pediatrics*, **112**, 1-7.

Coyle, P. & Jokelainen, P.T. (1982) Dorsal cerebral arterial collaterals of the rat. *Anat Rec*, **203**, 397-404.

Craig, A., Ling Luo, N., Beardsley, D.J., Wingate-Pearse, N., Walker, D.W., Hohimer, A.R. & Back, S.A. (2003) Quantitative analysis of perinatal rodent oligodendrocyte lineage progression and its correlation with human. *Exp Neurol*, **181**, 231-240.

Cremer, J.E. (1982) Substrate utilization and brain development. *J Cereb Blood Flow Metab*, **2**, 394-407.

Cruz, F., Scott, S.R., Barroso, I., Santisteban, P. & Cerdan, S. (1998) Ontogeny and cellular localization of the pyruvate recycling system in rat brain. *J Neurochem*, **70**, 2613-2619.

Cunningham, S., McColm, J.R., Wade, J., Sedowofia, K., McIntosh, N. & Fleck, B. (2000) A novel model of retinopathy of prematurity simulating preterm oxygen variability in the rat. *Invest Ophthalmol Vis Sci*, **41**, 4275-4280.

Danbolt, N.C. (2001) Glutamate uptake. *Prog Neurobiol*, **65**, 1-105.

Danbolt, N.C., Storm-Mathisen, J. & Kanner, B.I. (1992) An [Na^+ + K^+]coupled L-glutamate transporter purified from rat brain is located in glial cell processes. *Neuroscience*, **51**, 295-310.

Darland, D.C., Cain, J.T., Berosik, M.A., Saint-Geniez, M., Odens, P.W., Schaubhut, G.J., Frisch, S., Stemmer-Rachamimov, A., Darland, T. & D'Amore, P.A. (2011) Vascular endothelial growth factor (VEGF) isoform regulation of early forebrain development. *Dev Biol*, **358**, 9-22.

Davis, P.G., Tan, A., O'Donnell, C.P.F. & Schulze, A. (2004) Resuscitation of newborn infants with 100% oxygen or air: a systematic review and meta-analysis. *The Lancet*, **364**, 1329-1333.

Dean, J.M., Moravec, M.D., Grafe, M., Abend, N., Ren, J., Gong, X., Volpe, J.J., Jensen, F.E., Hohimer, A.R. & Back, S.A. (2011) Strain-specific differences in perinatal rodent oligodendrocyte lineage progression and its correlation with human. *Dev Neurosci*, **33**, 251-260.

Di Fiore, J.M., Bloom, J.N., Orge, F., Schutt, A., Schluchter, M., Cheruvu, V.K., Walsh, M., Finer, N. & Martin, R.J. (1996) A higher incidence of intermittent hypoxemic episodes is associated with severe retinopathy of prematurity. *J Pediatr*, **157**, 69-73.

Di Fiore, J.M., Kaffashi, F., Loparo, K., Sattar, A., Schluchter, M., Foglyano, R., Martin, R.J. & Wilson, C.G. (2012) The relationship between patterns of intermittent hypoxia and retinopathy of prematurity in preterm infants. *Pediatr Res*, **72**, 606-612.

Dobbing, J. & Sands, J. (1979) Comparative aspects of the brain growth spurt. *Early Hum Dev*, **3**, 79-83.

Dombrowski, G.J., Jr., Swiatek, K.R. & Chao, K.L. (1989) Lactate, 3-hydroxybutyrate, and glucose as substrates for the early postnatal rat brain. *Neurochem Res*, **14**, 667-675.

Duffy, T.E., Kohle, S.J. & Vannucci, R.C. (1975) Carbohydrate and energy metabolism in perinatal rat brain: relation to survival in anoxia *J Neurochem*, **24**, 271-276.

Dusick, J.R., Glenn, T.C., Lee, W.N., Vespa, P.M., Kelly, D.F., Lee, S.M., Hovda, D.A. & Martin, N.A. (2007) Increased pentose phosphate pathway flux after clinical traumatic brain injury: a [1,2-^{13}C2]glucose labeling study in humans. *J Cereb Blood Flow Metab*, **27**, 1593-1602.

Dyet, L.E., Kennea, N., Counsell, S.J., Maalouf, E.F., Ajayi-Obe, M., Duggan, P.J., Harrison, M., Allsop, J.M., Hajnal, J., Herlihy, A.H., Edwards, B., Laroche, S., Cowan, F.M., Rutherford, M.A. & Edwards, A.D. (2006) Natural history of brain lesions in extremely preterm infants studied with serial magnetic resonance imaging from birth and neurodevelopmental assessment. *Pediatrics*, **118**, 536-548.

Dzhala, V.I., Talos, D.M., Sdrulla, D.A., Brumback, A.C., Mathews, G.C., Benke, T.A., Delpire, E., Jensen, F.E. & Staley, K.J. (2005) NKCC1 transporter facilitates seizures in the developing brain. *Nat Med*, **11**, 1205-1213.

Eikenes, L., Løhaugen, G.C., Brubakk, A.-M., Skranes, J. & Håberg, A.K. (2010) Young adults born preterm with very low birth weight demonstrate widespread white matter alterations on brain DTI. *NeuroImage*, **54**, 1774-1785.

El-Khoury, N., Braun, A., Hu, F., Pandey, M., Nedergaard, M., Lagamma, E.F. & Ballabh, P. (2006) Astrocyte end-feet in germinal matrix, cerebral cortex, and white matter in developing infants. *Pediatr Res*, **59**, 673-679.

Eyjolfsson, E.M., Nilsen, L.H., Kondziella, D., Brenner, E., Haberg, A. & Sonnewald, U. (2011) Altered ^{13}C glucose metabolism in the cortico-striato-thalamo-cortical loop in the MK-801 rat model of schizophrenia. *J Cereb Blood Flow Metab*, **31**, 976-985.

Fabian, R.H., Perez-Polo, J.R. & Kent, T.A. (2008) Perivascular nitric oxide and superoxide in neonatal cerebral hypoxia-ischemia. *Am J Physiol Heart Circ Physiol*, **295**, H1809-1814.

Fan, T.W. & Lane, A.N. (2008) Structure-based profiling of metabolites and isotopomers by NMR *Prog Nucl Magn Res Spectrosc*, 69-117.

Favrais, G., van de Looij, Y., Fleiss, B., Ramanantsoa, N., Bonnin, P., Stoltenburg-Didinger, G., Lacaud, A., Saliba, E., Dammann, O., Gallego, J., Sizonenko, S., Hagberg, H., Lelievre, V. & Gressens, P. (2011) Systemic inflammation disrupts the developmental program of white matter. *Ann Neurol*, **70**, 550-565.

Felderhoff-Mueser, U., Bittigau, P., Sifringer, M., Jarosz, B., Korobowicz, E., Mahler, L., Piening, T., Moysich, A., Grune, T., Thor, F., Heumann, R., Bührer, C. & Ikonomidou, C. (2004) Oxygen causes cell death in the developing brain. *Neurobiol Dis*, **17**, 273-282.

Ferrari, D.C., Nesic, O.B. & Perez-Polo, J.R. (2010) Oxygen resuscitation does not ameliorate neonatal hypoxia/ischemia-induced cerebral edema. *J Neurosci Res*.

Field, T.M., Cohen, D., Garcia, R. & Greenberg, R. (1984) Mother-stranger face discrimination by the newborn. *Infant Behav Dev*, **7**, 19-25.

Fleiss, B. & Gressens, P. (2012) Tertiary mechanisms of brain damage: a new hope for treatment of cerebral palsy? *Lancet Neurol*, **11**, 556-566.

Folbergrova, J., Zhao, Q., Katsura, K. & Siesjo, B.K. (1995) N-tert-butyl-alpha-phenylnitrone improves recovery of brain energy state in rats following transient focal ischemia. *Proc Natl Acad Sci U S A*, **92**, 5057-5061.

Follett, P.L., Rosenberg, P.A., Volpe, J.J. & Jensen, F.E. (2000) NBQX attenuates excitotoxic injury in developing white matter. *J Neurosci*, **20**, 9235-9241.

Friebolin, H. (1993) *Basic One- and Two-Dimensional NMR Spectroscopy*. VCH Verlagsgesellschaft, Weinheim, Germany.

Geddes, J.W. & Wood, J.D. (1984) Changes in the amino acid content of nerve endings (synaptosomes) induced by drugs that alter the metabolism of glutamate and gamma-aminobutyric acid. *J Neurochem*, **42**, 16-24.

Gerstner, B., DeSilva, T.M., Genz, K., Armstrong, A., Brehmer, F., Neve, R.L., Felderhoff-Mueser, U., Volpe, J.J. & Rosenberg, P.A. (2008) Hyperoxia causes maturation-dependent cell death in the developing white matter. *J Neurosci*, **28**, 1236-1245.

Graeber, M.B. (2010) Changing face of microglia. *Science*, **330**, 783-788.

Grafe, M.R., Woodworth, K.N., Noppens, K. & Perez-Polo, J.R. (2008) Long-term histological outcome after post-hypoxic treatment with 100% or 40% oxygen in a model of perinatal hypoxic-ischemic brain injury. *Int J Dev Neurosci*, **26**, 119-124.

Halestrap, A.P. & Meredith, D. (2004) The SLC16 gene family-from monocarboxylate transporters (MCTs) to aromatic amino acid transporters and beyond. *Pflugers Arch*, **447**, 619-628.

Hartnett, M.E. & Penn, J.S. (2012) Mechanisms and Management of Retinopathy of Prematurity. *N Engl J Med*, **367**, 2515-2526.

Hassel, B., Sonnewald, U. & Fonnum, F. (1995) Glial-neuronal interactions as studied by cerebral metabolism of [2-^{13}C]acetate and [1-^{13}C]glucose: an ex vivo ^{13}C NMR spectroscopic study. *J Neurochem*, **64**, 2773-2782.

Haynes, R.L., Folkerth, R.D., Keefe, R.J., Sung, I., Swzeda, L.I., Rosenberg, P.A., Volpe, J.J. & Kinney, H.C. (2003) Nitrosative and oxidative injury to premyelinating oligodendrocytes in periventricular leukomalacia. *J Neuropathol Exp Neurol*, **62**, 441-450.

Herrero-Mendez, A., Almeida, A., Fernandez, E., Maestre, C., Moncada, S. & Bolanos, J.P. (2009) The bioenergetic and antioxidant status of neurons is controlled by continuous degradation of a key glycolytic enzyme by APC/C-Cdh1. *Nat Cell Biol*, **11**, 747-752.

Hertz, L. (2011) Astrocytic energy metabolism and glutamate formation — relevance for ^{13}C-NMR spectroscopy and importance of cytosolic/mitochondrial trafficking. *Magn Reson Imaging*, **29**, 1319-1329.

Hogstad, S., Svenneby, G., Torgner, I.A., Kvamme, E., Hertz, L. & Schousboe, A. (1988) Glutaminase in neurons and astrocytes cultured from mouse brain: kinetic properties and effects of phosphate, glutamate, and ammonia. *Neurochem Res*, **13**, 383-388.

Håberg, A., Qu, H., Sather, O., Unsgard, G., Haraldseth, O. & Sonnewald, U. (2001) Differences in neurotransmitter synthesis and intermediary metabolism between glutamatergic and GABAergic neurons during 4 hours of middle cerebral artery occlusion in the rat: the role of astrocytes in neuronal survival. *J Cereb Blood Flow Metab*, **21**, 1451-1463.

Inder, T.E., Huppi, P.S., Warfield, S., Kikinis, R., Zientara, G.P., Barnes, P.D., Jolesz, F. & Volpe, J.J. (1999) Periventricular white matter injury in the premature infant is followed by reduced cerebral cortical gray matter volume at term. *Ann Neurol*, **46**, 755-760.

Johnson, S. (2007) Cognitive and behavioural outcomes following very preterm birth. *Semin Fetal Neonatal Med*, **12**, 363-373.

Johnston, M.V. (2005) Excitotoxicity in perinatal brain injury. *Brain Pathol*, **15**, 234-240.

Kanamatsu, T. & Tsukada, Y. (1994) Measurement of amino acid metabolism derived from [1-^{13}C]glucose in the rat brain using ^{13}C magnetic resonance spectroscopy. *Neurochem Res*, **19**, 603-612.

Kanamatsu, T. & Tsukada, Y. (1999) Effects of ammonia on the anaplerotic pathway and amino acid metabolism in the brain: an ex vivo ^{13}C NMR spectroscopic study of rats after administering [2-^{13}C] glucose with or without ammonium acetate. *Brain Res*, **841**, 11-19.

Kinney, H.C., Haynes, R.L., Xu, G., Andiman, S.E., Folkerth, R.D., Sleeper, L.A. & Volpe, J.J. (2012) Neuron deficit in the white matter and subplate in periventricular leukomalacia. *Ann Neurol*, **71**, 397-406.

Koch, J.D., Miles, D.K., Gilley, J.A., Yang, C.P. & Kernie, S.G. (2008) Brief exposure to hyperoxia depletes the glial progenitor pool and impairs functional recovery after hypoxic-ischemic brain injury. *J Cereb Blood Flow Metab*, **28**, 1294-1306.

Kolb, B., Mychasiuk, R., Muhammad, A., Li, Y., Frost, D.O. & Gibb, R. (2012) Experience and the developing prefrontal cortex. *Proc Natl Acad Sci U S A*, **109**, 17186-17193.

Kondziella, D., Brenner, E., Eyjolfsson, E.M., Markinhuhta, K.R., Carlsson, M.L. & Sonnewald, U. (2006) Glial-neuronal interactions are impaired in the schizophrenia model of repeated MK801 exposure. *Neuropsychopharmacol*, **31**, 1880-1887.

Kreis, R., Hofmann, L., Kuhlmann, B., Boesch, C., Bossi, E. & Huppi, P.S. (2002) Brain metabolite composition during early human brain development as measured by quantitative in vivo 1H magnetic resonance spectroscopy. *Magn Reson Med*, **48**, 949-958.

Kunnecke, B., Cerdan, S. & Seelig, J. (1993) Cerebral metabolism of [1,2-^{13}C2]glucose and [U-^{13}C4]3-hydroxybutyrate in rat brain as detected by ^{13}C NMR spectroscopy. *NMR Biomed*, **6**, 264-277.

Kusaka, T., Matsuura, S., Fujikawa, Y., Okubo, K., Kawada, K., Namba, M., Okada, H., Imai, T., Isobe, K. & Itoh, S. (2004) Relationship between cerebral interstitial levels of amino acids and phosphorylation potential during secondary energy failure in hypoxic-ischemic newborn piglets. *Pediatr Res*, **55**, 273-279.

Larroque, B., Ancel, P.Y., Marret, S., Marchand, L., Andre, M., Arnaud, C., Pierrat, V., Roze, J.C., Messer, J., Thiriez, G., Burguet, A., Picaud, J.C., Breart, G. & Kaminski, M. (2008)

Neurodevelopmental disabilities and special care of 5-year-old children born before 33 weeks of gestation (the EPIPAGE study): a longitudinal cohort study. *Lancet*, **371**, 813-820.

Lehmenkuhler, A., Sykova, E., Svoboda, J., Zilles, K. & Nicholson, C. (1993) Extracellular space parameters in the rat neocortex and subcortical white matter during postnatal development determined by diffusion analysis. *Neuroscience*, **55**, 339-351.

Levine, S. (1960) Anoxic-ischemic encephalopathy in rats. *Am J Pathol*, **36**, 1-17.

Leviton, A., Fichorova, R.N., O'Shea, T.M., Kuban, K., Paneth, N., Dammann, O. & Allred, E.N. (2013) Two-hit model of brain damage in the very preterm newborn: small for gestational age and postnatal systemic inflammation. *Pediatr Res*, **73**, 362-370.

Leviton, A. & Gressens, P. (2007) Neuronal damage accompanies perinatal white-matter damage. *Trends Neurosci*, **30**, 473-478.

Lodygensky, G.A., West, T., Moravec, M.D., Back, S.A., Dikranian, K., Holtzman, D.M. & Neil, J.J. (2011) Diffusion characteristics associated with neuronal injury and glial activation following hypoxia-ischemia in the immature brain. *Magn Reson Med*, **66**, 839-845.

Lundstrom, K.E., Pryds, O. & Greisen, G. (1995) Oxygen at birth and prolonged cerebral vasoconstriction in preterm infants. *Arch Dis Child Fetal Neonatal Ed*, **73**, F81-86.

Maalouf, E.F., Duggan, P.J., Rutherford, M.A., Counsell, S.J., Fletcher, A.M., Battin, M., Cowan, F. & Edwards, A.D. (1999) Magnetic resonance imaging of the brain in a cohort of extremely preterm infants. *J Pediatr*, **135**, 351-357.

Malatesta, P., Hartfuss, E. & Gotz, M. (2000) Isolation of radial glial cells by fluorescent-activated cell sorting reveals a neuronal lineage. *Development*, **127**, 5253-5263.

Maltepe, E. & Saugstad, O.D. (2009) Oxygen in health and disease: regulation of oxygen homeostasis-clinical implications. *Pediatr Res*, **65**, 261-268.

Markram, H., Toledo-Rodriguez, M., Wang, Y., Gupta, A., Silberberg, G. & Wu, C. (2004) Interneurons of the neocortical inhibitory system. *Nat Rev Neurosci*, **5**, 793-807.

Martin, R.J., Wang, K., Koroglu, O., Di Fiore, J. & Kc, P. (2011) Intermittent hypoxic episodes in preterm infants: do they matter? *Neonatology*, **100**, 303-310.

Martinussen, M., Fischl, B., Larsson, H.B., Skranes, J., Kulseng, S., Vangberg, T.R., Vik, T., Brubakk, A.-M., Haraldseth, O. & Dale, A.M. (2005) Cerebral cortex thickness in 15-year-old adolescents with low birth weight measured by an automated MRI-based method. *Brain*, **128**, 2588-2596.

McKenna, M.C., Dienel, G.A., Sonnewald, U., Waagepetersen, H.S. & Schousboe, A. (2012) Energy Metabolism of the brain *Basic Neurochemistry*. Elsevier Inc, London, pp. 224-253.

McKenna, M.C., Sonnewald, U., Huang, X., Stevenson, J. & Zielke, H.R. (1996) Exogenous glutamate concentration regulates the metabolic fate of glutamate in astrocytes. *J Neurochem*, **66**, 386-393.

McQuillen, P.S. & Ferriero, D.M. (2004) Selective vulnerability in the developing central nervous system. *Pediatr Neurol*, **30**, 227-235.

McQuillen, P.S., Sheldon, R.A., Shatz, C.J. & Ferriero, D.M. (2003) Selective vulnerability of subplate neurons after early neonatal hypoxia-ischemia. *J Neurosci*, **23**, 3308-3315.

Melø, T.M., Nehlig, A. & Sonnewald, U. (2005) Metabolism is normal in astrocytes in chronically epileptic rats: a (13)C NMR study of neuronal-glial interactions in a model of temporal lobe epilepsy. *J Cereb Blood Flow Metab*, **25**, 1254-1264.

Melø, T.M., Nehlig, A. & Sonnewald, U. (2006) Neuronal-glial interactions in rats fed a ketogenic diet. *Neurochem Int*, **48**, 498-507.

Meng, S., Qiao, M., Scobie, K., Tomanek, B. & Tuor, U.I. (2006) Evolution of magnetic resonance imaging changes associated with cerebral hypoxia-ischemia and a relatively selective white matter injury in neonatal rats. *Pediatr Res*, **59**, 554-559.

Ment, L.R., Hirtz, D. & Hüppi, P.S. (2009) Imaging biomarkers of outcome in the developing preterm brain. *Lancet Neurol*, **8**, 1042-1055.

Micheva, K.D. & Beaulieu, C. (1995) Postnatal development of GABA neurons in the rat somatosensory barrel cortex: a quantitative study. *Eur J Neurosci*, **7**, 419-430.

Monier, A., Adle-Biassette, H., Delezoide, A.L., Evrard, P., Gressens, P. & Verney, C. (2007) Entry and distribution of microglial cells in human embryonic and fetal cerebral cortex. *J Neuropathol Exp Neurol*, **66**, 372-382.

Monier, A., Evrard, P., Gressens, P. & Verney, C. (2006) Distribution and differentiation of microglia in the human encephalon during the first two trimesters of gestation. *J Comp Neurol*, **499**, 565-582.

Moon, C., Lagercrantz, H. & Kuhl, P.K. (2013) Language experienced in utero affects vowel perception after birth: a two-country study. *Acta Paediatr*, **102**, 156-160.

Mori, S. & Zhang, J. (2006) Principles of diffusion tensor imaging and its applications to basic neuroscience research. *Neuron*, **51**, 527-539.

Mujsce, D.J., Christensen, M.A. & Vannucci, R.C. (1990) Cerebral blood flow and edema in perinatal hypoxic-ischemic brain damage. *Pediatr Res*, **27**, 450-453.

Nehlig, A. (2004) Brain uptake and metabolism of ketone bodies in animal models. *Prostaglandins Leukot Essent Fatty Acids*, **70**, 265-275.

Nelson, K.B. & Lynch, J.K. (2004) Stroke in newborn infants. *Lancet Neurol*, **3**, 150-158.

Neumann, H., Kotter, M.R. & Franklin, R.J. (2009) Debris clearance by microglia: an essential link between degeneration and regeneration. *Brain*, **132**, 288-295.

Niatsetskaya, Z.V., Charlagorla, P., Matsukevich, D.A., Sosunov, S.A., Mayurasakorn, K., Ratner, V.I., Polin, R.A., Starkov, A.A. & Ten, V.S. (2011) Mild hypoxemia during initial reperfusion alleviates the severity of secondary energy failure and protects brain in neonatal mice with hypoxic-ischemic injury. *J Cereb Blood Flow Metab*, **32**, 232-241.

Norenberg, M.D. & Martinez-Hernandez, A. (1979) Fine structural localization of glutamine synthetase in astrocytes of rat brain. *Brain Res*, **161**, 303-310.

Northington, F.J., Ferriero, D.M., Graham, E.M., Traystman, R.J. & Martin, L.J. (2001) Early neurodegeneration after hypoxia-ischemia in neonatal rat is necrosis while delayed neuronal death is apoptosis. *Neurobiol Dis*, **8**, 207-219.

Pape, K.E. & Wigglesworth, J.S. (1979) Blood supply to the developing brain *Haemorrhage, Ischemia and the Perinatal Brain*. William Heinemann Medical Books, London.

Patel, M.S. (1974) The relative significance of CO_2-fixing enzymes in the metabolism of rat brain. *J Neurochem*, **22**, 717-724.

Paxinos, G. & Watson, C. (2008) *The rat brain in stereotaxic coordinates*. Academic Press London, UK.

Penn, J.S., Henry, M.M., Wall, P.T. & Tolman, B.L. (1995) The range of PaO_2 variation determines the severity of oxygen-induced retinopathy in newborn rats. *Invest Ophthalmol Vis Sci*, **36**, 2063-2070.

Penn, J.S., Tolman, B.L. & Lowery, L.A. (1993) Variable oxygen exposure causes preretinal neovascularization in the newborn rat. *Invest Ophthalmol Vis Sci*, **34**, 576-585.

Perlman, J.M., Wyllie, J., Kattwinkel, J., Atkins, D.L., Chameides, L., Goldsmith, J.P., Guinsburg, R., Hazinski, M.F., Morley, C., Richmond, S., Simon, W.M., Singhal, N., Szyld, E., Tamura, M. & Velaphi, S. (2010) Neonatal resuscitation: 2010 International consensus on cardiopulmonary resuscitation and emergency cardiovascular care science with treatment recommendations. *Pediatrics*, **126**, e1319-e1344.

Pierson, C., Folkerth, R., Billiards, S., Trachtenberg, F., Drinkwater, M., Volpe, J. & Kinney, H. (2007) Gray matter injury associated with periventricular leukomalacia in the premature infant. *Acta Neuropathol*, **114**, 619-631.

Platt, M.J., Cans, C., Johnson, A., Surman, G., Topp, M., Torrioli, M.G. & Krageloh-Mann, I. (2007) Trends in cerebral palsy among infants of very low birthweight (<1500 g) or born prematurely (<32 weeks) in 16 European centres: a database study. *Lancet*, **369**, 43-50.

Pouwels, P.J., Brockmann, K., Kruse, B., Wilken, B., Wick, M., Hanefeld, F. & Frahm, J. (1999) Regional age dependence of human brain metabolites from infancy to adulthood as detected by quantitative localized proton MRS. *Pediatr Res*, **46**, 474-485.

Presti, A.L., Kishkurno, S.V., Slinko, S.K., Randis, T.M., Ratner, V.I., Polin, R.A. & Ten, V.S. (2006) Reoxygenation with 100% oxygen versus room air: late neuroanatomical and neurofunctional outcome in neonatal mice with hypoxic-ischemic brain injury. *Pediatr Res*, **60**, 55-59.

Puka-Sundvall, M., Sandberg, M. & Hagberg, H. (1997) Brain injury after hypoxia-ischemia in newborn rats: relationship to extracellular levels of excitatory amino acids and cysteine. *Brain Res*, **750**, 325-328.

Qu, H., Haberg, A., Haraldseth, O., Unsgard, G. & Sonnewald, U. (2000) (13)C MR spectroscopy study of lactate as substrate for rat brain. *Dev Neurosci*, **22**, 429-436.

Rabi, Y., Rabi, D. & Yee, W. (2007) Room air resuscitation of the depressed newborn: A systematic review and meta-analysis. *Resuscitation*, **72**, 353-363.

Rabi, Y., Yee, W., Chen, S.Y. & Singhal, N. (2006) Oxygen saturation trends immediately after birth. *J Pediatr*, **148**, 590-594.

Rabin, O., Deutsch, J., Grange, E., Pettigrew, K.D., Chang, M.C., Rapoport, S.I. & Purdon, A.D. (1997) Changes in cerebral acyl-CoA concentrations following ischemia-reperfusion in awake gerbils. *J Neurochem*, **68**, 2111-2118.

Ratner, V., Kishkurno, S.V., Slinko, S.K., Sosunov, S.A., Sosunov, A.A., Polin, R.A. & Ten, V.S. (2007) The contribution of intermittent hypoxemia to late neurological handicap in mice with hyperoxia-induced lung injury. *Neonatology*, **92**, 50-50-58.

Represa, A., Tremblay, E. & Ben-Ari, Y. (1989) Transient increase of NMDA-binding sites in human hippocampus during development. *Neurosci Lett*, **99**, 61-66.

Rice, J.E., 3rd, Vannucci, R.C. & Brierley, J.B. (1981) The influence of immaturity on hypoxic-ischemic brain damage in the rat. *Ann Neurol*, **9**, 131-141.

Rodriguez-Rodriguez, P., Fernandez, E., Almeida, A. & Bolanos, J.P. (2012) Excitotoxic stimulus stabilizes PFKFB3 causing pentose-phosphate pathway to glycolysis switch and neurodegeneration. *Cell Death Differ*, **19**, 1582-1589.

Rutherford, M., Counsell, S., Allsop, J., Boardman, J., Kapellou, O., Larkman, D., Hajnal, J., Edwards, D. & Cowan, F. (2004) Diffusion-weighted magnetic resonance imaging in term perinatal brain injury: a comparison with site of lesion and time from birth. *Pediatrics*, **114**, 1004-1014.

Sanchez, R.M. & Jensen, F.E. (2001) Maturational aspects of epilepsy mechanisms and consequences for the immature brain. *Epilepsia*, **42**, 577-585.

Saugstad, O.D., Ramji, S., Soll, R.F. & Vento, M. (2008) Resuscitation of newborn infants with 21% or 100% oxygen: an updated systematic review and meta-analysis. *Neonatology*, **94**, 176-182.

Schafer, D.P., Lehrman, E.K., Kautzman, A.G., Koyama, R., Mardinly, A.R., Yamasaki, R., Ransohoff, R.M., Greenberg, M.E., Barres, B.A. & Stevens, B. (2012) Microglia sculpt postnatal neural circuits in an activity and complement-dependent manner. *Neuron*, **74**, 691-705.

Schlapbach, L.J., Aebischer, M., Adams, M., Natalucci, G., Bonhoeffer, J., Latzin, P., Nelle, M., Bucher, H.U. & Latal, B. (2011) Impact of sepsis on neurodevelopmental outcome in a Swiss National Cohort of extremely premature infants. *Pediatrics*, **128**, e348-357.

Schmitz, T., Endesfelder, S., Reinert, M.-C., Klinker, F., Müller, S., Bührer, C. & Liebetanz, D. (2012) Adolescent hyperactivity and impaired coordination after neonatal hyperoxia. *Exp Neurol*, **235**, 374-379.

Schmitz, T., Ritter, J., Mueller, S., Felderhoff-Mueser, U., Chew, L.J. & Gallo, V. (2011) Cellular changes underlying hyperoxia-induced delay of white matter development. *J Neurosci*, **31**, 4327-4344.

Schousboe, A. (2000) Pharmacological and functional characterization of astrocytic GABA transport: a short review. *Neurochem Res*, **25**, 1241-1244.

Sedowofia, K., Giles, D., Wade, J., Cunningham, S., McColm, J.R., Minns, R. & McIntosh, N. (2008) Myelin expression is altered in the brains of neonatal rats reared in a fluctuating oxygen atmosphere. *Neonatology*, **94**, 113-122.

Segovia, K.N., McClure, M., Moravec, M., Luo, N.L., Wan, Y., Gong, X., Riddle, A., Craig, A., Struve, J., Sherman, L.S. & Back, S.A. (2008) Arrested oligodendrocyte lineage maturation in chronic perinatal white matter injury. *Ann Neurol*, **63**, 520-530.

Semple, B.D., Blomgren, K., Gimlin, K., Ferriero, D.M. & Noble-Haeusslein, L.J. (2013) Brain development in rodents and humans: Identifying benchmarks of maturation and vulnerability to injury across species. *Prog Neurobiol*, **106-107**, 1-16.

Shimabuku, R., Ota, A., Pereyra, S., Veliz, B., Paz, E., Nakachi, G., More, M. & Oliveros, M. (2005) Hyperoxia with 100% oxygen following hypoxia-ischemia increases brain damage in newborn rats. *Biol Neonate*, **88**, 168-171.

Sie, L.T., van der Knaap, M.S., Oosting, J., de Vries, L.S., Lafeber, H.N. & Valk, J. (2000) MR patterns of hypoxic-ischemic brain damage after prenatal, perinatal or postnatal asphyxia. *Neuropediatrics*, **31**, 128-136.

Sipilä, S., Huttu, K., Voipio, J. & Kaila, K. (2004) GABA uptake via GABA transporter-1 modulates GABAergic transmission in the immature hippocampus. *J Neurosci*, **24**, 5877-5880.

Sizonenko, S.V., Camm, E.J., Garbow, J.R., Maier, S.E., Inder, T.E., Williams, C.E., Neil, J.J. & Huppi, P.S. (2007) Developmental changes and injury induced disruption of the radial organization of the cortex in the immature rat brain revealed by in vivo diffusion tensor MRI. *Cereb Cortex*, **17**, 2609-2617.

Skranes, J.S., Nilsen, G., Smevik, O., Vik, T. & Brubakk, A.M. (1998) Cerebral MRI of very low birth weight children at 6 years of age compared with the findings at 1 year. *Pediatr Radiol*, **28**, 471-475.

Solberg, R., Andresen, J.H., Escrig, R., Vento, M. & Saugstad, O.D. (2007) Resuscitation of hypoxic newborn piglets with oxygen induces a dose-dependent increase in markers of oxidation. *Pediatr Res*, **62**, 559-563.

Solberg, R., Andresen, J.H., Pettersen, S., Wright, M.S., Munkeby, B.H., Charrat, E., Khrestchatisky, M., Rivera, S. & Saugstad, O.D. (2010) Resuscitation of hypoxic newborn piglets with supplementary oxygen induces dose-dependent increase in matrix metalloproteinase-activity and down-regulates vital genes. *Pediatr Res*, **67**, 250-256.

Sonnewald, U., Westergaard, N., Schousboe, A., Svendsen, J.S., Unsgard, G. & Petersen, S.B. (1993) Direct demonstration by [^{13}C]NMR spectroscopy that glutamine from astrocytes is a precursor for GABA synthesis in neurons. *Neurochem Int*, **22**, 19-29.

Stolp, H., Neuhaus, A., Sundramoorthi, R. & Molnar, Z. (2012) The long and the short of it: gene and environment interactions during early cortical development and consequences for long-term neurological disease. *Front Psychiatry*, **3**, 50.

Storm-Mathisen, J., Leknes, A.K., Bore, A.T., Vaaland, J.L., Edminson, P., Haug, F.M. & Ottersen, O.P. (1983) First visualization of glutamate and GABA in neurones by immunocytochemistry. *Nature*, **301**, 517-520.

Stubbs, D., DeProto, J., Nie, K., Englund, C., Mahmud, I., Hevner, R. & Molnar, Z. (2009) Neurovascular congruence during cerebral cortical development. *Cereb Cortex*, **19 Suppl 1**, i32-41.

Ten, V.S., Wu, E.X., Tang, H., Bradley-Moore, M., Fedarau, M.V., Ratner, V.I., Stark, R.I., Gingrich, J.A. & Pinsky, D.J. (2004) Late measures of brain injury after neonatal hypoxia-ischemia in mice. *Stroke*, **35**, 2183-2188.

Thornton, J.S., Amess, P.N., Penrice, J., Chong, W.K., Wyatt, J.S. & Ordidge, R.J. (1999) Cerebral tissue water spin-spin relaxation times in human neonates at 2.4 Tesla: Methodology and the effects of maturation. *Magn Reson Imaging*, **17**, 1289-1295.

Tkac, I., Rao, R., Georgieff, M.K. & Gruetter, R. (2003) Developmental and regional changes in the neurochemical profile of the rat brain determined by in vivo ^{1}H NMR spectroscopy. *Magn Reson Med*, **50**, 24-32.

Towfighi, J., Housman, C., Vannucci, R.C. & Heitjan, D.F. (1994) Effect of unilateral perinatal hypoxic-ischemic brain damage on the gross development of opposite cerebral hemisphere. *Biol Neonate*, **65**, 108-118.

Towfighi, J., Yager, J.Y., Housman, C. & Vannucci, R.C. (1991) Neuropathology of remote hypoxic-ischemic damage in the immature rat. *Acta Neuropathol*, **81**, 578-587.

Tremblay, E., Roisin, M.P., Represa, A., Charriaut-Marlangue, C. & Ben-Ari, Y. (1988) Transient increased density of NMDA binding sites in the developing rat hippocampus. *Brain Res*, **461**, 393-396.

Tremblay, M.E., Lowery, R.L. & Majewska, A.K. (2010) Microglial interactions with synapses are modulated by visual experience. *PLoS Biol*, **8**, e1000527.

Tuor, U.I., Hudzik, T.J., Malisza, K., Sydserff, S., Kozlowski, P. & Del Bigio, M.R. (2001) Long-term deficits following cerebral hypoxia-ischemia in four-week-old rats: correspondence between behavioral, histological, and magnetic resonance imaging assessments. *Exp Neurol*, **167**, 272-281.

Tyzio, R., Represa, A., Jorquera, I., Ben-Ari, Y., Gozlan, H. & Aniksztejn, L. (1999) The establishment of GABAergic and glutamatergic synapses on CA1 pyramidal neurons is sequential and correlates with the development of the apical dendrite. *J Neurosci*, **19**, 10372-10382.

Vaccarino, F.M., Fagel, D.M., Ganat, Y., Maragnoli, M.E., Ment, L.R., Ohkubo, Y., Schwartz, M.L., Silbereis, J. & Smith, K.M. (2007) Astroglial cells in development, regeneration, and repair. *Neuroscientist*, **13**, 173-185.

van de Looij, Y., Chatagner, A., Hüppi, P.S., Gruetter, R. & Sizonenko, S.V. (2011) Longitudinal MR assessment of hypoxic ischemic injury in the immature rat brain. *Magn Reson Med*, **65**, 305-312.

Vannucci, R., Brucklacher, R. & Vannucci, S. (2005) Glycolysis and perinatal hypoxic-ischemic brain damage. *Dev Neurosci*, **27**, 185-190.

Vannucci, R.C., Brucklacher, R.M. & Vannucci, S.J. (1997) Effect of carbon dioxide on cerebral metabolism during hypoxia-ischemia in the immature rat. *Pediatr Res*, **42**, 24-29.

Vannucci, R.C., Brucklacher, R.M. & Vannucci, S.J. (1999) CSF glutamate during hypoxia–ischemia in the immature rat. *Dev Brain Res*, **118**, 147-151.

Vannucci, R.C., Lyons, D.T. & Vasta, F. (1988) Regional cerebral blood flow during hypoxia-ischemia in immature rats. *Stroke*, **19**, 245-250.

Vannucci, R.C., Towfighi, J., Heitjan, D.F. & Brucklacher, R.M. (1995) Carbon dioxide protects the perinatal brain from hypoxic-ischemic damage: an experimental study in the immature rat. *Pediatrics*, **95**, 868-874.

Vannucci, R.C. & Vannucci, S.J. (2005) Perinatal hypoxic-ischemic brain damage: evolution of an animal model. *Dev Neurosci*, **27**, 81-86.

Vannucci, S.J., Reinhart, R., Maher, F., Bondy, C.A., Lee, W.-H., Vannucci, R.C. & Simpson, I.A. (1998) Alterations in GLUT1 and GLUT3 glucose transporter gene expression following unilateral hypoxia-ischemia in the immature rat brain. *Dev Brain Res*, **107**, 255-264.

Vannucci, S.J., Seaman, L.B., Brucklacher, R.M. & Vannucci, R.C. (1994) Glucose transport in developing rat brain: Glucose transporter proteins, rate constants and cerebral glucose utilization. *Mol Cell Biochem*, **140**, 177-184.

Vannucci, S.J., Seaman, L.B. & Vannucci, R.C. (1996) Effects of hypoxia-ischemia on GLUT1 and GLUT3 glucose transporters in immature rat brain. *J Cereb Blood Flow Metab*, **16**, 77-81.

Vannucci, S.J. & Simpson, I.A. (2003) Developmental switch in brain nutrient transporter expression in the rat. *Am J Physiol Endocrinol Metab*, **285**, E1127-1134.

Varoqui, H., Zhu, H., Yao, D., Ming, H. & Erickson, J.D. (2000) Cloning and functional identification of a neuronal glutamine transporter. *J Biol Chem*, **275**, 4049-4054.

Vento, M., Asensi, M., Sastre, J., Garcia-Sala, F., Pallardo, F.V. & Vina, J. (2001) Resuscitation with room air instead of 100% oxygen prevents oxidative stress in moderately asphyxiated term neonates. *Pediatrics*, **107**, 642-647.

Verney, C., Monier, A., Fallet-Bianco, C. & Gressens, P. (2010) Early microglial colonization of the human forebrain and possible involvement in periventricular white-matter injury of preterm infants. *J Anat*, **217**, 436-448.

Vitellaro-Zuccarello, L., Calvaresi, N. & Biasi, S. (2003) Expression of GABA transporters, GAT-1 and GAT-3, in the cerebral cortex and thalamus of the rat during postnatal development. *Cell Tissue Res*, **313**, 245-257.

Volpe, J.J. (2005) Encephalopathy of prematurity includes neuronal abnormalities. *Pediatrics*, **116**, 221-225.

Volpe, J.J. (2008) Neurology of the Newborn. In Elsevier, S. (ed), Philadelphia.

Volpe, J.J. (2009) Brain injury in premature infants: a complex amalgam of destructive and developmental disturbances. *Lancet Neurol*, **8**, 110-124.

Vrachnis, N., Vitoratos, N., Iliodromiti, Z., Sifakis, S., Deligeoroglou, E. & Creatsas, G. (2010) Intrauterine inflammation and preterm delivery. *Ann NY Acad Sci*, **1205**, 118-122.

Wallin, C., Puka-Sundvall, M., Hagberg, H., Weber, S.G. & Sandberg, M. (2000) Alterations in glutathione and amino acid concentrations after hypoxia-ischemia in the immature rat brain. *Dev Brain Res*, **125**, 51-60.

Wang, D.D. & Kriegstein, A.R. (2009) Defining the role of GABA in cortical development. *J Physiol*, **587**, 1873-1879.

Waniewski, R.A. & Martin, D.L. (1998) Preferential utilization of acetate by astrocytes is attributable to transport. *J Neurosci*, **18**, 5225-5233.

Weiss, M.D., Derazi, S., Rossignol, C., Varoqui, H., Erickson, J.D., Kilberg, M.S. & Anderson, K.J. (2003) Ontogeny of the neutral amino acid transporter SAT1/ATA1 in rat brain. *Dev Brain Res*, **143**, 151-159.

Welsh, F.A., Vannucci, R.C. & Brierley, J.B. (1982) Columnar alterations of NADH fluorescence during hypoxia-ischemia in immature rat brain. *J Cereb Blood Flow Metab*, **2**, 221-228.

White, T., Su, S., Schmidt, M., Kao, C.Y. & Sapiro, G. (2010) The development of gyrification in childhood and adolescence. *Brain and cognition*, **72**, 36-45.

Widerøe, M., Havnes, M.B., Morken, T.S., Skranes, J., Goa, P.-E. & Brubakk, A.-M. (2012) Doxycycline treatment in a neonatal rat model of hypoxia–ischemia reduces cerebral tissue and white matter injury: a longitudinal magnetic resonance imaging study. *Eur J Neurosci*, **36**, 2006-2016.

Wigglesworth, J.S. & Pape, K.E. (1978) An integrated model for haemorrhagic and ischaemic lesions in the newborn brain. *Early Hum Dev*, **2**, 179-199.

Wilbur, D.O. & Patel, M.S. (1974) Development of mitochondrial pyruvate metabolism in rat brain. *J Neurochem*, **22**, 709-715.

Xu, G., Broadbelt, K.G., Haynes, R.L., Folkerth, R.D., Borenstein, N.S., Belliveau, R.A., Trachtenberg, F.L., Volpe, J.J. & Kinney, H.C. (2011) Late development of the GABAergic system in the human cerebral cortex and white matter. *J Neuropathol Exp Neurol*, **70**, 841-858.

Yager, J.Y., Brucklacher, R.M. & Vannucci, R.C. (1991) Cerebral oxidative metabolism and redox state during hypoxia-ischemia and early recovery in immature rats. *Am J Physiol*, **261**, H1102-1108.

Yager, J.Y., Brucklacher, R.M. & Vannucci, R.C. (1992) Cerebral energy metabolism during hypoxia-ischemia and early recovery in immature rats. *Am J Physiol*, **262**, H672-677.

Yan, X.X., Zheng, D.S. & Garey, L.J. (1992) Prenatal development of GABA-immunoreactive neurons in the human striate cortex. *Brain Res Dev Brain Res*, **65**, 191-204.

Yu, A.C., Drejer, J., Hertz, L. & Schousboe, A. (1983) Pyruvate carboxylase activity in primary cultures of astrocytes and neurons. *J Neurochem*, **41**, 1484-1487.

8 Contributions

Paper I

Is not included due to copyright

Paper II

Long title: **Brain development after neonatal intermittent hyperoxia-hypoxia in the rat studied by longitudinal MRI and immunohistochemistry**

Short title: **O_2 fluctuations and long-term brain development**

Authors: Tora Sund Morken[1*], Axel Karl Gottfrid Nyman[2], Ioanna Sandvig[2], Sverre Helge Torp[1], Jon Skranes[1,3], Pål Erik Goa[4], Ann-Mari Brubakk[1,3], Marius Widerøe[2]

[1] Department of Laboratory Medicine, Children's and Women's Health, Norwegian University of Science and Technology (NTNU), N-7489 Trondheim, Norway

[2] Department of Circulation and Medical Imaging, Norwegian University of Science and Technology, N-7489 Trondheim, Norway

[3] Department of Pediatrics, St. Olav University Hospital, Central Norway Regional Health Authority, N-7006 Trondheim, Norway

[4] Department of Radiology, St. Olav University Hospital, Central Norway Regional Health Authority, N-7006 Trondheim, Norway

[*]Corresponding author:
Tora Sund Morken, MD
LBK, Medical Faculty, NTNU
MTFS
N-7489 Trondheim
Norway
Tel: +47 73 59 88 30 Fax: +47 73 55 13 50
e-mail: tora.s.morken@ntnu.no

Abstract

Background: Neonatal intermittent hyperoxia-hypoxia (IHH) is involved in the pathogenesis of retinopathy of prematurity. Whether similar oxygen fluctuations will create pathological changes in the grey and white matter of the brain is unknown.

Methods: From birth until postnatal day 14 (P14), two litters (total n=22) were reared in IHH: hyperoxia (50% O_2) interrupted by three consecutive two-minute episodes of hypoxia (12%O_2) every sixth hour. Controls (n = 8) were reared in room-air (20.9%O_2). Longitudinal MRI (Diffusion Tensor Imaging and T_2-mapping) was performed on P14 and P28 and retinal and brain tissue were examined for histopathological changes. Long-term neurodevelopment was assessed on P20 and P27.

Results: Mean, radial and axial diffusivity were higher in white matter of IHH versus controls at P14 ($p < 0.04$), while fractional anisotropy (FA) was lower in the hippocampal fimbria and tended to be lower in corpus callosum ($p = 0.08$) and external capsule ($p = 0.05$). White matter diffusivity in IHH was similar to controls at P28. Higher cortical vessel density ($p = 0.005$) was observed at P14. Cortical and thalamic T_2-relaxation time was longer in the IHH group at P14 ($p \leq 0.03$), and albumin leakage was present at P28. Rats in the IHH group ran for a longer time on a Rotarod than the control group ($p \leq 0.005$). Pups with lower bodyweight had more severe MRI alterations and albumin leakage.

Conclusion: IHH led to subtle reversible changes in brain white matter diffusivity, grey matter water content and vascular density. However, alterations in blood-brain barrier permeability may point to long-term effects. The changes seen after IHH exposure were more severe in animals with lower bodyweight. Future studies should aim at exploring possible interactions between IHH and growth restriction.

Introduction

Preterm born infants may be subject to pathological conditions in several organ systems like retinopathy of prematurity in the eye (ROP) and preterm encephalopathy. The severity of ROP is a predictor of neurodevelopmental outcome [1] and parallels postnatal head growth deficit [2]. The retina has been called a "window to the brain" since it is an extension of brain tissue [3], and it is conceivable that environmental insults during critical periods in development may contribute to both ROP and preterm encephalopathy. Exposure to unphysiological levels of oxygen may be such an environmental insult. In the retina it is the *fluctuations* and *range* between high (hyperoxic) and low (hypoxic) levels of oxygen that create ROP rather than either exposure alone [4,5], and even small fluctuations in oxygen concentration around a normoxic mean induce pathological changes [6]. Hyperoxia due to treatment combined with hypoxia due to apnoea is common in the sick premature child, and clinicians question whether such unphysiological oxygen levels will also affect long-term brain development [7]. In animal models this has been explored after neonatal hypoxia [8-10] or hyperoxia [11,12]. However, brain development following neonatal fluctuating oxygen levels, an exposure that would more closely mimic a clinical setting, is largely unexplored.

In ROP the coordinated formation of the neurovascular unit comprising neurons, endothelial cells, pericytes and astrocytes is disrupted [13]. Obliteration of immature vessels by hyperoxia leads to tissue hypoxia that in turn stimulates uncontrolled neovascularization, microbleedings, and eventually injury to the rapidly growing neural tissue of the retina [14]. The neurovascular unit may also be a target in the brain of preterm born children, a population where long-term pathological changes in grey and white matter are abundant [15,16]. Periventricular white matter is poorly vascularized due to arterial end-zones, and disturbances of vascular supply is likely involved in the development of periventricular leukomalacia (PVL) [17]. Furthermore, paucity of endothelial pericyte [18] and astrocyte coverage [19] in the germinal matrix of preterm born infants, a predilection site for intraventricular haemorrhage, indicates fragile vasculature. Vascularization of both the retina [20] and brain [21] occur in parallel to the brain growth spurt from gestational week 20 until term in humans and from birth until postnatal day 14 (P14) in the rat, a species that at birth is comparable to a very preterm human infant [22]. Both intermittent and continuous neonatal hypoxia reduce long-term myelination and induce angiogenesis in the

rat brain [10,23]. Furthermore, neonatal hyperoxia causes microvascular degeneration in grey matter [24] and maturation-dependent cell death in white matter [25,26]. It is conceivable that, both in the retina and brain, fluctuations between high and low oxygen levels disturb the coordinated formation of the neurovascular unit in a period of major growth and differentiation in both organs. Therefore, exposure of neonatal rats to a profile of intermittent hyperoxia-hypoxia (IHH) that cause ROP may induce a parallel disruption of neural and vascular tissue in the brain with ensuing white and grey matter injury.

To investigate this hypothesis we conducted a study of long-term brain development in rats exposed to IHH from birth until postnatal day 14. Outcome was evaluated with multimodal *in vivo* MRI combined with neurodevelopmental testing and detailed immunohistochemical studies of blood-brain barrier (BBB) permeability and vascular density.

Methods

Ethics Statement

Experiments were conducted in accordance with Guidelines set by the Norwegian Ethics Committee for Animal Research and approved by the responsible governmental authority (Forsøksdyrutvalget, permit no: 3748).

Oxygen Profiling

An A84 Oxycycler (Biospherix Ltd., Lacona, NY) was used to program a profile of intermittent hyperoxia-hypoxia (IHH) that create ROP in neonatal rats [27]. Continuous hyperoxia (50% O_2) was interrupted every sixth hour by three consecutive two – minute long episodes of hypoxia (12% O_2), each ten minutes apart (Figure 1). The ramp time between hyperoxia and hypoxia was approximately two minutes. Bedding was changed during a 50% cycle on day seven. The chamber was then opened for less than three minutes. Inside the chamber, oxygen was controlled via a sensor and a computerized feed-back system where nitrogen was used to lower and oxygen was used to raise the oxygen concentration. CO_2, temperature and relative humidity was continuously monitored and kept within physiological levels via the use of Soda lime (Anmedic AB, Sweden), ventilation and a built-in fan.

Experiment groups

Time-mated Sprague-Dawley rats were purchased from Scanbur AS (Nittedal, Norway). Within four hours after delivery of the last pup, litters with dam were placed in specialized controlled oxygen chambers in their cages (A-30524, Biospherix Ltd, Lacona, NY). To ensure a uniform age at start of exposure whole litters were exposed from birth. Two litters (A: n = 13 and B: n = 9) were exposed to intermittent hyperoxia-hypoxia (IHH) while one litter (controls: n = 8) was exposed to room-air (20.9 % O_2) from postnatal day 0 (P0) to postnatal day 14 (P14). Animals were kept on a 12:12 hours light: dark cycle and had food and water *ad libitum.* Half the animals were euthanized on P14 and the other half on P28 after MRI and neurodevelopmental testing.

MRI

MRI was performed on P14 (IHH: n = 22; control: n = 8) and P28 (IHH: n = 12; control: n = 4) using a 7T magnet (Biospec 70/20 AS, Bruker Biospin MRI, Ettlingen, Germany) with water-cooled (BGA-12, 400 mT/m) gradients. All animals were imaged longitudinally until euthanization. A volume resonator was used for RF transmission and actively decoupled head surface coils were used for RF reception. During scanning the anaesthetized (2% isoflurane in 30% O_2/70% N_2) pups lay prone in a dedicated water-heated bed (Bruker Biospin MRI) and the head of every animal was fixated in the same position with tooth-bar, nose-mask and polystyrene. Temperature and respiration were monitored during the scanning procedure. On P14 and P28 coronal T_2-maps were obtained with a turbo spin-echo (RARE) sequence: Effective TE = 16, 48, 80, 120 ms; TR = 3750 ms; RARE - factor = 4; FOV = 25 x 20 mm^2; MTX = 160 x 96 reconstructed to 164 x 128; 15 slices á 0.75 mm. DTI was performed with an EPI sequence using 30 directions and b = 1000ms; 5 b0 images and TE = 32; TR = 3750ms; FOV = 25.6 x 25.6 mm^2; MTX = 128 x 128 and 15 coronal slices á 0.75 mm.

Magnetic Resonance Image Analysis

In-house developed software was used for calculating T_2-maps (MATLAB ver. R2010a, Math Works Inc., Natick, MA), and ImageJ (v1.42q, National Institute of Health, Bethesda, MD) was used for image analysis. T_2-maps were calculated by fitting a mono-exponential model to the signal intensity of the images with different TE-values. Regions of interest (ROI) were drawn in the parasagittal cortex, thalamus, hippocampus and putamen in two slices corresponding to –3.25 mm and –1.5 mm from the bregma [28] (Supplementary Figure 1). For brain volume measurements the areas of both hemispheres were drawn manually on the T_2-maps in each image slice and the total brain volumes were calculated and compared between groups. DTI-analyses were performed with the tools of the FMRIB software library (FSL ver. 4.1.4, Oxford Centre for Functional MRI of the Brain, Oxford, UK; www.fmrib.ox.ac.uk/fsl). Images were pre-processed to reduce artefacts due to motion and eddy current distortions by affine transformation and co-registration of the diffusion encoded images to the b0 images. Brains were segmented out using the Brain Extraction Tool before FDT ver2.0 (FMRIB's Diffusion Toolbox; both part of FSL) was used to fit a voxelwise diffusion tensor model to the diffusion image data. Maps for the fractional anisotropy (FA), mean, radial and axial diffusivity were created. To limit partial volume effects, ROI were manually drawn in

the centre of white matter structures at all relevant image slices on the FA maps and combined to five volumes of interest: corpus callosum (body), external capsule, internal capsule, hippocampal fimbriae and white matter (comprising all of the aforementioned areas, see Supplementary Figure 1). Mean FA, radial, axial and mean diffusivity were calculated in each of these volumes of interest in each animal. Due to low signal-to-noise (SNR) in the deeper brain structures in the diffusion weighted images on P28, masks were only drawn in the body of the corpus callosum where SNR was adequate for robust calculations of DTI metrics at this time-point (IHH: n = 6, control: n = 4).

Rotarod

On P20 and P27 rats were tested on a Rotarod (Bioseb, Vitrolles, France) in four consecutive trials with increasing rotation from 0 to 40 rpm within 2 minutes. The time the animals ran on the rotating rod was recorded.

Histology

Rats were euthanized by an overdose of pentobarbital (300 mg/kg; Vétoquinol, Lure Cedex, France). For fixation an intracardial perfusion of 4% paraformaldehyde (Fluka Chemie AG, Buchs, Switzerland) in phosphate-buffered saline (Oxoid Limited, Hampshire, UK) was given. Eyes were enucleated and the orbita were inspected for gross abnormalities. Thereafter the retina of the left eye was dissected and whole-mounted onto Super Frost object glass (Thermo Fisher Scientific Inc., Waltham, MA) while the right eye and the brain were paraffin-embedded. Only a few retinas were successfully whole-mounted in each group (IHH: n = 2; control: n = 1). Coronal brain sections corresponding to –3.25 mm from the bregma [28] and retinal cross-sections (4 µm) were cut and stained with Haematoxylin & Eosin (H&E; Cell Path Ltd., Newtown, UK and Sigma-Aldrich Inc., St. Louis, MO) and examined for morphological changes.

Immunohistochemistry

Brain sections were incubated with anti-rat-albumin (1:16000) (Nordic Immunology, Eindhoven, the Netherlands) for albumin leakage, Biotinylated *Griffonia (Bandeiraea) Simplicifolia* Lectin I Isolectin B4 (1 µg/ml) (Vector Laboratories Inc., Burlingame, CA) for vascular density, anti-glial fibrillary acid protein (GFAP; 1:200) (Cymbus Biotechnology,

Southampton, UK) for astrogliosis and anti-ED1-FITC (1:400) (Serotec, Raleigh, NC) for cluster of differentiation 68 (CD68) positive activated microglia. Sections were then incubated with labelled polymer HRP anti-rabbit (Dako A/S, Glostrup, Denmark), streptavidin-conjugated FITC (Vector Laboratories Inc.), horse-anti-mouse-biotin (Vector Laboratories Inc.) and rat-anti-FITC-biotin (Roche, Basel, Switzerland). Visualization was performed using a Vectastain ABC kit (Vector Laboratories Inc.) and a Diaminobenzidine (DAB) kit (Vector Laboratories Inc.). Images of brain sections were captured with a MIRAX MIDI system (Carl Zeiss MicroImaging GmbH, Jena, Germany) and examined. The presence (score = 1) or not (score = 0) of increased albumin immunoreactivity in the neuropil in the hippocampus, cortex, thalamus and hypothalamus was scored. Vessel density was quantified in three areas of the cortex (parietal and temporal), thalamus, hippocampus (CA2, CA3 and dentate gyrus) and periventricular white matter at x 400 magnification using ImageJ and normalized relative to control. The result was averaged for each animal and the mean was compared between groups. GFAP and CD68-stained sections were evaluated qualitatively for changes between groups. Following incubation with Isolectin B4 (12.5 μg/ml) overnight and thereafter with streptavidin-conjugated FITC, retinal wholemounts were analyzed qualitatively for neovascularization and maturation of the retinal vascular bed.

Statistical Analysis

To test for differences in mean between experiment groups and between time-points in the same individual, paired and unpaired two-tailed Student's *t*-tests were applied, respectively. Between-litter differences were analyzed with one-way ANOVA followed by post-hoc tests with Bonferroni correction for multiple comparisons. A $p < 0.05$ was chosen as level of significance. Data are presented as mean ± 95 % confidence interval. Analyses were performed in SPSS version 16.0 (SPSS Inc., Chicago, IL).

Results

Retinal changes

At P14 orbital macroscopic bleedings were observed in four out of ten IHH animals and in none of the controls. Furthermore, haemorrhage in the ganglion cell layer and/or inner and outer nuclear layer were seen in five out of nine animals in the IHH group, often in all three layers and on several locations (Figure 2 a-d). Similar bleedings were observed in one control animal in one location. At P28 areas of neovascularization were observed in retinal wholemounts of both IHH animals (Figure 2 g-h) but not in the control (Figure 2 e-f), and the control retinal vasculature appeared more remodelled compared to IHH.

Bodyweight

On P14 litter A weighed less (n = 13, mean = 21.2 ± 0.6 g) than litter B (n = 9, mean = 27.4 ± 0.5g) and controls (n = 8, mean = 25.8 ± 1.1g; $p < 0.01$) while B was heavier than controls ($p = 0.01$). At P28 mean weight of B (79.6 ± 2.6g) was higher than that of A (73.8 ± 2.7g, $p = 0.01$) but none were different from mean weight of controls (76.3 ± 3.4g).

Brain volume

At P14, litter A (809.8 ± 20.7µl) had lower brain volume than litters B (871.8 ± 33.0µl) and C (875.4 ± 21.5µl; $p = 0.01$*)* while litter B and C did not differ. At P28 mean volume of A (1002.0 ± 31.0µl, $p = 0.01$) was lower than that of B (1081.2 ± 11.2µl) but none were different from controls (1049.4 ± 48.1µl).

Histopathology

No pathological changes were seen in the H & E brain sections with regards to neuropil, neurons, glial cells, vessels or leptomeninges. There were especially no extravasations of erythrocytes, inflammation or eosinophilic degeneration in neurons observed.

Immunohistochemistry

A generalized positive immunoreaction for albumin was seen in both IHH and controls in the neuropil at P14 and in the hypothalamus, a circumventricular organ void of BBB [29], at P28 (Figure 3 a & c). However, only in the IHH group was focal perivascular albumin leakage above control levels observed in the neuropil at P28 (Figure 3 e & f). Although albumin leakage was present in most animals in both litters in the IHH group (A: 6/7 animals versus B: 3/5 animals), litter A had multiple larger areas (Figure 3e), while those of litter B were singular smaller areas similar to those observed in control animals. Cortical vascular density of the IHH animals was higher than controls at P14 (p = 0.005, see Figure 4) and tended to be higher in the thalamus *(*p = 0.07). At P28 vascular density was similar to controls. GFAP staining was not elevated in the IHH versus controls, nor was there increased activation of microglia at either time-point (data not shown).

T_2 maps

Visual evaluation of T_2-maps did not reveal differences in grey or white matter. However, at P14 the measured T_2-relaxation time was higher in the IHH group than in controls in cortex (p = 0.02) and thalamus (p = 0.03) (Table 1), but similar on P28. In both groups T_2-relaxation time decreased from P14 to P28 (p < 0.003). At P14 litter A had a higher mean T_2 relaxation time than litter B in all areas (p < 0.006), and than controls in cortex and thalamus (p < 0.001, Figure 7).

Diffusion Tensor Imaging

At P14, mean, radial and axial diffusivity were higher in the IHH than in the control group in all areas of white matter (p < 0.04) except axial diffusivity in the external capsule (p = 0.09). Fractional anisotropy (FA) was lower in the hippocampal fimbriae (p = 0.001) and tended to be lower in the external capsule (p = 0.05) and corpus callosum (p = 0.08, see Figure 5) in the IHH group. At P28 there was no difference in white matter diffusivity of the corpus callosum between IHH and controls, but there was a significant increase in FA (p = 0.03) and decrease in radial (p = 0.008) and mean (p = 0.009) diffusivity from P14 to P28 in the IHH group (Table 2). Litter A had a lower mean FA in all of white matter, corpus callosum and hippocampal fimbria than B and controls (p < 0.02, Figure 8). Furthermore, radial diffusivity in A was higher than that of B and controls in all areas (p < 0.01). Mean diffusivity for litter A was

higher than litter B in the internal capsule (p = 0.001) and in all areas compared to controls (p < 0.005). Axial diffusivity in the internal capsule was higher in litter A than controls (p = 0.04). At P28 there were no differences in DTI parameters between litters (data not shown).

RotaRod

The IHH group ran for a longer time on the RotaRod than controls at both P20 (p = 0.003) and P27 (p = 0.004, Figure 6).

Discussion

White matter

Diffusion Tensor MRI is an excellent method to study directional free water diffusion and thereby *in vivo* white matter microstructural development and myelination [30]. During the first postnatal weeks the white matter of rats undergoes maturational changes such as increased oligodendrocyte coverage and myelination of white matter axons. This maturation is reflected in the measured water diffusion with decreasing mean diffusivity, increasing fractional anisotropy (FA) and decreasing radial diffusivity [31] of the white matter. We report three major findings from DTI of white matter structures performed at P14 and P28 after IHH exposure: 1) higher mean, axial and radial diffusivity among IHH animals at P14; 2) lower FA among IHH animals at P14; 3) no difference in diffusivity at P28. The two first observations indicate a less structured white matter with increased extracellular versus intracellular water content at P14. A normalization of white matter diffusivity long-term similar to what was observed in the present study has earlier been reported after neonatal hypoxia-ischemia [32]. Albeit DTI data were limited at P28, we speculate that alterations in diffusivity after neonatal IHH may be related to white matter maturational delay rather than to permanent injury. Such an interpretation is supported by studies reporting that neonatal intermittent hypoxia delay the maturation of oligodendrocytes rather than injure axons permanently [33] and that neonatal hyperoxic exposure cause a similar maturational delay [34]. Delayed white matter maturation with subsequent hypomyelination is also observed in preterm infants with diffuse white matter injury [35]. However, our DTI findings contrast reports of permanent white matter diffusivity alterations after neonatal hypoxia [36] and hyperoxia [12]. Our profile of IHH had lower hyperoxia (50% versus 80%) and shorter hypoxia (three two-minute episodes every sixth hour versus ten days continuous exposure) than the aforementioned studies. This less severe exposure may have caused transient white matter affection with a preserved ability to catch-up maturation rather than a permanent injury, which may explain the observed normalization of white matter diffusivity after IHH exposure over time.

Grey matter

Higher grey matter T_2-relaxation time in response to intermittent hyperoxia-hypoxia (IHH) indicates increased water content, and alterations in angiogenesis and BBB-formation may explain the increased vascular density and albumin leakage long-term. The angiogenic effect of hypoxia [37] has been extensively studied in the adult, but not the neonatal brain [38]. On the other hand, hyperoxia causes microvascular degeneration in the neonatal brain [24] possibly inducing tissue hypoxia. By exposing the neonatal brain to a combination of high and low oxygen levels as in IHH, such vasoobliteration by hyperoxia may have potentiated the angiogenic effect of the hypoxic episodes. Moreover, the normalization of vascular density in the IHH group at P28 may possibly be mediated via apoptosis of the newly-formed endothelium [23,39]. However, the concomitant long-term albumin leakage indicates that BBB-integrity was permanently altered even though vessel density returned to normal levels.

The decrease in T_2-relaxation time in normal brain tissue during maturation of the brain coincides with a reduction in free extracellular water as neurons mature [40,41]. Although the BBB is not fully developed at neonatal age [42] most of the functional barrier properties i.e. glucose and albumin transporters are [29]. Thus the relatively high brain water content and high concentration of albumin in the cerebrospinal fluid (CSF) at this age [29] may explain the observed albumin-immunoreactivity in the neuropil at postnatal day 14. The suggested presence of a transcellular route for albumin transport [43] is supported by visible albumin in intracellular vesicles in the choroid plexus cells at both P14 and P28 (Figure 4 b & d).

Rotarod

The IHH animals ran longer on the Rotarod than controls, contrary to what would be expected if IHH exposure had given motor function deficits. It is unlikely that this was caused by an improved motor function after IHH exposure. However, during consecutive trials several animals in the control group were able to turn around and apparently willingly jump off the rotating rod, thereby resulting in shorter time spent on the rod. None of the IHH animals showed this behaviour. Neonatal hyperoxia has been shown to impair memory in rats [11] and although behavioural tests were not performed in the present study, we

speculate that differences in memory may explain the observed longer time spent on a Rotarod after IHH exposure.

Retina

It should be noted that classic avascular zones with subsequent prominent neovascularization such as those seen in models for ROP with 24 hours exposure of alternating hyper- and hypoxia [4] have not been observed after IHH [27], or after fluctuating oxygen levels around a normoxic mean [6]. Nevertheless, in line with earlier reports [27], the highly clinically relevant profile of neonatal IHH in our study created retinopathy seen as macro- and microscopic haemorrhages.

Implications for further research

The strength of our study is the longitudinal design with MRI, immunohistochemistry and neurodevelopmental testing, enabling the comparison of *in vivo* grey and white matter changes to detailed histopathological characterization and long-term outcome. However, the exploration of brain development after neonatal IHH has raised several questions:

(I) Does intrauterine and postnatal growth influence susceptibility to injury from IHH? Rat pups born in larger litters have a lower bodyweight at birth and in the whole suckling period [44], indicating that intrauterine growth determines postnatal body weight gain. Even though no intervention was applied to induce growth restriction in our study, pups from the most numerous litter with the lowest bodyweight and brain volume had the most severe alterations in many parameters of brain development. This finding could have been caused by confounding maturational differences due to age with IHH exposure. However, because of rigorous control of the time of birth, the age of the pups was comparable in the present study. Nevertheless, lower body weight may lead to later achievement of developmental milestones [44]. Such a maturational delay may have contributed to the differences observed in white matter diffusivity and in T_2 relaxation time, since as mentioned earlier, changes in these parameters are part of normal brain development. However, the albumin leakage over the BBB that was most pronounced in pups with the lowest bodyweight was a pathological finding that could not have been related to maturation. Therefore, albeit the limited number of litters, this study may imply that growth restriction, even within the

normal range [45], may sensitize the brain to adverse events such as IHH. Indeed, birth weight at term within the normal range correlates with longitudinal brain volume development [46]. Furthermore, being born small-for-gestational-age (SGA) deteriorates neurodevelopmental outcome [47] and delays white matter maturation at term-equivalent age in preterms [48]. To explore if an interaction between growth and IHH exists, studies where growth restriction is a controlled condition should be performed.

(II) What is the role of key cellular players in the formation of BBB integrity like pericytes [49] and mediators of angiogenesis like vascular endothelial growth factor (VEGF) [37] in the alterations observed after IHH? Endothelial coverage of pericytes closes the time-window when immature vessels are vulnerable to obliteration by hyperoxia [50], and hypoxia causes the same cells to migrate away from vessels, further destabilizing the endothelium [51]. Furthermore, although angiogenesis in tissue hypoxia is most likely beneficial, its mediator VEGF increases vessel permeability [52]. Future studies should probe whether alterations in pericyte development and VEGF secretion form a causal basis for the observations of increased vascular density, higher T_2 relaxation time and long-term BBB leakage reported in the present study.

Conclusion

IHH led to subtle changes in brain white matter diffusivity, grey matter water content and vascular density. However, alterations in BBB permeability may indicate permanent long-term effects. The formation of the neurovascular unit may represent a common site of injury in both the retina and the brain. Alterations after IHH exposure were more severe in low-weight animals. Future studies should aim at exploring whether an interaction between inhibited postnatal growth and IHH exist.

Acknowledgements

The authors acknowledge Kathrin Torseth and Eli Johannesen (Cellular and Molecular Imaging Core Facility, NTNU) for performing the immunohistochemical staining and Paulo Girão (Medical Faculty, NTNU) for scanning the histological sections. The MRI was performed at the MR Core Facility at NTNU.

References

1. Msall ME, Phelps DL, DiGaudio KM, Dobson V, Tung B, et al. (2000) Severity of neonatal retinopathy of prematurity is predictive of neurodevelopmental functional outcome at age 5.5 years. Pediatrics 106: 998-1005.
2. Lofqvist C, Engstrom E, Sigurdsson J, Hard AL, Niklasson A, et al. (2006) Postnatal head growth deficit among premature infants parallels retinopathy of prematurity and insulin-like growth factor-1 deficit. Pediatrics 117: 1930-1938.
3. Msall ME (2006) The retina as a window to the brain in vulnerable neonates. Pediatrics 117: 2287-2289.
4. Penn JS, Henry MM, Wall PT, Tolman BL (1995) The range of PaO2 variation determines the severity of oxygen-induced retinopathy in newborn rats. Invest Ophthalmol Vis Sci 36: 2063-2070.
5. Di Fiore JM, Kaffashi F, Loparo K, Sattar A, Schluchter M, et al. (2012) The relationship between patterns of intermittent hypoxia and retinopathy of prematurity in preterm infants. Pediatr Res 72: 606-612.
6. Cunningham S, McColm JR, Wade J, Sedowofia K, McIntosh N, et al. (2000) A novel model of retinopathy of prematurity simulating preterm oxygen variability in the rat. Invest Ophthalmol Vis Sci 41: 4275-4280.
7. Martin RJ, Wang K, Koroglu O, Di Fiore J, Kc P (2011) Intermittent hypoxic episodes in preterm infants: do they matter? Neonatology 100: 303-310.
8. Schwartz ML, Vaccarino F, Chacon M, Li Yan W, Ment LR, et al. (2004) Chronic neonatal hypoxia leads to long term decreases in the volume and cell number of the rat cerebral cortex. Semin Perinatol 28: 379-388.
9. Ment LR, Schwartz M, Makuch RW, Stewart WB (1998) Association of chronic sublethal hypoxia with ventriculomegaly in the developing rat brain. Dev Brain Res 111: 197-203.
10. Ogunshola OO, Stewart WB, Mihalcik V, Solli T, Madri JA, et al. (2000) Neuronal VEGF expression correlates with angiogenesis in postnatal developing rat brain. Dev Brain Res 119: 139-153.
11. Ramani M, van Groen T, Kadish I, Bulger A, Ambalavanan N (2013) Neurodevelopmental impairment following neonatal hyperoxia in the mouse. Neurobiol Dis 50: 69-75.
12. Schmitz T, Endesfelder S, Reinert M-C, Klinker F, Müller S, et al. (2012) Adolescent hyperactivity and impaired coordination after neonatal hyperoxia. Exp Neurol 235: 374-379.
13. Chen J, Smith LE (2007) Retinopathy of prematurity. Angiogenesis 10: 133-140.
14. Hartnett ME, Penn JS (2012) Mechanisms and Management of Retinopathy of Prematurity. N Engl J Med 367: 2515-2526.
15. Vangberg TR, Skranes J, Dale AM, Martinussen M, Brubakk A-M, et al. (2006) Changes in white matter diffusion anisotropy in adolescents born prematurely. NeuroImage 32: 1538-1548.
16. Martinussen M, Fischl B, Larsson HB, Skranes J, Kulseng S, et al. (2005) Cerebral cortex thickness in 15-year-old adolescents with low birth weight measured by an automated MRI-based method. Brain 128: 2588-2596.
17. Khwaja O, Volpe JJ (2008) Pathogenesis of cerebral white matter injury of prematurity. Arch Dis Child Fetal Neonatal Ed 93: F153-161.
18. Braun A, Xu H, Hu F, Kocherlakota P, Siegel D, et al. (2007) Paucity of pericytes in germinal matrix vasculature of premature infants. J Neurosci 27: 12012-12024.

19. El-Khoury N, Braun A, Hu F, Pandey M, Nedergaard M, et al. (2006) Astrocyte end-feet in germinal matrix, cerebral cortex, and white matter in developing infants. Pediatr Res 59: 673-679.
20. Roth AM (1977) Retinal vascular development in premature infants. Am J Ophthalmol 84: 636-640.
21. Wigglesworth JS, Pape KE (1978) An integrated model for haemorrhagic and ischaemic lesions in the newborn brain. Early Hum Dev 2: 179-199.
22. Yager JY, Ashwal S (2009) Animal models of perinatal hypoxic-ischemic brain damage. Pediatr Neurol 40: 156-167.
23. Kanaan A, Farahani R, Douglas RM, LaManna JC, Haddad GG (2006) Effect of chronic continuous or intermittent hypoxia and reoxygenation on cerebral capillary density and myelination. Am J of Physiol-Reg I 290: R1105-R1114.
24. Sirinyan M, Sennlaub F, Dorfman A, Sapieha P, Gobeil F, Jr., et al. (2006) Hyperoxic exposure leads to nitrative stress and ensuing microvascular degeneration and diminished brain mass and function in the immature subject. Stroke 37: 2807-2815.
25. Vottier G, Pham H, Pansiot J, Biran V, Gressens P, et al. (2011) Deleterious effect of hyperoxia at birth on white matter damage in the newborn rat. Dev Neurosci 33: 261-269.
26. Gerstner B, DeSilva TM, Genz K, Armstrong A, Brehmer F, et al. (2008) Hyperoxia causes maturation-dependent cell death in the developing white matter. J Neurosci 28: 1236-1245.
27. Coleman RJ, Beharry KDA, Brock RS, Abad-Santos P, Abad-Santos M, et al. (2008) Effects of brief, clustered versus dispersed hypoxic episodes on systemic and ocular growth factors in a rat model of oxygen-induced retinopathy. Pediatr Res 64: 50-55
28. Paxinos G, Watson C (2008) The rat brain in stereotaxic coordinates. London, UK: Academic Press
29. Saunders NR, Liddelow SA, Dziegielewska KM (2012) Barrier mechanisms in the developing brain. Front Pharmacol 3: 46.
30. Mori S, Zhang J (2006) Principles of diffusion tensor imaging and its applications to basic neuroscience research. Neuron 51: 527-539.
31. Bockhorst KH, Narayana PA, Liu R, Ahobila-Vijjula P, Ramu J, et al. (2008) Early postnatal development of rat brain: In vivo diffusion tensor imaging. J Neurosci Res 86: 1520-1528.
32. Morken TS, Widerøe M, Vogt C, Lydersen S, Havnes M, et al. (2012) Longitudinal diffusion tensor and manganese-enhanced MRI detect delayed cerebral gray and white matter injury after hypoxia-ischemia and hyperoxia. Pediatr Res 73: 171-179.
33. Cai J, Tuong CM, Zhang Y, Shields CB, Guo G, et al. (2011) Mouse intermittent hypoxia mimicking apnoea of prematurity: effects on myelinogenesis and axonal maturation. J Pathol 226: 495-508.
34. Brehmer F, Bendix I, Prager S, van de Looij Y, Reinboth BS, et al. (2012) Interaction of inflammation and hyperoxia in a rat model of neonatal white matter damage. PLoS One 7: e49023.
35. Buser JR, Maire J, Riddle A, Gong X, Nguyen T, et al. (2012) Arrested preoligodendrocyte maturation contributes to myelination failure in premature infants. Ann Neurol 71: 93-109.

36. Chahboune H, Ment LR, Stewart WB, Rothman DL, Vaccarino FM, et al. (2009) Hypoxic injury during neonatal development in murine brain: correlation between in vivo DTI findings and behavioral assessment. Cereb Cortex 19: 2891-2901.
37. Shweiki D, Itin A, Soffer D, Keshet E (1992) Vascular endothelial growth factor induced by hypoxia may mediate hypoxia-initiated angiogenesis. Nature 359: 843-845.
38. Baburamani AA, Ek CJ, Walker DW, Castillo-Melendez M (2012) Vulnerability of the developing brain to hypoxic-ischemic damage: contribution of the cerebral vasculature to injury and repair? Front Physiol 3: 424.
39. Pichiule P, LaManna JC (2002) Angiopoietin-2 and rat brain capillary remodeling during adaptation and deadaptation to prolonged mild hypoxia. J Appl Physiol 93: 1131-1139.
40. Lehmenkuhler A, Sykova E, Svoboda J, Zilles K, Nicholson C (1993) Extracellular space parameters in the rat neocortex and subcortical white matter during postnatal development determined by diffusion analysis. Neuroscience 55: 339-351.
41. Thornton JS, Amess PN, Penrice J, Chong WK, Wyatt JS, et al. (1999) Cerebral tissue water spin-spin relaxation times in human neonates at 2.4 Tesla: Methodology and the effects of maturation. Magn Reson Imaging 17: 1289-1295.
42. Butt AM, Jones HC, Abbott NJ (1990) Electrical resistance across the blood-brain barrier in anaesthetized rats: a developmental study. J Physiol 429: 47-62.
43. Dziegielewska KM, Habgood MD, Møllgård K, Stagaard M, Saunders NR (1991) Species-specific transfer of plasma albumin from blood into different cerebrospinal fluid compartments in the fetal sheep. J Physiol 439: 215-237.
44. Chahoud I, Paumgartten FJ (2009) Influence of litter size on the postnatal growth of rat pups: is there a rationale for litter-size standardization in toxicity studies? Environ Res 109: 1021-1027.
45. Palmer AK, Ulbrich BC (1997) The cult of culling. Fundam Appl Toxicol 38: 7-22.
46. Walhovd KB, Fjell AM, Brown TT, Kuperman JM, Chung Y, et al. (2012) Long-term influence of normal variation in neonatal characteristics on human brain development. Proc Natl Acad Sci U S A 109: 20089-20094.
47. Leviton A, Fichorova RN, O'Shea TM, Kuban K, Paneth N, et al. (2013) Two-hit model of brain damage in the very preterm newborn: small for gestational age and postnatal systemic inflammation. Pediatr Res 73: 362-370.
48. Lepomaki V, Matomaki J, Lapinleimu H, Lehtonen L, Haataja L, et al. (2013) Effect of antenatal growth on brain white matter maturation in preterm infants at term using tract-based spatial statistics. Pediatr Radiol 43: 80-85.
49. Daneman R, Zhou L, Kebede AA, Barres BA (2010) Pericytes are required for blood-brain barrier integrity during embryogenesis. Nature 468: 562-566.
50. Benjamin LE, Hemo I, Keshet E (1998) A plasticity window for blood vessel remodelling is defined by pericyte coverage of the preformed endothelial network and is regulated by PDGF-B and VEGF. Development 125: 1591-1598.
51. Gonul E, Duz B, Kahraman S, Kayali H, Kubar A, et al. (2002) Early pericyte response to brain hypoxia in cats: an ultrastructural study. Microvasc Res 64: 116-119.
52. Schoch HJ, Fischer S, Marti HH (2002) Hypoxia-induced vascular endothelial growth factor expression causes vascular leakage in the brain. Brain 125: 2549-2557.

Figures

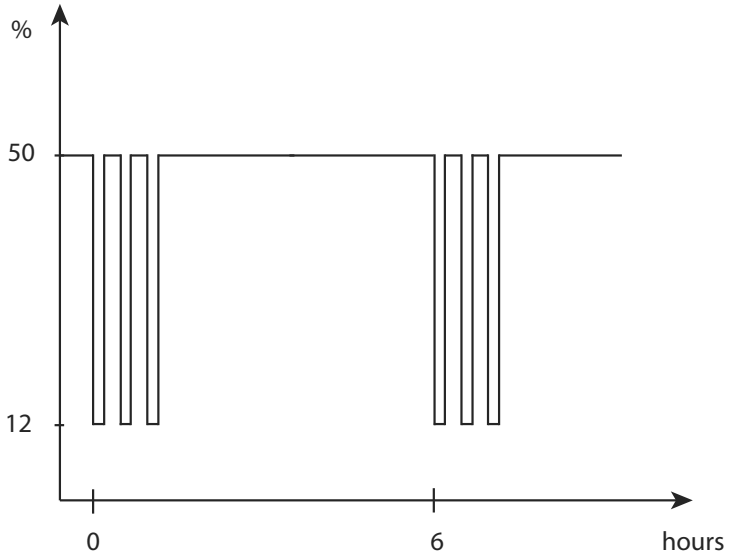

Figure 1 Experimental profile of intermittent hyperoxia-hypoxia
Every sixth hour of hyperoxia (50 % O_2) was interrupted by a cluster of three consecutive episodes of hypoxia (12 % O_2) 10 minutes apart, each of 2 minutes. This profile was applied continuously from < 4 hours after birth until postnatal day 14.

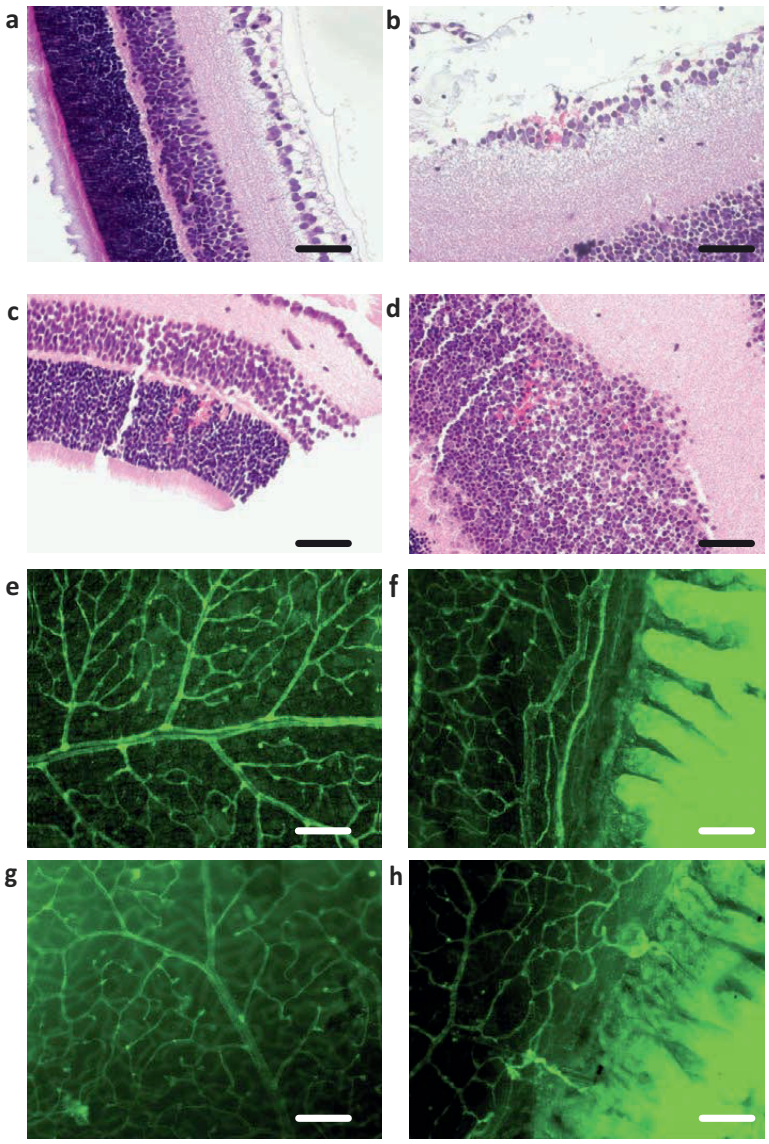

Figure 2 Retina

(a-d): H&E retinal slices from control (a) and IHH animals at P14 (b-d) showing haemorrhage in the ganglion cell layer (b), inner nuclear layer (c) and outer nuclear cell layer (d). (e-h): Retinal wholemounts stained with endothelial-specific Biotinylated *Griffonia (Bandeiraea) Simplicifolia* Lectin I Isolectin B4 from controls at P28 with a mature vascular bed (e) with no vasculature extending beyond the ora serrata (f). Vascular bed in IHH animal at P28 with less remodelling (g) and areas of vascularization beyond the ora serrata (h). (a-d): x400 magnification; scale bar = 50 µm. (e-h): x100 magnification; scale bar = 200 µm. Abbreviations, IHH, intermittent hyperoxia-hypoxia; P14, postnatal day 14; P28, postnatal day 28.

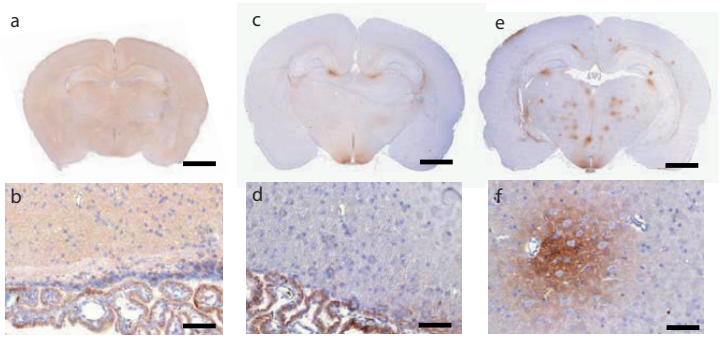

g

	IHH	controls
cortex	8/12	1/4
hippocampus	3/12	0/4
thalamus	5/12	1/4
hypothalamus	11/12	4/4

Figure 3 Albumin

Albumin immunoreactivity (brown stain) at P14 (a-b) and P28 in controls (c-d) and IHH (e-f). Note several spots of albumin immunoreactivity in the cortex and thalamus of the IHH animal at P28, and positive immunoreactivity for albumin in both experiment groups. Albumin is present in intracellular vesicles in neuroependymal cells in the ventricles (b & d). (g) The sum of positive scores for albumin leakage in the neuropil of the respective brain areas are presented as fractions of the maximum possible score in each experiment group at P 28. (a, c & e): scale bar = 2 mm (b, d & f): scale bar = 50 µm at x 400 magnification. Abbreviations: IHH, intermittent hyperoxia-hypoxia; P14, postnatal day 14; P28, postnatal day 28.

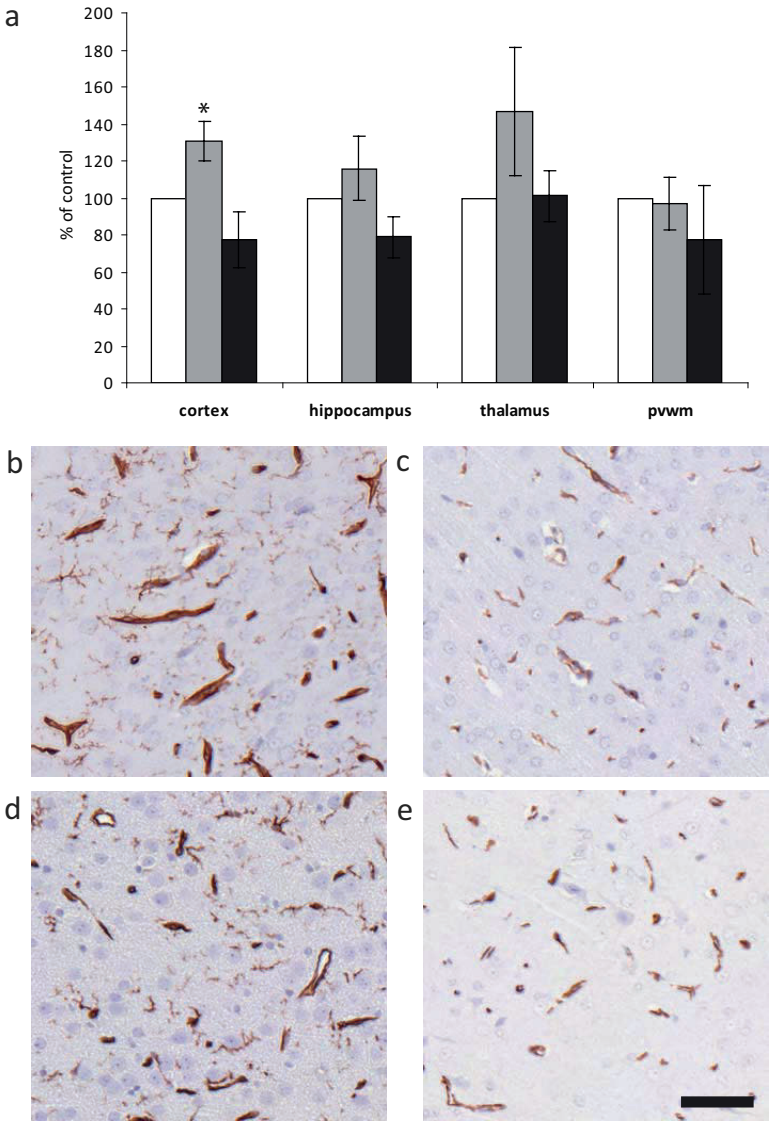

Figure 4 Vascular density

(a) Vascular density as % of controls (white columns, n = 4) in IHH animals at postnatal day 14 (grey columns; IHH: n = 10) and postnatal day 28 (black columns; IHH: n = 12). Data are expressed as mean ± 95% confidence intervals. (b-e) x400 magnification of lectin-stained endothelium in IHH (upper row) and control (lower row) at P14 (b & d) and P28 (c & e). *p = 0.005 IHH vs. control. Scale bar = 50 µm. Abbreviations: IHH, intermittent hyperoxia-hypoxia; pvwm, periventricular white matter.

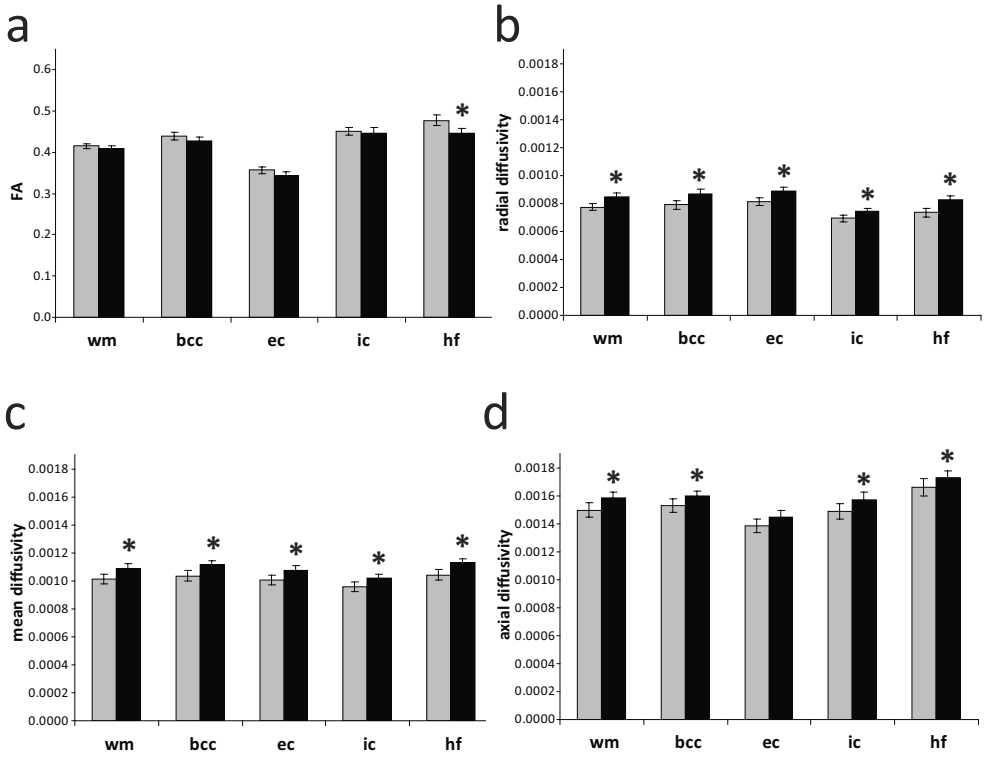

Figure 5 DTI on postnatal day 14

Fractional anisotropy (a); radial (b); mean (c) and axial diffusivity (d) in white matter areas of controls (grey columns, n = 8) and IHH (black columns, n = 22). Mean, axial and radial diffusivity are shown in units of mm^2/s. Data are presented as mean ± 95% confidence interval.* $p < 0.04$. Abbreviations: wm: all of white matter; bcc: corpus callosum (body); ec: external capsule; ic: internal capsule; IHH, intermittent hyperoxia-hypoxia; hf: hippocampal fimbriae.

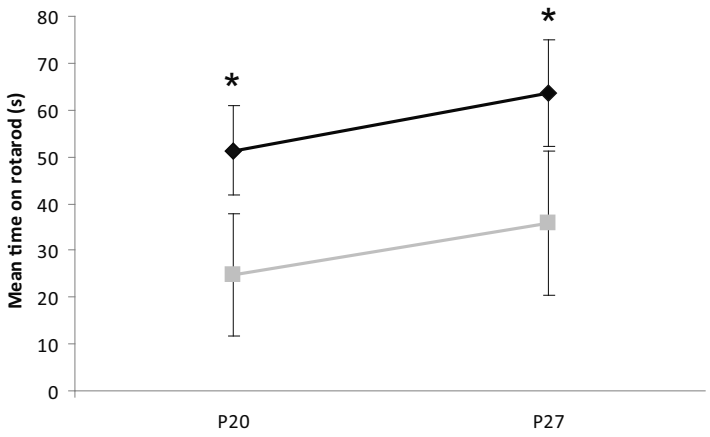

Figure 6 Rotarod testing

Mean time on a Rotarod on P20 and P27 of IHH (n = 12, black diamonds) and controls (n = 4, grey boxes). *$p \leq 0.04$ IHH vs. control. Data are presented as mean ± 95% confidence intervals. Abbreviations: IHH, intermittent hyperoxia-hypoxia; P20, postnatal day 20; P27, postnatal day 27.

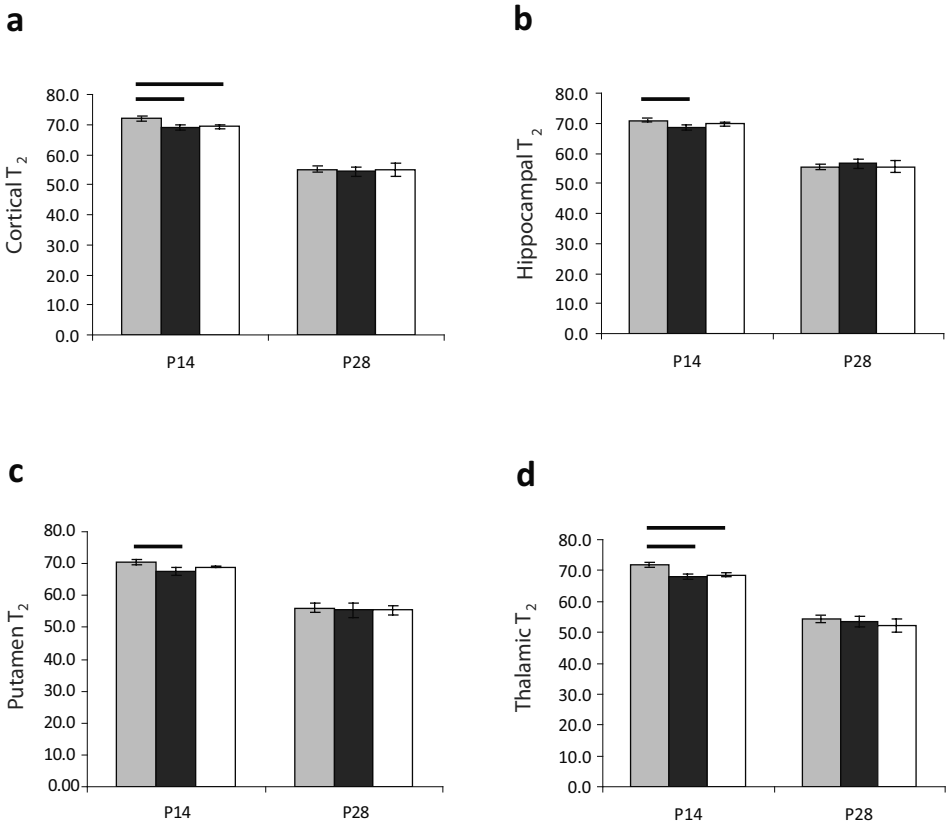

Figure 7 Litter differences in T_2

T_2-relaxation time in the brain at P14 in litter A (grey columns, n = 13), litter B (black columns, n = 9) and C (white columns, n = 8) in the cortex (a), hippocampus (b), putamen (c) and thalamus (d). T_2-relaxation times are shown in units of milliseconds. Differences between litters are marked where significant ($p < 0.05$). Data are presented as mean ± 95% confidence interval. Abbreviations: IHH, intermittent hyperoxia-hypoxia; P14: postnatal day 14; P28: postnatal day 28.

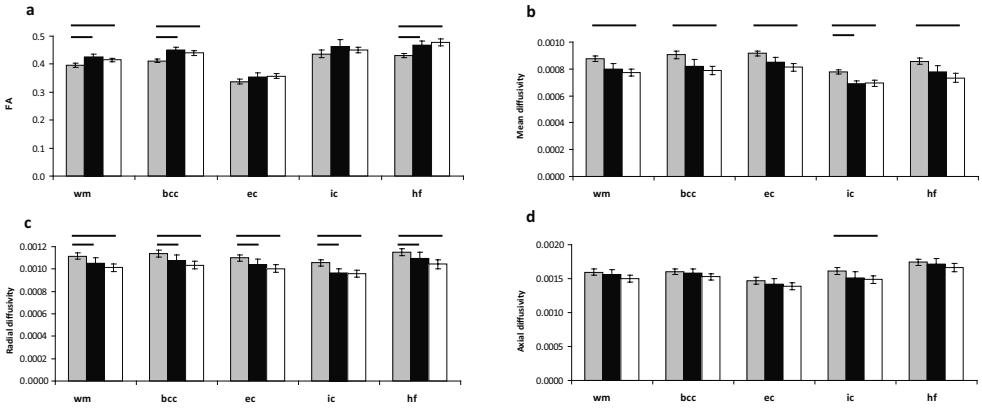

Figure 8 Litter differences in DTI metrics

Fractional anisotropy (a); mean (b), radial (c) and axial diffusivity (d) in white matter areas of litter A (grey columns, n = 13), B (black columns, n = 9) and controls (white columns, n = 8) on postnatal day 14. Mean, axial and radial diffusivity are shown in units of mm^2/s. Data are presented as mean ± 95% confidence interval. Differences between litters are marked where significant ($p < 0.05$). Abbreviations: wm: all of white matter; bcc: corpus callosum (bcc); ec: external capsule; ic: internal capsule; IHH, intermittent hyperoxia-hypoxia; hf: hippocampal fimbriae.

Supplementary Information:

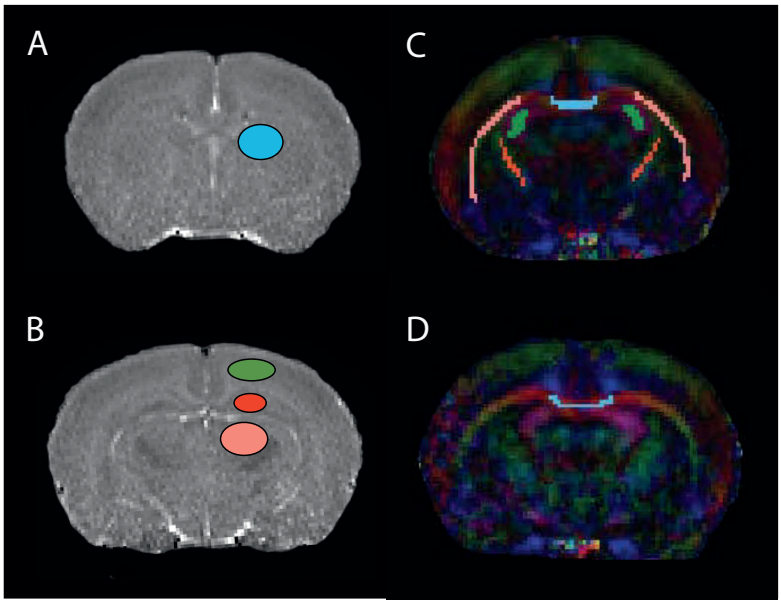

Figure 1 Regions of Interest in T_2 and FA-maps
(a) T_2-map corresponding to –1.5 mm from the bregma with regions of interest (ROI) marked in putamen (blue). (b) T_2 -map corresponding to –3.25 mm from the bregma with ROI in parasagittal cortex (green), hippocampus (red) and thalamus (pink). (c) Colour-encoded directional FA-maps from postnatal day 14 (c) and 28 (d) with ROI in corpus callosum (blue), hippocampal fimbriae (green), internal capsule (red) and external capsule (pink). The ROI in corpus callosum encompassed three slices anterior and three posterior to the one shown. The ROI in hippocampal fimbriae, external and internal capsule encompassed two posterior to the one shown.

Tables

		cortex	hippocampus	putamen	thalamus
		(msec)			
IHH	**P14**	70.7 ± 0.8*	69.9 ± 0.9	69.3 ± 0.9	70.2 ± 1.0*
	P28	54.9 ± 0.8†	56.0 ± 0.6†	55.9 ± 1.3†	54.1 ± 0.8†
control	**P14**	69.3 ± 0.7	69.7 ± 1.1	69.0 ± 0.2	68.5 ± 1.1
	P28	54.9 ± 2.1†	55.6 ± 2.4 †	55.4 ± 1.4†	52.2 ± 1.2†

Table 1 T_2 relaxation time

T_2-relaxation time in the brain at P14 (IHH: n = 22; control: n = 8) and P28 (IHH: n = 12; control: n= 4). Data are presented as mean ± 95% confidence interval. *p < 0.05 P14 IHH vs. P14 control. †p < 0.003 P14 vs. P28 within each experiment group. Abbreviations: IHH, intermittent hyperoxia-hypoxia; P14: postnatal day 14; P28: postnatal day 28.

		FA	radial diffusivity	mean diffusivity (mm^2/s)	axial diffusivity
IHH	**P14**	0.44 ± 0.02	0.00090 ± 0.00005*	0.00115 ± 0.00005*	0.00166 ± 0.00004*
	P28	0.52 ± 0.05†	0.00072 ± 0.00005†	0.00103 ± 0.00003†	0.00164 ± 0.00005
control	**P14**	0.44 ± 0.02	0.00078 ± 0.00002	0.00103 ± 0.00001	0.00153 ± 0.00003
	P28	0.48 ± 0.05	0.00077 ± 0.00005	0.00103 ± 0.00004	0.00154 ± 0.00009

Table 2 Diffusion tensor metrics of the corpus callosum at postnatal day 14 and 28

DTI metrics in animals with DTI of the corpus callosum at both P14 and P28 in IHH (n = 6) and controls (n = 4). Data are presented as mean ± 95% confidence interval.* p < 0.02 P14 IHH vs. P14 control, †$p \leq 0.03$ P14 IHH vs. P28 IHH. Abbreviations: FA, fractional anisotropy; IHH, intermittent hyperoxia-hypoxia; P14, postnatal day 14; P28, postnatal day 28.

Paper III

Is not included due to copyright

Paper IV